Crustal Structure of Active Deformation Zones in Africa: Implications for Global Crustal Processes

C. J. Ebinger, D. Keir, I. D. Bastow, K. Whaler, J. O. S. Hammond, A. Ayele, M. S. Miller, Christel Tiberi, S. Hautot

AGU PUBLICATIONS

Tectonics

REVIEW ARTICLE
10.1002/2017TC004526

Special Section:
An appraisal of Global Continental Crust: Structure and Evolution

Crustal Structure of Active Deformation Zones in Africa: Implications for Global Crustal Processes

C. J. Ebinger[1], D. Keir[2,3], I. D. Bastow[4], K. Whaler[5], J. O. S. Hammond[6], A. Ayele[7], M. S. Miller[8], C. Tiberi[9], and S. Hautot[10]

[1]Department of Earth and Environmental Sciences, Tulane University of Louisiana, New Orleans, LA, USA, [2]Dipartimento di Scienze della Terra, Università degli Studi di Firenze, Florence, Italy, [3]Ocean and Earth Science, University of Southampton, Southampton, UK, [4]Department of Earth Science and Engineering, Imperial College London, London, UK, [5]School of GeoSciences, University of Edinburgh, Edinburgh, UK, [6]Department of Earth and Planetary Sciences, Birkbeck, University of London, London, UK, [7]Institute of Geophysics, Space Science, and Astronomy, Addis Ababa University, Addis Ababa, Ethiopia, [8]Research School of Earth Sciences, Australian National University, Canberra, ACT, Australia, [9]Géosciences Montpellier, UMR5243-CNRS, Université Montpellier, Montpellier, France, [10]Imagir sarl, Brest, France

Key Points:
- In African rifts that formed within the last 7 Myr, ~20% of the crust is new magmatic material
- In mature rift sectors, the surface area of the rift has doubled in ~ 10 Myr, and intrusive volumes are 30% or more
- Plate rupture is achieved through catastrophic magma intrusion events in 15–20 km thick transitional crust

Correspondence to:
C. J. Ebinger,
cebinger@tulane.edu

Citation:
Ebinger, C. J., Keir, D., Bastow, I. D., Whaler, K., Hammond, J. O. S., Ayele, A., … Hautot, S. (2017). Crustal structure of active deformation zones in Africa: Implications for global crustal processes. *Tectonics*, *36*. https://doi.org/10.1002/2017TC004526

Received 24 FEB 2017
Accepted 4 SEP 2017
Accepted article online 13 NOV 2017

Abstract The Cenozoic East African rift (EAR), Cameroon Volcanic Line (CVL), and Atlas Mountains formed on the slow-moving African continent, which last experienced orogeny during the Pan-African. We synthesize primarily geophysical data to evaluate the role of magmatism in shaping Africa's crust. In young magmatic rift zones, melt and volatiles migrate from the asthenosphere to gas-rich magma reservoirs at the Moho, altering crustal composition and reducing strength. Within the southernmost Eastern rift, the crust comprises ~20% new magmatic material ponded in the lower crust and intruded as sills and dikes at shallower depths. In the Main Ethiopian Rift, intrusions comprise 30% of the crust below axial zones of dike-dominated extension. In the incipient rupture zones of the Afar rift, magma intrusions fed from crustal magma chambers beneath segment centers create new columns of mafic crust, as along slow-spreading ridges. Our comparisons suggest that transitional crust, including seaward dipping sequences, is created as progressively smaller screens of continental crust are heated and weakened by magma intrusion into 15–20 km thick crust. In the 30 Ma Recent CVL, which lacks a hot spot age progression, extensional forces are small, inhibiting the creation and rise of magma into the crust. In the Atlas orogen, localized magmatism follows the strike of the Atlas Mountains from the Canary Islands hot spot toward the Alboran Sea. CVL and Atlas magmatism has had minimal impact on crustal structure. Our syntheses show that magma and volatiles are migrating from the asthenosphere through the plates, modifying rheology, and contributing significantly to global carbon and water fluxes.

1. Overview

The geological record of the African continent spans three quarters of Earth history. Key events occurred in the Archaean when the West African, Congo, Kaapvaal, Zimbabwe, and Tanzanian cratons formed, followed by Palaeoproterozoic accretion of cratons. Unusually, only the northern and northwestern margins of the African plate have been involved in orogeny since the end Pan-African (~500 Ma), when a Himalayan-scale collision formed along eastern Africa and orogenies ringed the Zimbabwe-Kaapvaal-Congo cratons of southern and western Africa (e.g., Muhongo & Lenoir, 1994; Shackleton, 1986; Van Hinsbergen et al., 2011). Each of these processes has left an indelible signature on Africa's crust and contributed to the formation and destruction of continental topography.

Excluding the collisional belts of NW Africa (e.g., Miller & Becker, 2014), the predominant tectonic processes since the Pan-African have been magmatism and extension that have increased the surface area and volume of African crust, as outlined in this paper. Southeastern Africa was affected by rifting and flood magmatism at 184–179 Ma (Ferrar-Karroo flood basalts) prior to the separation of Africa and Antarctica (e.g., Duncan et al., 1997), and large sectors of western Africa experienced flood magmatism at 137–127 Ma (Etendeka-Parana flood basalts) as the south Atlantic opened (e.g., Mohriak et al., 2012; Turner et al., 1994). Central, southern, and eastern Africa were affected by the Mesozoic rifting and breakup of Gondwana that left scars such as the Central African rift system and the widespread extensional basins from Somalia to S. Africa (e.g., Burke, 1996; Veevers et al., 1994). Over the past ~45 Ma, Africa again has experienced kimberlitic to flood magmatism and plateau uplift, followed by diachronous rifting from Egypt south to South Africa and southwest

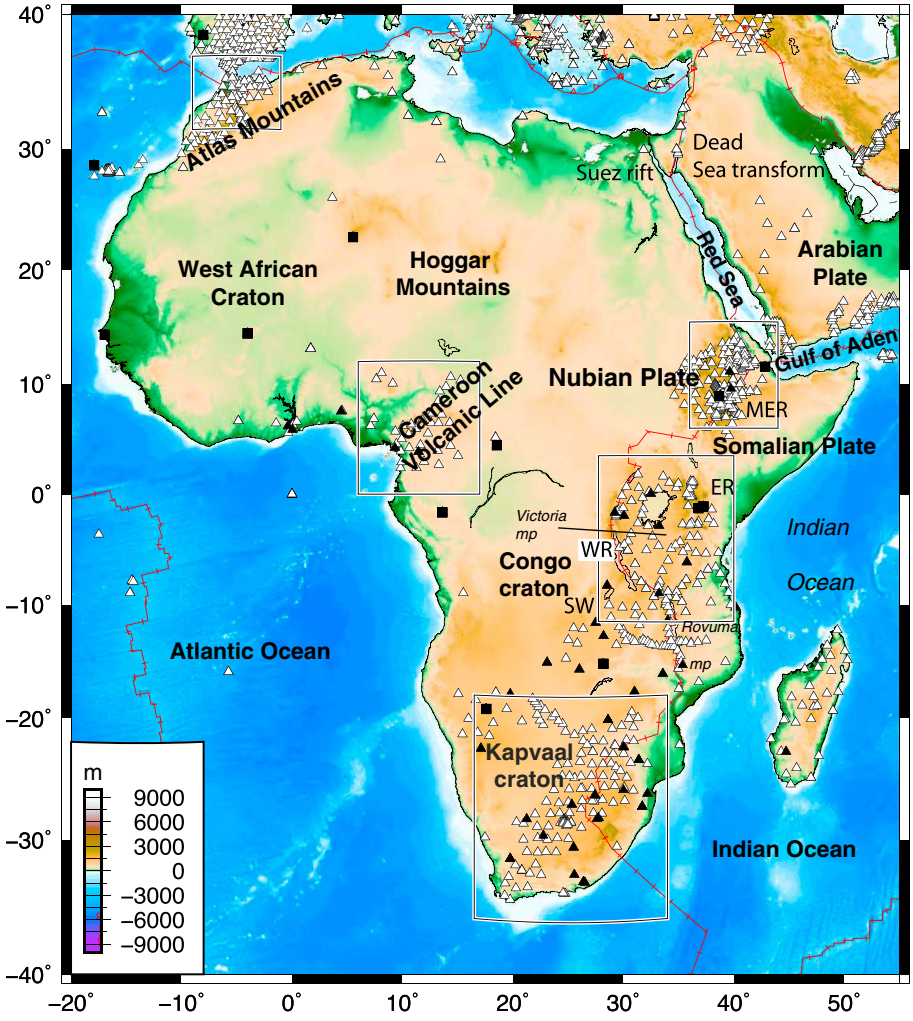

Figure 1. Topography of Africa with major plates (after Bird, 2003). Landforms and tectonic features labeled. White triangles are temporary seismic networks, whereas black solid shapes are permanent seismic stations. Stations used in controlled source experiments shown in Figures 5 and 7. Boxes enclose regions with crustal thickness information constrained from receiver functions in Figures 2 and 3. Subregions are explored in more detail in subsequent figures.
SW = Southwestern rift, WR = Western rift, ER = Eastern rift, MER = Main Ethiopian Rift, Rovuma mp = Rovuma microplate, Victoria mp = Victoria microplate.

through Botswana (e.g., Ebinger & Scholz, 2012) (Figure 1). The Tertiary rift basins and magmatic provinces include all stages and styles in the evolution of cratonic rift zones: incipient rifting in the Okavango to incipient seafloor spreading in the Afar depression, amagmatic sectors in the Western and Southwestern rift to the large igneous province in Ethiopia-Yemen, and sectors that transect Paleozoic lithosphere of variable thickness and composition (e.g., Corti, 2009; Ebinger & Scholz, 2012; Rooney et al., 2017) (Figures 1–4). Oligocene-Recent magmatism with little extension modifies crustal structure beneath West-Central Africa along the Cameroon Volcanic Line (CVL) (Figure 3). Perhaps owing to the very slow movement of the African plate since collision with Europe initiated at ~40 Ma, domal uplift and magmatism without faulting also characterize northern Africa (e.g., Hoggar-Tibesti; Bond, 1978; Brown & Girdler, 1980; Rosenbaum & Lister, 2004) (Figure 1).

Over the past few decades, multiple geoscientific experiments have yielded fundamental new constraints on the structure, composition, and evolution of the crust beneath extensional basin systems in Africa and between Africa and Arabia (e.g., Berckhemer et al., 1975; Prodehl & Mechie, 1991a, 1991b; Tokam et al., 2010; Wölbern et al., 2010). Controlled source seismic experiments provide absolute velocity control and details along largely 2-D profiles of crust and, where seismic sources are large, the upper mantle (e.g.,

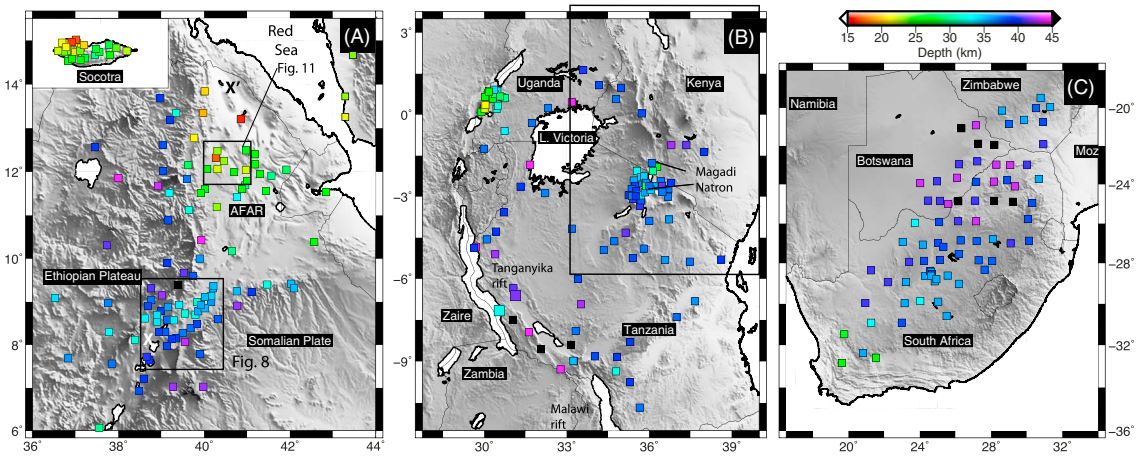

Figure 2. Crustal thickness in East Africa constrained using receiver function analysis. Boxes in Figure 2a enclose area of Figure 8 and Figure 11. Box in Figure 2b encloses area shown in Figure 5. Data are sourced from (a) Ethiopia-Yemen plateau regions and the Gulf of Aden Island of Socotra (Ahmed et al., 2014, 2013; Dugda & Nyblade, 2006; Hammond et al., 2011; Stuart et al., 2006), (b) East Africa (Dugda et al., 2005; Hodgson et al., 2017; Plasman et al., 2017; Tugume et al., 2012; Wölbern et al., 2010), and (c) Southern Africa (Nguuri et al., 2001; Kgaswane et al., 2009).

Keller et al., 1994; Maguire et al., 2006; Ruegg, 1975; Stuart et al., 1985). Receiver functions provide constraints on velocity contrasts at the Moho and, in some areas, intracrustal and intramantle reflectors, beneath each permanent or temporary seismic station (e.g., Gao et al., 2013; Hammond et al., 2011; Hodgson et al., 2017; Plasman et al., 2017) (e.g., Figures 2 and 3). Crustal tomography provides a 3-D image of the velocity structure and serves to connect velocity variations between the 2-D controlled source profiles and receiver function point measurements. Ambient noise and arrival time tomography methods, however, rarely image the lower crust owing to sparse ray coverage from local earthquakes and array aperture for ambient noise (e.g., Accardo et al., 2017; Daly et al., 2008; Kim et al., 2012; Korostelev et al., 2015). Magnetotelluric data provide 2-D profiles and point measurements of crust and upper mantle electrical resistivity

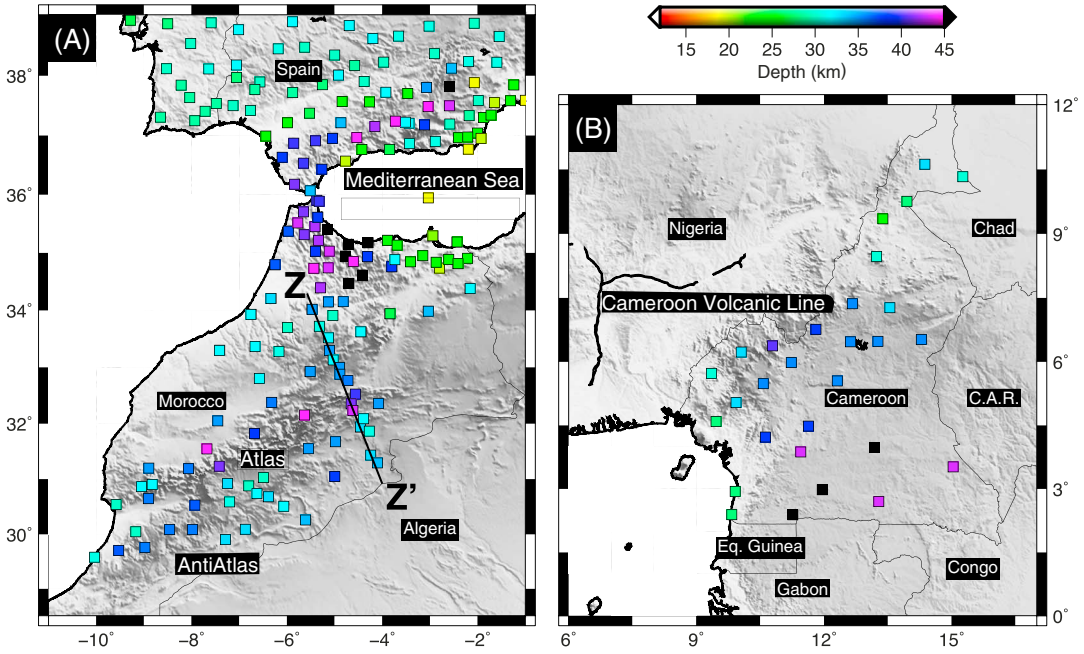

Figure 3. Crustal thickness in (a) the Atlas orogen (Africa-Eurasia collision) and (b) Cameroon Volcanic Line constrained using receiver function analysis. Z-Z′ denotes location of profile shown in Figure 14. Data from Figure 3a are Cooper and Miller (2014), Jessell et al. (2016), Mancilla and Diaz (2012); Miller and Becker (2014), and Spieker et al. (2014) and Figure 3b are sourced from Tokam et al. (2010) and Gallacher and Bastow (2012).

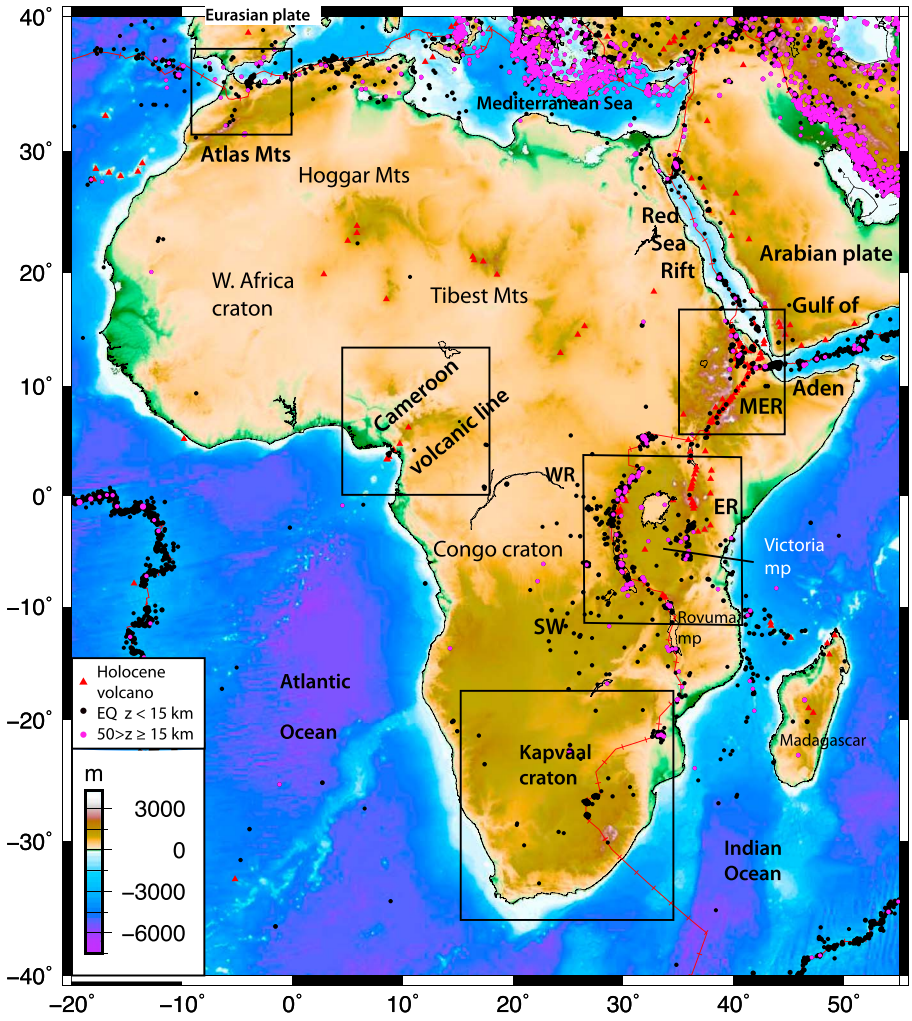

Figure 4. Topography of Africa with major plates, and 1976–2016 seismicity from the NEIC catalogue, and Holocene to Recent volcanoes from the Global Volcanism Program (http://volcano.si.edu/). ER = Eastern rift, WR = Western rift, SW = Southwestern arm, Rovuma mp = Rovuma microplate, Victoria mp = Victoria microplate. Large Archaean cratons with deep roots labeled; small Tanzania craton lies between the ER and WR. Lower crustal earthquakes with depths greater than 15 km are highlighted in magenta. Boxes enclose regions with crustal thickness information constrained from receiver functions in Figures 2 and 3.

properties, including resistivity versus depth and azimuthal anisotropy of electrical conductivity (e.g., Selway et al., 2014; Whaler & Hautot, 2006). Magnetotelluric data are more sensitive to the presence of melt than seismic methods. Although models of gravity anomalies are highly nonunique, when constrained or jointly inverted with independent 2-D and 3-D data sets, the spatial patterns of gravity anomalies provide additional information on 3-D density variations (e.g., Roecker et al., 2017; Tiberi et al., 2005). The combination of magnetotelluric, seismic, and gravity data in separate and joint inversions enables tighter constraints on material properties and, in some instances, provides new insights into the distinction between magmatic fluids, aqueous fluids, and volatiles within the crust and their role in crustal deformation.

This contribution synthesizes our current understanding of crustal modification in tectonically active cratonic rift zones and mountain belts and lays out a road map for future studies of African rift and orogenic zones. Several large-scale crust and mantle imaging experiments have acquired promising data sets in incipient and weakly extended, magma-poor rift sectors (e.g., Gao et al., 2013; Hodgson et al., 2017; Shillington et al., 2016), but a synthesis of crustal structure of early stage rifts is premature. Our focus is to characterize crustal structure in zones of active deformation in the East African rift, Cameroon Volcanic Line (CVL), and

Atlas Mountains. The review of along-axis variations in the East African rift affords the opportunity to compare and contrast magma-rich rift sectors, providing insights on the evolution of the continental crust in response to stretching and magmatism. This synthesis and comparison offers new insights into the nature of "transitional" crust beneath late-stage rifts (e.g., Fuis & Mooney, 1990; Persaud et al., 2016) and passive margins worldwide (e.g., Skogseid et al., 2000; Van Avendonk et al., 2009). Comparison and contrast with the magmatically modified crust beneath the Atlas Mountains and CVL add to our understanding of fluid and volatile migration through the African crust.

Section 2 provides a broad-brush summary of the geodynamical context of active deformation in Africa. Section 3 outlines the role of magma intrusion during the first 5–7 Myr of rifting in cratonic lithosphere, using examples from the southern sector of the Eastern (Gregory) rift. Sections 4 and 5 address the role of magmatism and thinning in the formation of crust transitional between continental and oceanic. The Horn of Africa is one of few areas worldwide where this transition is occurring, and comparisons with the well-studied Salton Trough and northern Gulf of California (e.g., Fuis & Mooney, 1990; Persaud et al., 2016) inform our understanding of magmatic modification along passive margins worldwide. In section 6, we journey across the continent, where warm asthenosphere rises beneath the eastern edge of the Congo craton and the southern margin of a preexisting Mesozoic rift zone. This linear belt of Cenozoic eruptive volcanic centers, neither the CVL, exhibits the age progression, mechanical stretching, magmatic modification displayed in parts of East Africa nor along linear volcanic tracks in oceanic plates. Here too, volatiles have likely played a central role in magmatic modification of Africa's crust. Section 7 presents a review of crustal structure and its relation to mantle dynamics beneath the Atlas Mountains where compressional tectonics may inhibit upward migration of melt, leading to the localized, linear trend of magmatism linked instead to the Canary Island hot spot. This integration of constraints on crustal structure beneath zones of active rifting and orogenesis in Africa shows that magma and volatiles are migrating from the asthenosphere through the plates, modifying lithospheric rheology and significantly contributing to global carbon and water fluxes.

2. Geodynamic Settings

The slow-moving African continent moves at 3–7 mm y^{-1} NW to WNW and collides with the Eurasian plate (e.g., Serpelloni et al., 2007). Africa has unusually high elevation, in large part owing to the broad plateau uplifts associated with mantle plumes and volcanic construction in the large igneous provinces of the East African Rift System (EARS) and the CVL and the unextended Hoggar and Tibesti volcanic uplifts (Figure 1). Extension effectively increases the surface area of continental landmasses and creates continental platforms. Magmatism during rifting creates new continental crust through dike and sill intrusion and surface construction, but the rates and volumes of crustal accretion are poorly constrained (Lee et al., 2016; Thybo & Artemieva, 2013), in part motivating this comparative study.

2.1. East African Rift System

Active faulting and magmatism occur across a large part of the African continent between the Horn of Africa southwest to the Okavango region of Botswana and in a second diffuse arm that continues from southwestern Ethiopia to southeastern Mozambique, including offshore regions of the Indian Ocean, such as the Davie Ridge (Figures 1 and 2). The southern Red Sea, Main Ethiopian, and Eastern, Western, and Southwestern rift systems have developed atop broad topographic plateaux, whereas the Malawi rift and its southeastward continuation transect low elevation regions in Mozambique (Figure 2).

The broad plateaus, their corresponding negative Bouguer gravity anomalies, low upper mantle seismic velocities, and the large volume and geochemistry of eruptive volcanic products have been cited as evidence for one or more mantle plumes beneath sections, or all, of the uplifted zones of Africa (e.g., Ebinger & Sleep, 1998; Marty & Yirgu, 1996; Nyblade & Robinson, 1994; Sengör & Burke, 1978). Global and local tomography and geochemical studies reveal low-velocity zones caused by one or a combination of elevated temperatures and the presence of melt in the asthenosphere (e.g., Adams et al., 2012; Debayle et al., 2001; Fishwick & Bastow, 2011; Mulibo & Nyblade, 2013; O'Donnell et al., 2013; Ritsema et al., 1999; Rooney et al., 2011; Simmons et al., 2007; Weeraratne et al., 2003). Although gaps remain in our knowledge of the Western rift and beneath the Indian Ocean, the lowest *P* and *S* wave velocity regions underlie the Main Ethiopian Rift (MER) and the Eastern rift zone and the isolated volcanic provinces of

the Western rift (e.g., Adams et al., 2012; Bastow et al., 2008; Fishwick, 2010; O'Donnell et al., 2013). The Ethiopia-Yemen and East African Plateaux are separated by an ~300 km wide topographic depression that is underlain by crust stretched during Mesozoic rifting, allowing the possibility that the two plateaux are actually one uplifted region extending from southern Africa to the Red Sea: the African superplume province (e.g., Kendall & Lithgow-Bertelloni, 2016; Nyblade & Robinson, 1994; Ritsema et al., 1999).

Thermal-mechanical modeling indicates that widespread Mesozoic rift zones spanning the breadth and length of Africa would have been actively subsiding and underlain by thinned lithosphere at the onset of flood magmatism. At ~40 Ma the earliest flood basalts were erupted in southwestern Ethiopia and northern Kenya, suggesting that these thinned and heated regions may have been inherently weaker than surrounding regions (e.g., Hendrie et al., 1994; Morley et al., 1999) or may have ponded anomalously hot mantle material susceptible to decompression melting (e.g., Ebinger & Sleep, 1998). Edge-driven convection may enhance magma production and lithospheric heating at the edges of the deeply rooted Tanzania and Congo cratons where kimberlitic and carbonatitic magmatism has occurred since ~40 Ma (e.g., Ebinger & Sleep, 1998; King & Anderson, 1998; King & Ritsema, 2000). The geochemistry of Eocene-Recent eruptive volcanic products points to a mantle plume origin for the Ethiopia-Yemen flood basalt sequences, but the East African plateau region south of Ethiopia shows more spatial variability (e.g., Chakrabarti et al., 2009; Furman, 2007, Furman et al., 2006; Halldórsson et al., 2014; Pik et al., 2006; Rooney et al., 2011).

Although sub-Saharan Africa is widely separated from subducting slabs that carry fluids to the mantle, and the last orogenesis occurred over 500 Myr ago, African volcanoes and active fault systems transfer large volumes of exsolved volatiles, and xenoliths are heavily metasomatized (e.g., Chesley et al., 1999; Frezzotti et al., 2010; Reisberg et al., 2004; Rooney et al., 2017; Trestrail et al., 2017; Vauchez et al., 2005). The lithospheric heating and fluid migration modify crust and mantle density, geothermal gradients, and hydration state, which are the primary controls on the lithospheric strength (e.g., Bürgmann & Dresen, 2008; Hacker et al., 2015; Lowry & Pérez-Gussinyé, 2011). Mineral physics, seismic and magnetotelluric (MT) imaging, and xenoliths provide increasing evidence that hydration state and high partial pressures of CO_2 and temperature significantly influence the rheology, density, seismic velocity, and thermodynamics of minerals (e.g., Guerri et al., 2015; Selway et al., 2014; Schmandt & Humphreys, 2010; Vauchez et al., 2005; Wada et al., 2008). Gas and fluid phases also change the frictional properties of fault zones (e.g., Niemeijer & Spiers, 2006). Thus, heat transfer and the migration of magmatic fluids and exsolved gases through the thinning plate beneath rift zones may play a key role in strain localization during early stage rifting (e.g., Buck, 2004; Lee et al., 2016; Maccaferri et al., 2011; Muirhead et al., 2016; Rooney et al., 2017), as outlined in this review paper.

2.2. Cameroon Volcanic Line

The CVL formed between the northern edge of the deeply rooted Congo craton and the Benue trough, a highly extended Cretaceous rift system that connected to basins in eastern Sudan and Kenya (e.g., Benkhelil, 1989; Fairhead & Binks, 1991; Poudjom Djomani et al., 1997) (Figure 3). The CVL straddles the continent-ocean boundary (Figure 3). Intriguingly, 42 Ma to Recent volcanism along the CVL displays no clear age progression (e.g., Fitton, 1980; Halliday et al., 1990; Marzoli et al., 2000; Nkouathio et al., 2008), an observation that has prompted numerous workers to explore beyond the classic plate-plume hypothesis for hot spot development to explain the CVL. Alternatives have included decompression melting beneath reactivated shear zones in the lithosphere (e.g., Fairhead, 1988; Fairhead & Binks, 1991; Freeth, 1979; Moreau et al., 1987), small-scale upper mantle convection that may advect mantle lithosphere (e.g., King & Anderson, 1998; King & Ritsema, 2000), and delamination (e.g., De Plaen et al., 2014; Fourel et al., 2013). It has also been suggested that lateral flow of buoyant asthenosphere, beneath continental lithosphere thinned extensively during Mesozoic rifting, may now be contributing to the younger volcanism along the line (Ebinger & Sleep, 1998). In support of this hypothesis, Perez-Gussinyé et al. (2009) constrained lithospheric strength via study of effective elastic plate thickness (*Te*) across the African continent using coherence analysis of topography and Bouguer anomaly data. Their study revealed corridors of relatively weak lithosphere that continue across the African continent from the Afar region to Cameroon, where *Te* is also depressed in comparison to the surrounding cratons.

2.3. Atlas Mountains

The Atlas Mountains of Morocco are a 2,000 km long intracontinental compressional belt that strikes ENE from Morocco into Algeria and Tunisia (Figures 1, 3, and 4). The structure was formed by reactivation of Triassic-Jurassic age normal faults that originally formed during the opening of the North Atlantic, followed by the Cenozoic collision of Africa with Eurasia (e.g., Gomez et al., 2000; Pique et al., 2002). Unlike some of the other orogenic belts around the Mediterranean, the origin of the topography of the Atlas is not directly linked to slab rollback (e.g., Dewey et al., 1989; Faccenna et al., 2004; Wortel & Spakman, 2000). The unusually high topography, modest tectonic shortening, thin lithosphere, and localized alkali volcanism may be explained by upwelling of a hot mantle anomaly linked to the Canary island hot spot (e.g., Duggen et al., 2009; Miller et al., 2015; Miller & Becker, 2014).

3. Embryonic Rifting of Cratonic Lithosphere and the Role of Volatiles

A long-standing question in plate tectonics involves the initiation of rifting in strong cratonic lithosphere, where the inherent strength of the plate is greater than the far-field and gravitational potential energy forces available (e.g., Bott, 1990; Flesch & Bendick, 2012; Stamps et al., 2014). Where magma is generated, the buoyancy forces of magma add to the tectonic stress, and dike intrusion may accommodate extension at one eighth the force required to overcome friction along a fault (e.g., Bialas et al., 2010; Buck, 2004). Yet only very small melt volumes can be generated beneath thick lithosphere; magma-assisted rifting is unlikely in lithosphere greater than ~ 100 km thick, unless the upper mantle is anomalously hot, carbonated, and hydrated (e.g., Dixon et al., 2008; Turner et al., 1994). The $<$7 Myr old Eastern rift in southern Kenya and northern Tanzania provides a unique opportunity to address this paradigm: faulting and magmatism occur in deeply rooted lithosphere, and crust and mantle xenoliths constrain compositions (Figure 5). This region is one of the most seismically active regions in East Africa, and both teleseismically and locally detected earthquakes span the entire crustal thickness (e.g., Albaric et al., 2014; Craig et al., 2011; Lee et al., 2016; Yang & Chen, 2010) (Figure 4).

The Eastern (Gregory) rift marks the divergent plate boundary between the slowly opening ($\leq$6 mm/y) Nubia and Somalia plates (e.g., Birhanu et al., 2016; Saria et al., 2014) (Figures 4 and 5). The Eastern rift splays into a broad zone of ~80 km long, seismically active faults, and isolated eruptive centers at its southern termination in northern Tanzania (Figures 4 and 5). The southern sector of the Eastern rift developed after ~6 Ma, based on ^{40}Ar-^{39}Ar dating of volcanic samples and carbon dating of abundant fossil remains in the Olduvai and Natron basins (e.g., Ashley et al., 2009; Mana et al., 2012, 2015). Sedimentary basin thicknesses increase to almost 10 km where the East African rift overprints Mesozoic rift basins in northern Kenya (e.g., Hendrie et al., 1994).

Although heat flow data show little-to-no elevation of geotherms beneath the 1.5–2 km rift flanks, magmatic systems within basins have locally elevated geotherms (e.g., Nyblade et al., 1990; Simiyu, 2010; Wheildon et al., 1994). The geochemistry and petrology of mantle xenoliths indicate that the lithosphere beneath the craton (west), rift, and Pan-African belt (east) has been metasomatized in large part by magmatic fluids and volatiles (e.g., Aulbach et al., 2011; Mattsson et al., 2013; Rudnick et al., 1993). Uniquely, voluminous CO_2 emissions derived from magma degassing occur along the seismically active border fault systems bounding basins (Lee et al., 2016) at distances $>$20 km from the active carbonatitic volcano, Oldoinyo Lengai (Figure 5). The volume of fault zone degassing along faults and from volcanoes may be 11% of the global CO_2 budget (Lee et al., 2016). The localized metasomatism, magma intrusion, and magma degassing may have weakened the cratonic lithosphere to enable rift initiation at the edge of the deeply rooted Tanzania craton. Crustal xenoliths from Archaean crust (west) and Pan-African crust (east) are mafic granulites (Jones et al., 1983; Mansur et al., 2014) (Figure 5). Yield strength envelopes for granulitic lower crust indicate that it is too weak to explain the unusual lower crustal seismicity in this rift sector (e.g., Wang et al., 2012; Weinstein et al., 2017).

3.1. Crustal Velocities, Thinning, and Evidence for Intrusions

Seismic refraction/wide-angle reflection, arrival time and mantle tomography, MT, and gravity data acquired as part of the KRISP94 (Kenya Rift International Seismic Project) with profile locations shown in Figure 5 provide details of Archaean and Late Proterozoic crust, as well as rift structure. Data from two temporary seismic arrays spanning three rift segments of the Eastern rift, including the active Oldoinyo Lengai volcano, provide

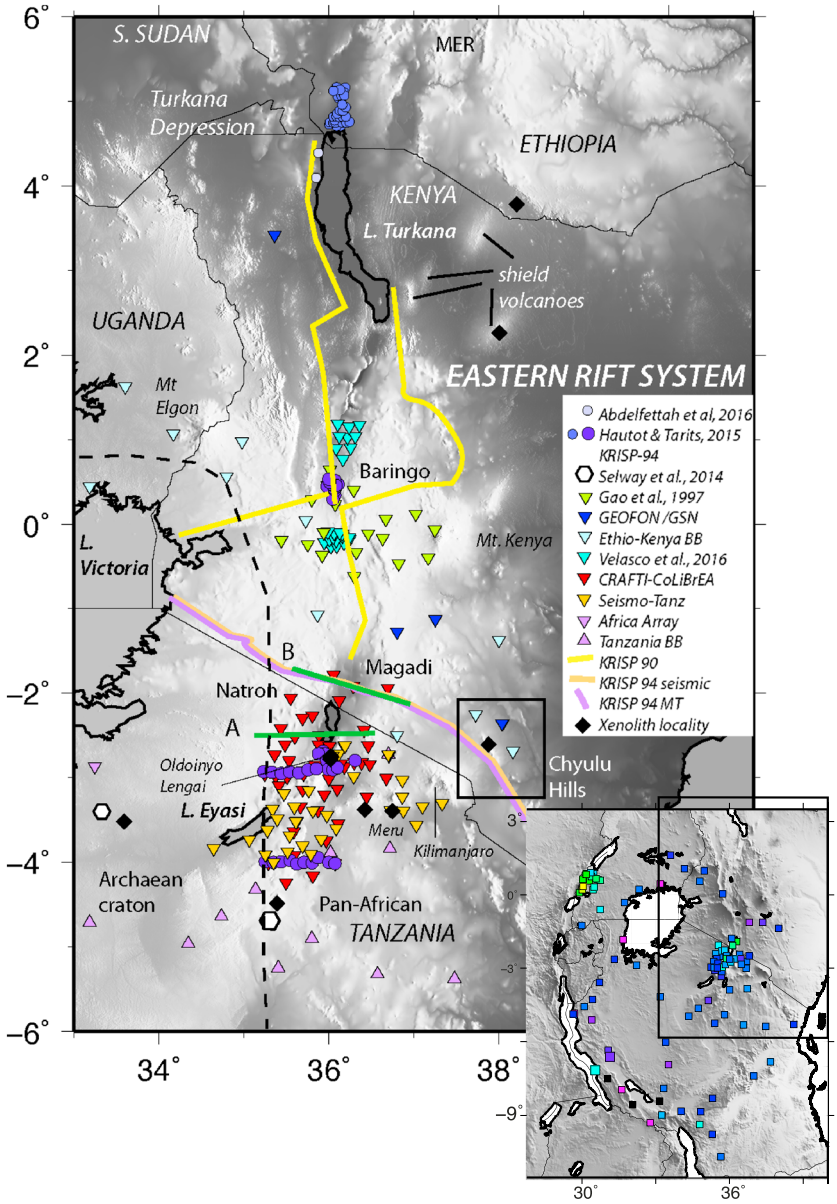

Figure 5. Compilation of seismic and magnetotelluric (MT) data sets from the Eastern rift system, with respect to crust and mantle xenolith localities. Inset places study area within context of region shown in Figure 2b. Green bold lines show the locations of cross sections of the Natron (A-A′) and Magadi (B-B′) basins shown in Figure 6. Magadi and Natron are early-stage magmatic rift basins described in the text. Black box encloses the Chyulu Hills off-rift magmatic zone. Black dashed line is the approximate surface contact between Archaean and Pan-African crust. Triangles and inverted triangles are locations of broadband seismic data sets (Albaric et al., 2014; Dugda et al., 2005; Gao et al., 1997; Last et al., 1997; Plasman et al., 2017; Tugume et al., 2012; Velasco et al., 2011; Weinstein et al., 2017), and circles and hexagons are locations of intermediate and long-period MT recordings (Abdelfettah et al., 2016; Hautot et al., 2000; Hautot & Tarits, 2015; Sakkas et al., 2002; Selway et al., 2014; Simpson, 2000). Bold lines are approximate locations of the Kenya Rift International Seismic Project (KRISP) wide angle reflection/refraction and MT profiles as outlined in Prodehl et al. (1994) and Khan et al. (1999).

critical insights into magmatic modification and crustal stretching processes within the faulted basins and beneath the numerous eruptive volcanic centers (Ibs-von Seht et al., 2001; Plasman et al., 2017; Roecker et al., 2017) (Figures 2b and 5).

The uppermost crust is dominated by the ~3–7 km thick sedimentary basins that formed in the Oligocene-Recent zones of crustal stretching (e.g., Hendrie et al., 1994; Morley et al., 1999; Morrissey & Scholz, 2014). Upper crustal velocities in crystalline basement are 6.0–6.3 km/s. The sometimes-reflective boundary

between upper and middle crust is marked by a velocity increase to ~6.5 km/s (Birt et al., 1997; Keller et al., 1994). Lower crustal velocities are variable but 6.7–6.9 km/s on average. Last et al. (1997) and Dugda et al. (2005) analyzed receiver functions from widely spaced stations spanning the Archaean-Pan-African suture in the southernmost (Tanzania) and central (Kenya) sectors of the Eastern rift (Figures 2 and 5). Last et al. (1997) find no change in crustal thickness crossing the Archaean-Proterozoic boundary through the central Manyara rift. Dugda et al. (2005) find slightly thicker crust in the Pan-African belt east of the rift (39–42 km) than west of the rift beneath the Tanzania craton (37–38 km), and normal Poisson's ratios of 0.24–0.27, indicating little or no crustal thinning or magmatic modification outside the rift zones.

Geophysical data from the Magadi-Natron-Manyara sector of the Eastern rift reveal crustal thinning and magma intrusion across the rift zone and low-velocity, high V_P/V_S bodies beneath some volcanoes. Moho depth determined from receiver functions and the KRISP94 profile varies between 28 and 41 km beneath the rift valley and rift shoulders, respectively (Figures 2b, 6a, and 6b). The thickest crust (41 km) underlies the Crater Highlands, a wedge of uplifted basement, and $<$6 Myr volcanic constructs (Plasman et al., 2017). The V_P/V_S ratio depicts a lateral variability, with zones of high V_P/V_S strongly correlated with the location of volcanic edifices. Unusually high lower crustal velocities of 7.1–7.2 km/s in the lowermost crust beneath the Magadi basin have been interpreted as evidence for cooled gabbroic crustal intrusions (e.g., Thybo et al., 2000) or cumulates (Christensen & Mooney, 1995). Beneath the Natron basin, Plasman et al. (2017) find local low-velocity zones with a strong reflective signature, and high V_P/V_S (1.83–1.98) in the lower crust, interpreted as magma bodies. Based on wide-angle reflection-refraction studies, the mantle reflection, *PmP*, is high amplitude but only at low frequencies. At high frequencies, reverberative phases are observed and modeled as an approximately 4 km thick series of mafic sills (Thybo et al., 2000).

At a greater depth of ~60 km, an intramantle interface roughly mimics the step-like and symmetrically outward dipping geometry of the Moho (Plasman et al., 2017). Intramantle reflectors were also detected in refraction/wide-angle reflection profiling in the northern part of the Eastern rift (Mechie, Keller, et al., 1994; Keller et al., 1994), and in the Main Ethiopian Rift, as outlined in section 4. A narrow zone of thinned mantle lithosphere is imaged directly beneath the fault bounded rift basins: ~90 km thick versus $>$125 km outside the rift zone (Green et al., 1991; Ritsema et al., 1999), consistent with *P-T* conditions of eruptive volcanic products (Macdonald, 1994; Mechie, Fuchs, et al., 1994). Along the length of the rift, velocities in the mantle just below the Moho from *Pn* analyses are 7.5–7.7 km/s, significantly lower than values beneath the flanks and stable interior: 8.0–8.1 km/s (Maguire et al., 1994; Mechie, Keller, et al., 1994). The magnitude of the velocity decrease is 0.3 km/s larger than predicted from higher geothermal gradients, suggesting that partial melt within the upper mantle also contributes to the observed velocity reduction beneath the rift (Mechie, Fuchs, et al., 1994).

If we assume an initial crustal thickness of 40 km, the ~28 km thick crust beneath the Natron and Magadi basins crustal thickness estimated from wide-angle refraction/reflection studies and receiver function studies indicates ~30% extension achieved in $<$7 Myr. The volume increase from magma intrusion may bias crustal stretching estimates to smaller values.

3.2. Crustal Magmatic Plumbing Systems

KRISP-94 MT experiments crossing the Proterozoic suture, the Magadi rift basin and flanks, and the off-rift Quaternary-Recent Chyulu Hills eruptive centers reveal not only the shallow basin structure but also several high conductivity zones interpreted as active and ancient intrusives. Using a 2-D inversion, Simpson (2000) report high conductivity lower crust, and Meju and Sakkas (2007) use a 3-D inversion to image narrow high conductivity zones rising to ~8 km subsurface beneath the central rift and beneath the Chyulu hills. Seismic tomography models reveal similar patterns. Tomography models of local earthquake *P* and *S* wave arrival times indicate a ~10 km wide, linear low-velocity zone beneath the central Magadi basin, which may be a zone of fractured or intruded rock (Ibs-von Seht et al., 2001) (Figure 6c). For the Magadi-Natron-Manyara sector, Roecker et al. (2017) jointly inverted ambient noise, arrival time, and gravity data to image V_P, V_S, and V_P/V_S in the crust shallower than ~25 km. The most significant features are (1) low *P* and *S* wave speeds underlying the rift zone; (2) a relatively high wave speed, ~10 km wide tabular feature located along the western edge of the Natron and Manyara rifts; and (3) areas with low (1.65–1.71) values of V_P/V_S in the upper crust, with the lowest ratios along the boundaries of the rift zones (Roecker et al., 2017). The low *P* and *S* wave

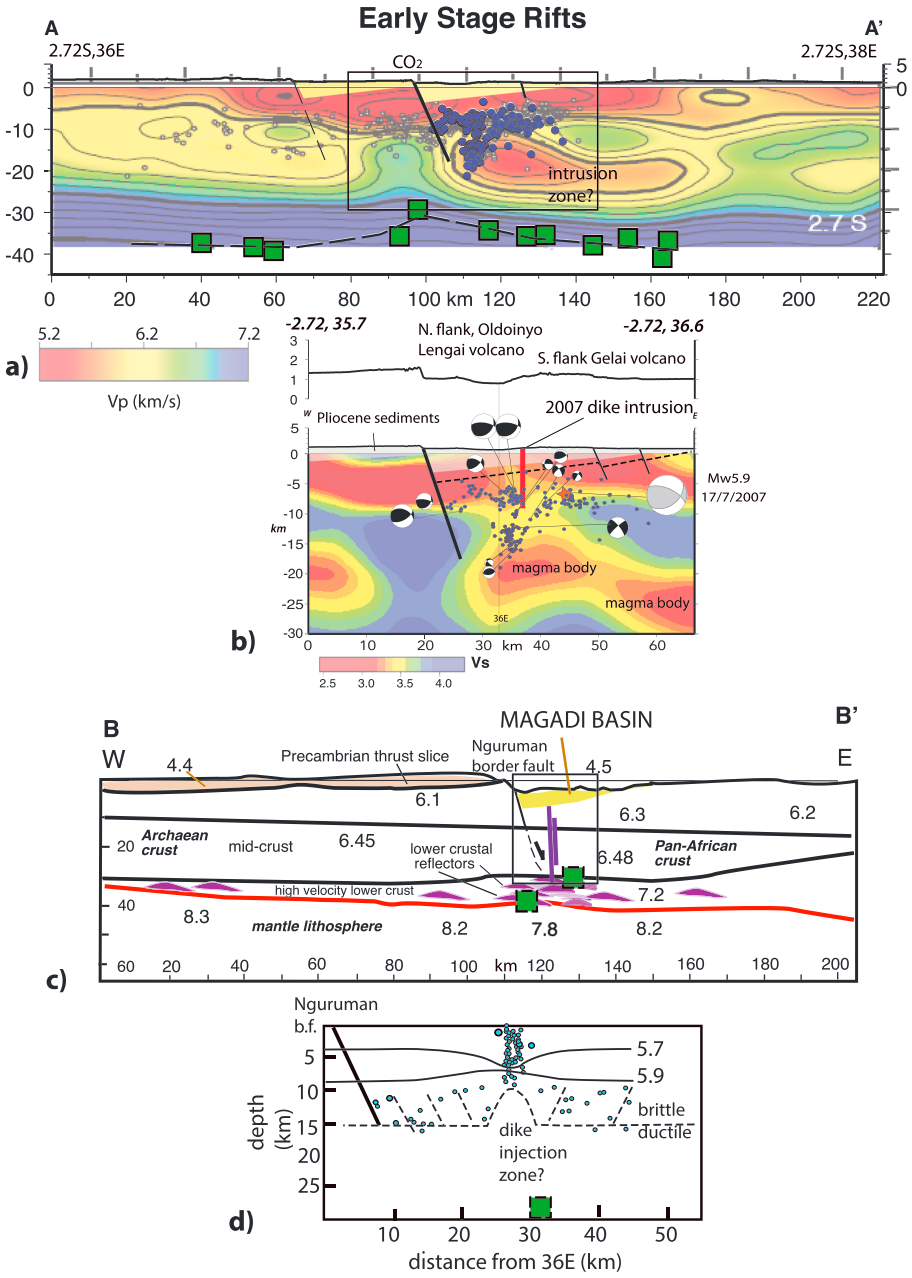

Figure 6. Cross sections of crustal structure illustrating evolutionary changes in rift structure (see Figure 5 for profile locations). With each diagram, we show a detailed velocity model with seismicity across the active rift zone, from a variety of tomographic studies. Red bold line is refraction/reflection Moho. Purple lozenges indicate zones of underplate or mafic lower crustal sills. For simplicity, dikes are sourced from the mantle, and shallow magma chambers, although multiple magma reservoirs may exist. Green squares are receiver function estimates of crustal thickness. (a) Early-stage rifting in the ~3 Myr old Natron basin. *P* and *S* wave velocities from joint ambient noise, arrival time, and gravity inversion (Roecker et al., 2017). Precise earthquake locations lying within 5 km of the line of section projected onto the line of the profile from Weinstein et al. (2017), receiver function crustal thickness estimates from Plasman et al. (2017). (b) Increasing modification in the adjoining, ~ 7 Myr Magadi basin region (Birt et al., 1997). Bottom upper crustal section from arrival time tomography study of Ibs-von Seht et al. (2001), with earthquakes within 20 km projected onto the line of profile. Receiver functions from Plasman et al. (2017).

speeds at midcrustal levels beneath the rift valley correlate with Holocene-Recent eruptive centers, and the tabular (in plan view), high-wave speed feature is the uplifted footwall of the Natron basin, with crust on the hanging wall intruded and experiencing magma degassing along the fault zone (Lee et al., 2016; Weinstein et al., 2017) (Figure 6a). Given the high levels of CO_2 outgassing observed at the surface and the sensitivity of

V_P/V_S to pore fluid compressibility, Roecker et al. (2017) suggest that the low V_P/V_S values that correlate with zones of active CO_2 degassing at the surface are caused by the volcanic plumbing in the upper crust being suffused by a gaseous CO_2 above a deeper, crystalline mush with high V_P/V_S, and high reflectivity in some areas (Plasman et al., 2017).

In a detailed study of the off-axis Chyulu hills shield cone province (Figure 5), Sakkas et al. (2002) find steeply dipping high conductivity zones at depths 1–8 km and 9–18 km, interpreted as magma intrusions. Similarly, in a MT study of the Baringo rift segment to the north, Hautot et al. (2000) suggest that Mesozoic sediments underlie a 4 km-thick African rift sequence and interpret a high-density magma intrusion with top no shallower than 6 km. Within the southern Natron basin, pancake-shaped zones of persistent $M_L \leq 4.5$ earthquakes above the inferred lower crustal crystal-rich mush zone at depths of 6–11 km below sea level may be stacked sills, with the variable fractionation depths feeding the wide range of magma compositions at Oldoinyo Lengai and the adjacent monogenetic cone complex (Roecker et al., 2017; Weinstein et al., 2017).

Guth (2016) provides coarse estimates of eruptive magma volumes both from map data and from seismically imaged basin fill, which combine to 310,000 km^3. Because her work includes only basins in Kenya and ignores the Eastern rift in northern Tanzania and southwestern Ethiopia, we extrapolate estimates of intrusive volumes to the same region. For a conservative estimate of intrusive volumes, we assume 20% new magmatic material (underplate and intrusions into the central rift zone, 8 km thick) for a 70 km wide rift zone that is 600 km long; intrusive volumes are at least 336,000 km^3. The total volume is at least 43,000 km^3 per million years, assuming all sectors are 15 Myr old (average age of Eastern rift).

3.3. Constraints on Lower Crustal Deformation in Early Stage Rifts

Although lower crustal earthquakes occur in magmatic and amagmatic rift basins in Africa, we focus on lower crustal earthquakes in magmatic rift sectors. The Magadi, Natron, and Manyara basins are all associated with earthquakes in the lower crust, as relocated from local seismic networks (Albaric et al., 2014; Ibs-von Seht et al., 2001; Mulibo & Nyblade, 2009; Roecker et al., 2017) and from teleseismic studies (Craig et al., 2011; Shudofsky et al., 1987; Yang & Chen, 2010). Within the Natron basin, precisely relocated earthquakes occur at depths of 20–27 km along a projection of the border fault to the base of the crust, consistent with thermomechanical models of basin and flank morphology and gravity anomalies (e.g., Sippel et al., 2017). Volumetrically significant gas fluxes measured near these deeply penetrating fault zones bounding basins indicate that the border faults serve as conduits for CO_2 exsolved from active magma intrusions (Lee et al., 2016). Lower crustal seismicity also occurs around lower crustal mush zones, and the inferred sill complexes where high fluid pressures may induce hydraulic fracture (Weinstein et al., 2017).

Laboratory experiments simulating lower crustal conditions demonstrate that granulite is weak, particularly if the rock contains a small weight percent of water (Wang et al., 2012). Although cooled magmatic underplate or cumulates may locally strengthen the lower crust, the high V_P/V_S ratios in the lower crust and CO_2 degassing along faults that penetrate to the lower crust indicate active intrusion processes and locally hot, weak lower crust (Plasman et al., 2017; Roecker et al., 2017). A strong, mafic lower crust, therefore, seems an unlikely explanation for widespread lower crustal seismicity in this sector of the Eastern rift. Instead, slip along border faults that penetrate to lower crustal levels, locally high pore fluid pressures, as indicated by volatile degassing, and active magma intrusion are explanations for the unusual lower crustal earthquakes in magmatically active early stage rift zones.

3.4. Summary: Early Stage Magmatic Rift Zones

Half-graben basins bounded by steep border faults that penetrate to lower crustal levels characterize the $<$7 Myr southern sector of the Eastern (Gregory) rift. Seismic, gravity, MT, seismicity, and xenolith studies show widespread magmatic underplating, with high levels of magmatic CO_2 degassing along border faults, as well as through active volcanoes. Although much of the area was affected by magmatism between 6 and 1 Ma, during the past ~1 Ma, eruptive centers have formed within the central Magadi and Natron basins. Tomographic imaging and seismicity indicate that the central volcanoes and monogenetic cones are sourced by one or more lower crustal magma chamber(s) overlain by stacked sills that may explain the wide range of lava compositions. Dike and sill intrusions have reached 8–10 km subsurface, in patterns similar to the Main Ethiopian Rift outlined below. Sharp contrasts in velocity and V_P/V_S between hanging wall and footwall suggest that magmatic modification has localized to the faulted basin area.

4. Magma-Rich Continental Rifting—The Main Ethiopian Rift

The Horn of Africa captures the combined processes of crustal stretching and intrusion at various stages of continental breakup. The Ethiopian rift is the northernmost sector of the EARS, which is the incipient boundary between the Nubia and Somalia plates (Figures 2a and 7). It encompasses early to midstage continental rift sectors, and it captures the transition from deformation along 50–100 km long border fault systems to zones of magma intrusion. Here we focus our synthesis on how geophysics and petrology are providing improved understanding of where and how magma migrates and ponds in the crust during progressive rift development. Some of these patterns mimic along-strike patterns noted in the $<$7 Myr old Natron-Magadi rift sectors (section 3) and highlight strain and structural changes associated with the rise of magma to upper crustal levels.

The Main Ethiopian Rift (MER) formed within the Precambrian metamorphic crustal basement of the Pan-African orogenic belt that exhibits N-S to NNE-SSW suture zones (Berhe, 1990; Vail, 1983) and NW-SE oriented strike-slip faults in Ethiopia (Brown, 1970; Purcell, 1976). The central and northern sectors of the MER developed between 18 and 10 Ma, respectively (e.g., Rooney et al., 2013; Woldegabriel et al., 1990; Wolfenden et al., 2004). Between 18 and 12 Ma, large offset border faults commonly marked by chains of eruptive centers formed along one or both sides of the rift (e.g., Chernet et al., 1998; Rooney et al., 2014) (Figure 7). South of ~7.5°N, seismically active faults in a broad depression effectively link the ~30 Myr Eastern rift to the MER, across a broad zone of subparallel and time-transgressive basins (e.g., Ebinger et al., 2000; Morley et al., 1992). Further north, within the basin bounded by Miocene border faults, the rift floor is segmented into a series of Quaternary-to-Recent aligned volcanic centers cut by small offset normal fault systems, referred to as magmatic segments (Corti, 2008, 2009; Ebinger & Casey, 2001; Mazzarini et al., 2013) (Figure 7). The magmatic segments are the locus of magma intrusion and are underlain by high-velocity zones interpreted as gabbroic intrusions, as outlined below (Figure 8). GPS data show that the axial volcanic segments are the locus of current extension (Bilham et al., 1999), with the surface geology suggesting that this has been the case since the Quaternary (Ebinger & Casey, 2001). Plate kinematic models constrained by marine magnetic anomaly patterns and geodetic data require that some extension across the MER took place by about 16 Ma (DeMets & Merkouriev, 2016).

As outlined below, crustal structure in Ethiopia is constrained using receiver functions, wide-angle controlled source seismology, MT, and inversion of gravity data. Combined, these results provide important clues to extensional processes that modify the crust during rifting.

4.1. Crustal Velocities, Thinning, and Evidence for Intrusion

Stuart et al. (2006) and Hammond et al. (2011) analyzed receiver functions from broadband stations in the Ethiopian rift, building on results of earlier studies of data from widely spaced networks (Dugda et al., 2005; Dugda & Nyblade, 2006) (Figures 2a and 5). The EAGLE controlled source wide-angle experiment constrained across-rift and along-axis variations in crustal structure, as well as the uplifted flanks of the Ethiopian flood basalt province (Figures 8, 9, and 10a). EAGLE comprised two ~400 km long profiles: one cross rift (Figure 9) and one rift axial profile (Maguire et al., 2006). A dense network of stations was deployed over the intersection of the two profiles to provide 3-D images of the along-axis segmentation patterns (Keranen et al., 2004; Mackenzie et al., 2005; Maguire et al., 2006) (Figure 7). Figure 10 compares receiver function results projected onto the line of controlled source and MT profiles to facilitate comparisons of crustal thickness estimates from seismic tomography, reflection, and MT results. Crustal thicknesses are similar to those determined using receiver functions, but absolute determination of V_P and variations thereof provides further insights.

The crust beneath the Somalian plate east of the rift is 38–40 km thick (Figures 2a and 7). The crust on the Nubian plate west of the rift is of similar thickness but thickens to 41–43 km between ~9°N and 12°N. MT data show significant differences between the lowermost crust beneath the plateaux on either side of the rift (Figure 9): thicker and resistive beneath the Somalian Plateau, thinner with higher conductivity beneath the Ethiopian Plateau in agreement with the interpretation of underplate there (Mackenzie et al., 2005; Rooney et al., 2017). This region of thicker crust lies at the northern edge of an off-rift upper mantle low-velocity structure imaged by traveltime tomography (e.g., Bastow et al., 2008, 2005; Hammond et al., 2013). At the surface, this upper mantle low-velocity zone and thicker crust on the northwestern rift shoulder is

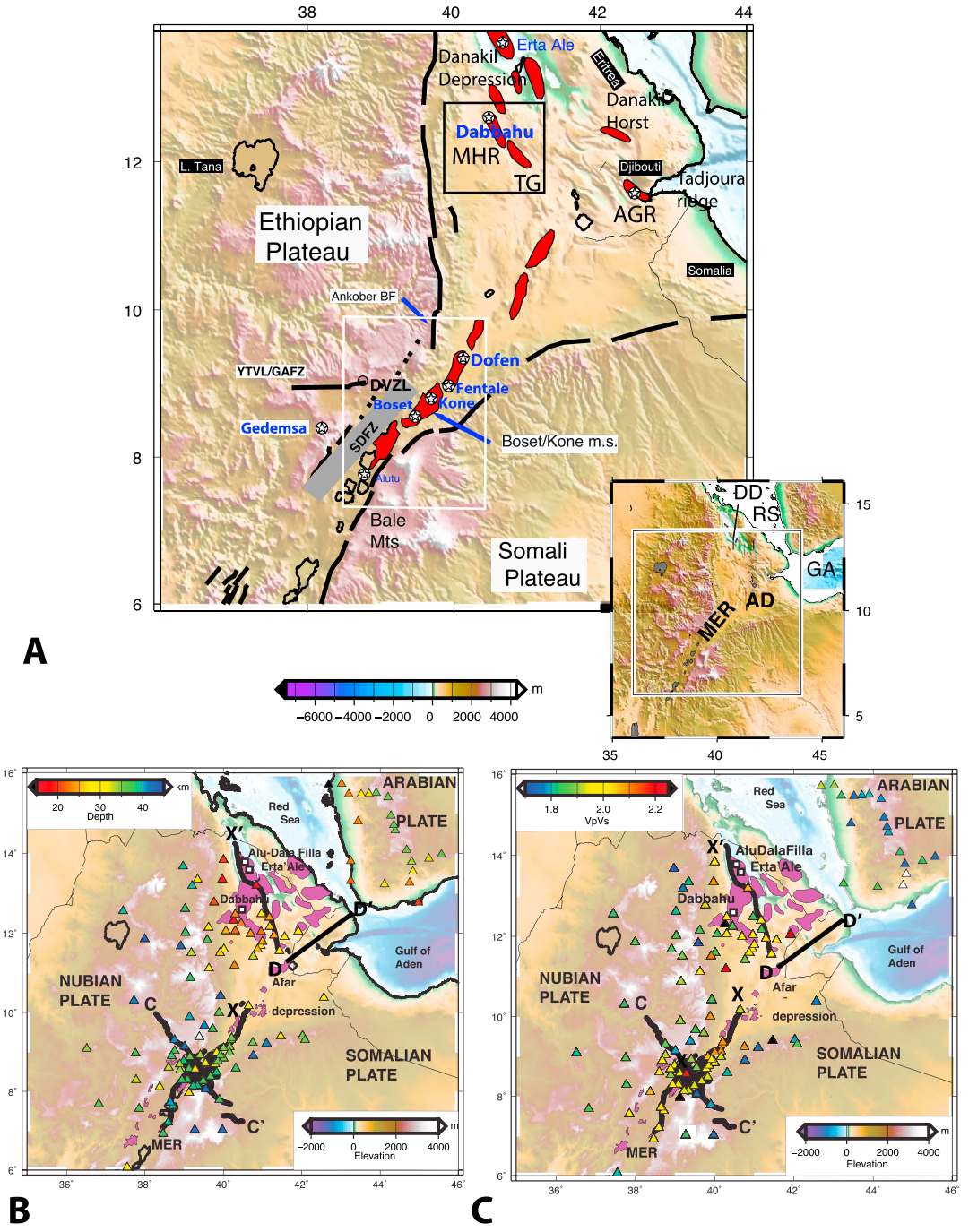

Figure 7. (a) Topography and bathymetry of the horn of Africa region. Red shapes are Quaternary to Recent magmatic segments along the rift axis. Black lines are Oligocene to Recent border faults. White circles are Holocene volcanoes named in the manuscript. SDFZ is Silti Debre Zeit Fault Zone and DVZL is Debre Zeit Volcanic Lineament. YTVL: Yerer Tullu-Wellel Volcanic Lineament. GAFZ: Guder Ambo Fault Zone. MHR: Manda Harraro rift. TG is Tendaho Graben. AGR is Asal-Ghoubbet Rift. C-C′ and D-D′ indicate endpoints of crustal profiles shown in Figures 9 and 10. White box encloses area shown in Figure 8, and black box encloses area shown in Figure 11. X-X′ indicate endpoints of crustal profile shown in Figure 12. (b) Variations in crustal thickness with magenta indicating Quaternary lava flows. (c) Variations in V_P/V_S in the region determined from receiver function analysis with magenta indicating Quaternary lava flows (Ahmed et al., 2014; Dugda & Nyblade, 2006; Hammond et al., 2011; Stuart et al., 2006).

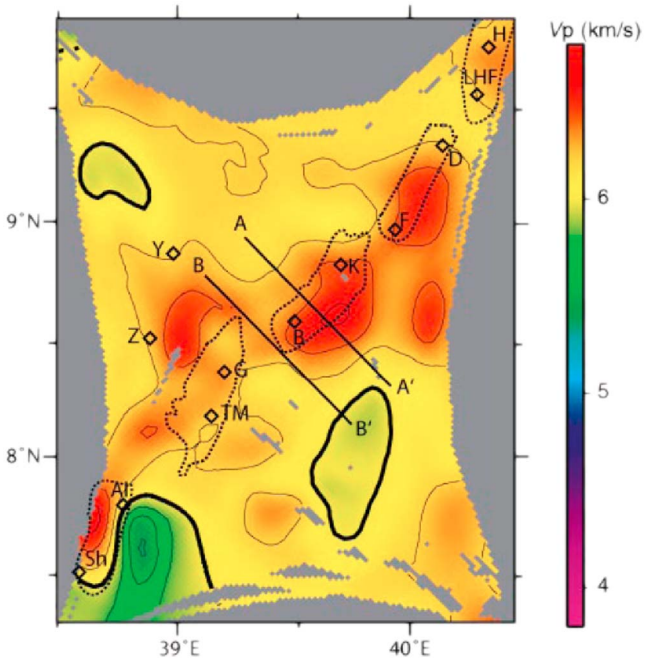

Figure 8. High-velocity zones underlying magmatic segments of the central MER as imaged in horizontal slice of V_P at 10 km below rift topography, from controlled source and earthquake arrival time tomography (Keranen et al., 2004). Location of box shown in Figure 7a. Dashed lines enclose Quaternary-Recent magmatic segments. Diamonds denote locations of Quaternary-Recent eruptive centers: Sh = Shala; Al = Aluto; TM = Tullu Moje; G = Gedemsa; B = Boset; K = Kone; F = Fentale; D = Dofen; LHF = Liyado-Hayk field; H = Hertale. A-A′ notes the location of the velocity profile shown in Figure 10b. Profile C-C′ (Figure 9) is centered on A-A′, and it continues NW and SE of Profile A-A′. B-B′ is shown in the original Keranen et al. (2004) paper.

marked by a chain of Miocene-Quaternary eruptive centers, the Yerer-Tullul Wellel volcanic lineament (YTVL; Abebe et al., 1998) (Figure 7). Magmatic underplating during the early stages of rifting may have thickened and strengthened crust to the north and localized later strain and magmatism (e.g., Keranen & Klemperer, 2008; Kim et al., 2012). It should be borne in mind that receiver function Moho depth estimates for the Ethiopian Plateau are shallower than those inferred by wide-angle reflection analysis: receiver functions appear sensitive primarily to the top, not the bottom of the 8–12 km thick mafic layer(s) in the lower crust (e.g., Stuart et al., 2006).

Along the rift axis, crustal thickness varies from around 38 km in the south to 30 km in the north, with most of the change in Moho depth occurring just south of the Boset-Kone magmatic segment where the rift floor drops in elevation into the Afar depression (Figures 2a and 7). The change in crustal thickness from ~40 km beneath the rift shoulders to 30 km in the rift implies a minimum stretching factor of 1.5 (28 km) or considerably less than the stretching factor ~2 estimated by plate kinematic models (42 km; DeMets & Merkouriev, 2016). Stretching factors estimated from crustal thickness alone will underestimate total extension, as outlined below.

The crust is interpreted to be slightly more mafic ($V_P/V_S > 1.85$) beneath the Ethiopian Plateau than the Somalian Plateau ($V_P/V_S \approx 1.80$) (Figures 2a and 7c). This could either be due to Oligocene to Recent magmatic activity or different prerift crustal compositions. Regions of volcanism inside and on the side of the rift (e.g., Silti Debre Zeit Fault zone, SDFZ) are characterized by thinned crust and $V_P/V_S > 2.0$, indicative of partial melt within the crust (Figure 7c). Seismic, MT, gravity, and petrological data image or require significant magma volumes, particularly in the lower crust of these magmatic rift zones (Cornwell et al., 2006; Hammond et al., 2011; Keir et al., 2011a, 2011b; Whaler & Hautot, 2006). For example, elevated V_P/V_S ratios in regions of thinning likely indicate that both solidified and still partially molten intrusions contribute to extension (Hammond et al., 2011, 2013).

Using spatial variations in V_P imaged by wide-angle controlled source seismology, it has been possible to infer spatial variations in amount of intrusion. Along the rift, V_P in the lower crust ranges from 6.6 to 7.2 km/s, peaking at 7.1–7.2 km/s in the lowermost crust between Gedemsa and Fentale volcanoes in the central part of the MER (Figures 7 and 9). Elevated wave speeds of >6.8 km/s have been interpreted as evidence for gabbroic crustal intrusions (e.g., Keranen et al., 2004; Mackenzie et al., 2005; Maguire et al., 2006). In the upper crust, 3-D controlled source tomography shows significant variation in V_P, with discrete high V_P (>6.4 km/s) zones beneath the magmatic segments (Figures 8 and 9). The >7 km/s velocities and high densities inferred from forward and inverse models of gravity data indicate that the magmatic segments are underlain by gabbroic material (e.g., Cornwell et al., 2006; Mahatsente et al., 1999; Tiberi et al., 2005). The observed pattern of segmented high-velocity zones was reproduced by gabbroic bodies that rise to 10 km below the surface, indicating that 30% of the crust beneath the magmatic segments is new igneous material (Keranen et al., 2004).

The observations corroborate the surface geology evidence that axial magma intrusion, likely in the form of gabbroic cumulates from crustal magma chambers, fed sheeted dykes. The dikes, as well as faults above the dikes, accommodate most of the deformation across the rift, based on time-averaged and active deformation patterns (Casey et al., 2006; Keir et al., 2015). New GPS data confirm that active deformation occurs across the Ethiopian Plateau (Birhanu et al., 2016), which hosts aligned chains of Quaternary eruptive centers, high-conductivity lower crust, and lower crustal seismicity (Keir et al., 2011a, 2011b) (e.g., Figure 10).

4.2. Crustal Magma Plumbing Systems

The interpretation of gravity and electrical conductivity anomalies has been used to construct an ever more detailed picture of the crustal magma plumbing system accommodating extension during breakup and

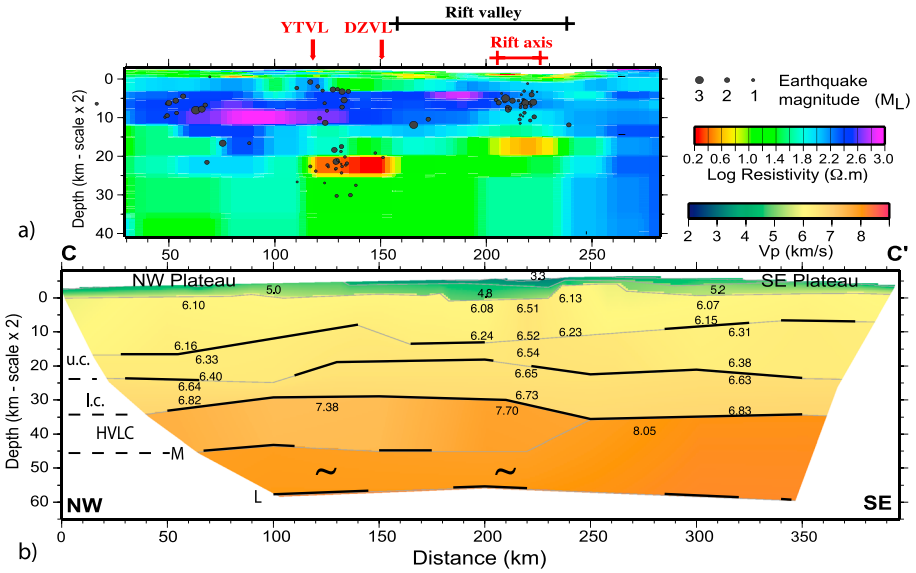

Figure 9. Rift cross sections comparing several geophysical properties of the crust across the MER. The position of C-C′ is labeled on Figure 7a. (a) The 2-D resistivity structure of the crust along a portion of A-A′ determined using MT methods (Whaler & Hautot, 2006). The shallow low-velocity parts of the model are interpreted as sediments and volcanic and volcaniclastic rocks filling in the subsiding basins of the MER, extending between ~ 150 and 250 km of C-C′ (Keranen et al., 2004; Mackenzie et al., 2005). (b) Profile C-C′ is the *P* wave velocity model of the crust determined using controlled source reflection/refraction (Mackenzie et al., 2005) with earthquake hypocenters (gray dark circles) recorded during October 2001 to January 2003 and located within 20 km either side (dashed lines) of the profile projected onto the section. Labels are u.c., upper crust; l.c., lower crust; HVLC, high-velocity lower crust; M, Moho.

sourcing active off-axis volcanoes (Figure 9). In the MER, Cornwell et al. (2006) conducted a cross-rift gravity survey and Whaler and Hautot (2006) a cross-rift MT survey, coincident with wide-angle Line 1 (Figure 9). Major features of the gravity study are an axial low-density upper mantle or high-density lower crustal zone which is modeled as a ~50 km wide body with a density of 3,190 kg/m^3, supporting interpretations of a mafic underplate layer beneath the northwestern rift flank (Cornwell et al., 2006). Two high-density (3,000 kg/m^3) upper crustal bodies underlie the MER: a 20 km wide axial body and a 12 km wide off-axis body, both of which are likely gabbroic in composition.

MT data provide some of the best evidence for the emplacement and migration of melt during breakup. Major features of the MT survey are a conductive body at 20–25 km depth beneath the rift axis interpreted as a middle-to-lower crustal magma reservoir (Figure 9). A second highly conductive region at 25–35 km depth is beneath the rift flank near the SDFZ and YTVL (Figures 6 and 8). The lower crustal high conductivity zone coincides with seismicity, leading to its interpretation as a pressurized magma reservoir beneath the rift flank volcanoes (Keir et al., 2009) (Figure 9). Ambient noise tomography reveals low V_S (<3.2 km/s) beneath the magmatic segments, suggesting that the zones of solidified axial intrusions still include a small fraction of partial melt (Kim et al., 2012). Lower crustal melt retention is also consistent with high V_P/V_S ratios imaged in the upper crust beneath the rift axis using local earthquake tomography (Daly et al., 2008). Petrological analyses along the SDFZ indicate that erupted lavas fractionated at a range of crustal depths, in line with the geophysical observations (Rooney et al., 2011, 2014, 2007). A shallow conductive lens at <1 km depth underlying Boset Volcano is most likely indicative of either a shallow hydrothermal or a magmatic system (Whaler & Hautot, 2006).

Farther south in the MER, Samrock et al. (2015) collected broadband MT data over the Aluto volcanic center (Figure 7a). They found no middle or lower crustal conductor there, despite models of geodetic data indicating melt storage and migration at <10 km depths (Biggs et al., 2011). These observations have subsequently been interpreted as resulting from a locked, crystal-rich mush which lacks the connectivity to provide high bulk electrical conductivity (Hutchison et al., 2016). Samrock et al.'s (2015) data did, however, indicate a conductor beneath the SDFZ to the northwest of Aluto, with top surface at ~12 km depth. Both observations have subsequently been confirmed as melt storage beneath rift flank volcanoes by a 110 km long MT

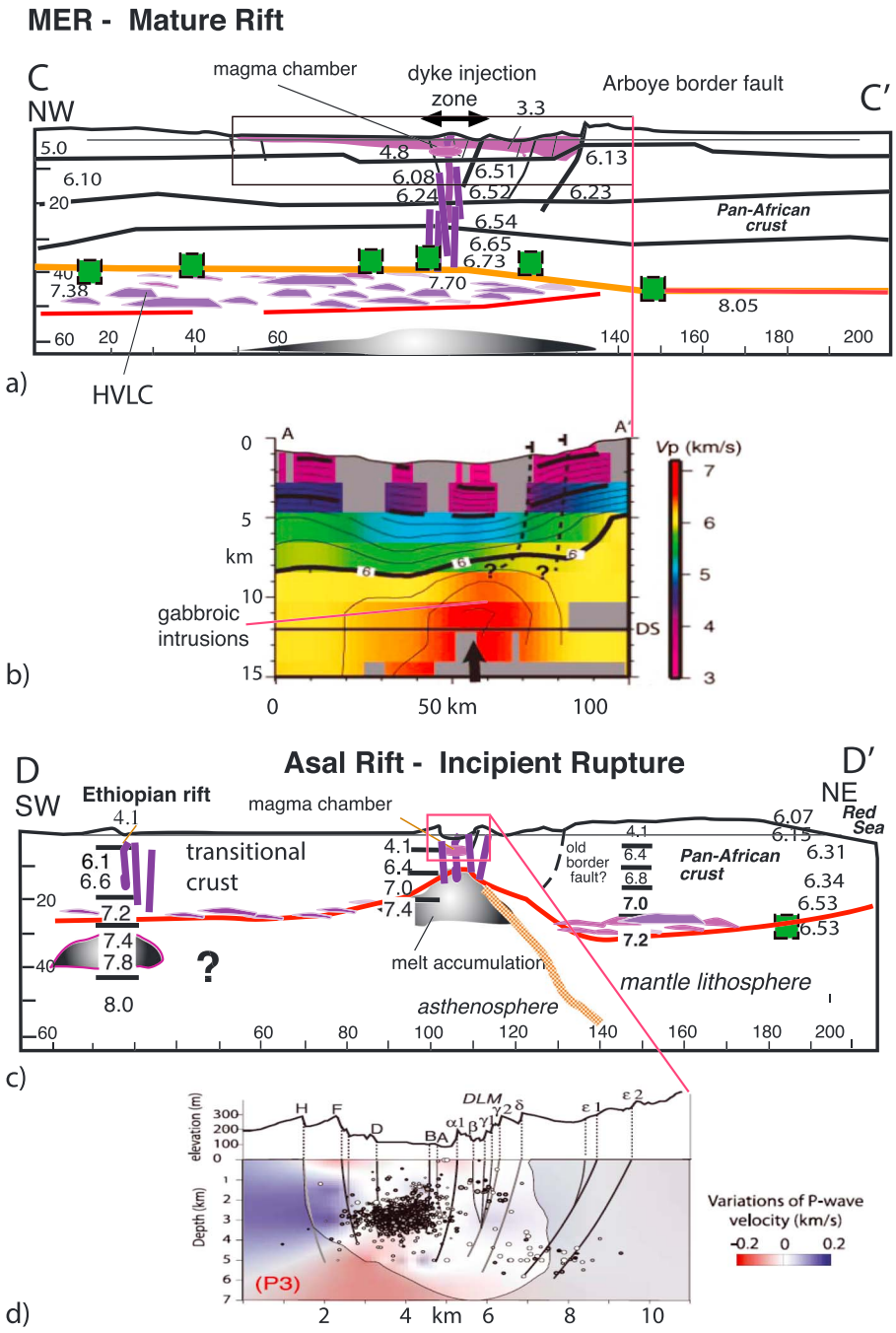

Figure 10. Cross sections of crustal structure illustrating evolutionary changes between the mature Main Ethiopian Rift and incipient seafloor spreading in the Asal rift (see Figure 7a for profile locations). With each diagram, we show a detailed velocity model with seismicity across the active rift zone. Red bold line is refraction/reflection Moho; orange line indicates top of thick underplate zone marked by purple lozenges (mafic lower crustal sills). For simplicity, dikes are sourced from the mantle, and shallow magma chambers, although multiple magma reservoirs may exist. Green squares are receiver function estimates of crustal thickness (Figure 2a). (a) Cross section C-C′ of the ~12 Myr old MER sector transitional between continental and oceanic rifting. Flood magmatism prior to rifting may contribute to the thick underplate. (b) Shorter profile through 3-D V_P tomography model (A-A′; Figure 8) shows gabbroic intrusions into lower and middle crust beneath the magmatic segment (Keranen et al., 2004). (c) Incipient seafloor spreading in the Asal rift at the westernmost end of the Gulf of Aden rift based on velocity data from Makris and Ginzburg (1987) and Ruegg (1975) and structure from Doubre et al. (2007). (d) Shorter profile from 3-D V_P tomography model shows detail across rift. Greek letters refer to specific faults with measured slip rates and colors from Doubre et al. (2007).

profile centered on Aluto and orthogonal to the rift axis, which included deeper-probing long-period MT measurements (Hübert et al., 2016).

4.3. Summary of Mature Rift Crustal Structure

Geophysical and petrological studies indicate that intrusion and fluid release into the lower crust occur beneath the rift and parts of the uplifted plateau region, 40 Myr after the onset of flood magmatism. This long-lived magmatism produces a high-velocity, high *P* wave lower crust with or without low *S* wave velocities. Within the fault-bounded basins, border faults are largely inactive, and strain is localized to $<$20 km wide magmatic segments: zones of localized magma intrusion, volcanic construction, and dense faulting. At least 30% of the crust beneath the magmatic segments is new igneous material. Comparison of refraction/wide-angle reflection Moho and receiver function Moho reveals a discrepancy: the receiver function analyses image the top of the high-velocity lower crust in zones of active magma intrusion and provide minimum constraints on intrusive magma volumes.

5. Late Stage Continental Breakup and Initiation of Seafloor Spreading: The Afar Depression

The Afar depression encompasses the rift-rift-rift triple junction between the Nubian, Somalian, and Arabian plates: The Red Sea (Arabia-Nubia) and Gulf of Aden (Arabia-Somalia) rifts that bound the Arabian plate and the East African rift (Nubia-Somalia) (e.g., Beyene & Abdelsalam, 2005; Manighetti et al., 1998; McKenzie & Davies, 1970; Mohr, 1972) (Figure 7). The cumulative extension in Afar is much higher than in the MER, and it therefore is the ideal setting to understand the final stages of continental breakup (e.g., Doubre et al., 2007; Stab et al., 2016; Wolfenden et al., 2005). Well-established seafloor spreading with seafloor spreading anomalies is observed in some sectors of the Red Sea (Ligi et al., 2011) and in the Gulf of Aden (e.g., Leroy et al., 2010).

Rifting of Arabia from Africa to form the Red Sea and Gulf of Aden rift zones preceded rifting in the Main Ethiopian Rift by $>$10 Myr, based on structural, stratigraphic, and plate kinematic data (e.g., Chernet et al., 1998; Corti, 2009; DeMets & Merkouriev, 2016; Wolfenden et al., 2004). Stratal relations of dated volcanic sequences and aligned eruptive centers indicate that some border faults along the western margin of Afar began at 29–31 Ma, approximately coeval with the highest magma production rates in the Ethiopia-Yemen flood basalt province (e.g., Ayalew et al., 2006; Wolfenden et al., 2005). Faulting and basin subsidence had begun by about 35 Ma along large portions of the Gulf of Aden but without magmatism (Leroy et al., 2010). As in the Ethiopian rift, structural and geomorphological analyses indicate that extensional strain was initially focused on large offset border faults, and subsequently, extension has become more localized to axial volcanic segments (Hayward & Ebinger, 1996; Sembroni et al., 2016; Wolfenden et al., 2005) (Figure 7).

The comparatively long history of flood magmatism and faulting has produced unusual crust; the structure and composition of the 18–25 km thick crust beneath Afar are transitional between continental and oceanic (e.g., Makris & Ginzburg, 1987; Mohr, 1989). Its structure informs magmatic passive margin studies in the Red Sea and worldwide. Specifically, debate continues regarding the nature of crust beneath thick sequences of seaward dipping volcanic layers that mask basement structure (e.g., Franke et al., 2007; Van Avendonk et al., 2009). Is the Afar crust, which is slightly thicker than normal oceanic crust, completely new igneous material intruded as sheeted dikes fed from lower crustal magma chamber(s), as along mid-ocean ridges with slow opening rates, or is it a combination of highly stretched continental crust with magmatic intrusions and metamorphosed sediments?

Active deformation processes in the Afar depression provide important clues (e.g., Keir et al., 2009; Pagli et al., 2012). Constraints on crustal structure primarily come from teleseismic receiver function studies (Ayele et al., 2004; Dugda et al., 2005; Hammond et al., 2011; Stuart et al., 2006), wide-angle seismic surveys (Berckhemer et al., 1975; Maguire et al., 2006; Makris & Ginzburg, 1987), gravity (Lewi et al., 2015; Redfield et al., 2003; Tessema & Antoine, 2004; Tiberi et al., 2005), and MT studies (Desissa et al., 2013; Didana et al., 2014, 2015; Johnson et al., 2016; Van Ngoc et al., 1981). A primary focus is to address the links between crustal thinning, magma intrusion, and subsidence to address a long-standing debate in plate tectonics: When does seafloor spreading start?

5.1. Crustal Thinning and Intrusive Bodies

Over the past 30 Myr, the zone of stretched and subsiding crust has broadened to about 300 km in central Afar, whereas the zone of active deformation has narrowed to intensely faulted, <20 km wide and ~50 km long magmatic segments fed from central magma chambers. Similar to the shoulders of the Ethiopian rift, receiver function analysis shows that the crust beneath the Ethiopia-Yemen Plateau is 40–45 km thick. It is ~35 km thick beneath the Somalian Plateau (Dugda et al., 2005; Hammond et al., 2011; Keranen et al., 2009; Stuart et al., 2006), similar to average crustal thickness of 35 km beneath the plateau of western Yemen (Ahmed et al., 2013) (Figures 2a and 9). The Danakil horst, separating the two subparallel arms of the Red Sea rift in the offshore and in Afar, is underlain by ~30 km thick crust. In general, the Ethiopian, Somalian, and Yemen Plateaux have V_P/V_S of 1.7–1.9, whereas localized regions of thicker (~30 km thick) crust within Afar have V_P/V_S of 1.8–1.9 (Dugda et al., 2005; Hammond et al., 2011; Reed et al., 2014; Stuart et al., 2006) (Figure 7c). $V_P/V_S \leq 1.85$ can be explained compositionally (Christensen, 1996; Hacker et al., 2015), but observations of $V_P/V_S > 1.85$ strongly suggest present-day melt in rift-parallel fractures and cracks, with anisotropy contributing to the high V_P/V_S values (Hammond, 2014). Ambient noise tomography images low *Vs* in the middle to upper crust (Korostelev et al., 2015), consistent with the high V_P/V_S (>1.9) imaged with receiver functions (Hammond et al., 2011), with both indicating melt-filled pore spaces/fractures.

Within the fault-bounded depression that includes the MER, southern Red Sea, and Gulf of Aden rifts, distinct differences occur. The <10 Myr old northern sector of the MER in Afar cuts through crust originally stretched and intruded as Arabia and Africa separated to form the third arm of the triple junction. The superposition of two rift systems (Red Sea, MER) causes a striking northward decrease in crustal thickness from ~35 km in the central MER to ~25 km in southern Afar (e.g., Figure 7b). What remains unclear, however, is the ratio of intrusive to extrusive volumes and total mechanical stretching.

In central Afar, the crust is 20–25 km thick beneath the current locus of volcanism and strain in the Manda-Harraro rift (MHR) and Tendaho Graben (TG), which are the southernmost segments of the Red Sea rift arm (Reed et al., 2014) (Figure 7). Currently active and abandoned magmatic segments are the locus of the greatest crustal thinning (<20 km), and they are separated by bands of ~30 km thick, intruded crust (Hammond et al., 2011). This "ridge-jump" pattern was created as the magma storage systems supplying magmatic segments jumped laterally across the broad Afar triple junction zone (Hammond et al., 2011). Further suggestion of ridge migration comes from thermal modeling (Daniels et al., 2014) and Medynski et al.'s (2015) inference of chemically distinct, alternately active magma chambers. The spatial arrangement of subparallel, migrating magma accretion zones is similar to patterns observed on passive margins worldwide, and predicted in ridge-jump seaward-dipping accretion models (Buck, 2017).

As outlined in section 5.3 and Van Ngoc et al. (1981), MT results indicate at least two of the magmatic segments: the MHR segment in the southern Red Sea and the Asal-Ghoubbet segment in the Gulf of Aden rifts extend in a fashion similar to a mid-ocean ridge (Figure 7). During intense faulting and fissural eruption episodes, dikes sourced from magma chambers near the center of magmatic segments achieved meters of rift opening and created up to 60 km long columns of mafic crust in periods of days (e.g., Abdallah et al., 1979; Ayele et al., 2009; Barnie et al., 2016; Keir et al., 2009).

Gravity and magnetic data from a 50 km long, ~1 m station density profile across the Tendaho basin provide indirect evidence that the intense dike intrusion events produce narrow columns of new igneous crust, similar to processes on slow-spreading ridges (Bridges et al., 2012). Here the magnetic data show near-symmetrical anomalies across the center of the rift, whose scale, shape, and magnitude are similar to those observed in nearby seafloor spreading centers in the Gulf of Aden. These data, together with the Bouguer gravity field, are consistent with symmetrical sheeted mafic dike complex intruded into the upper ~10 km of the crust and capped by 2–3 km thick basin fill of fissural basalts and sediments (Bridges et al., 2012). The observations provide evidence that most crustal extension is facilitated by magma intrusion, mimicking the extensional processes at slow-spreading mid-ocean ridges. Thus, it is possible that the first magnetic anomalies recorded at volcanic rifted margins form in comparatively thick (~15 km thick) crust originally classified as "transitional crust" (e.g., Bridges et al., 2012; Bronner et al., 2011; Rooney et al., 2014).

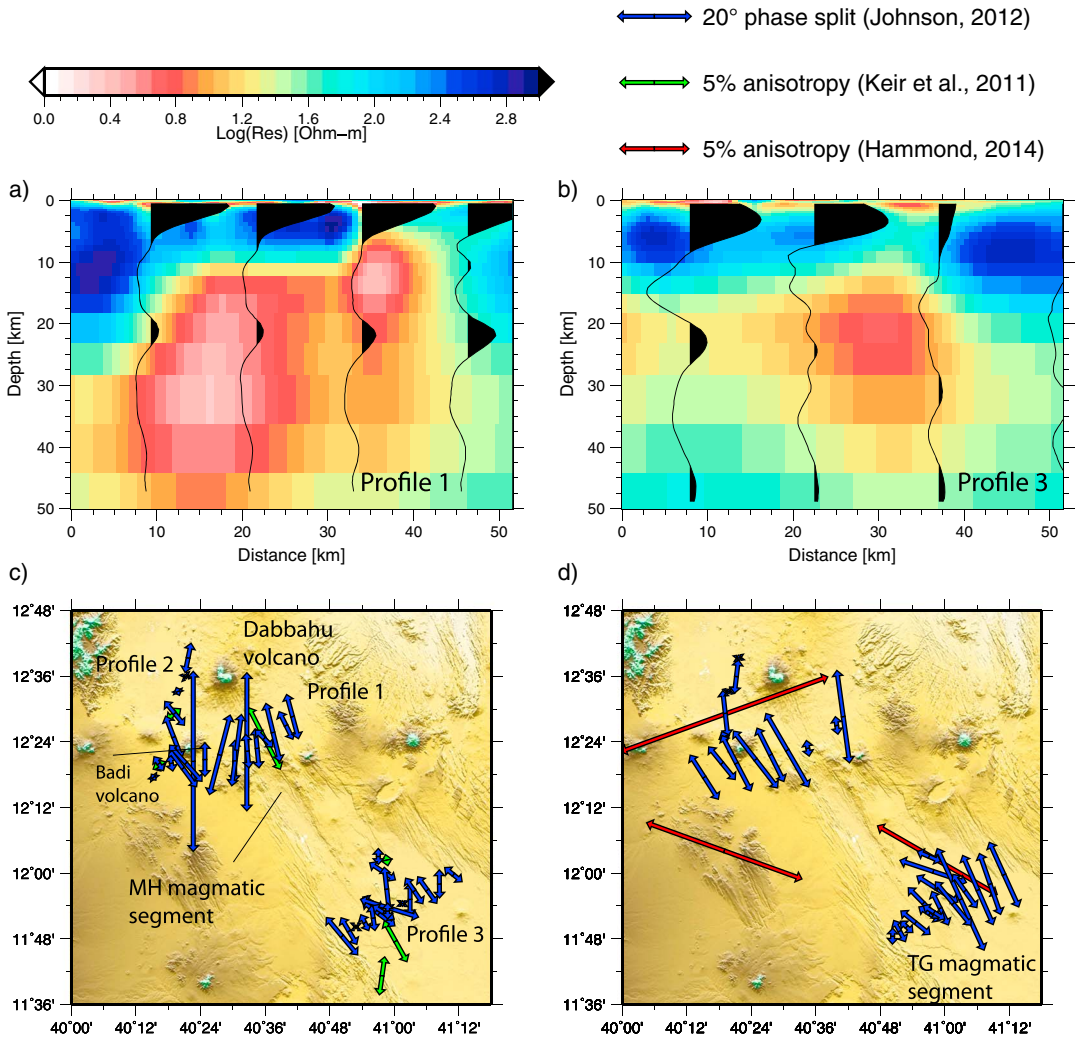

Figure 11. Comparison of MT and seismic models of crustal structure and anisotropy: (a) Magnetotelluric results for Profile 1 (Desissa et al., 2013). (b) Magnetotelluric results for Profile 3 (Johnson et al., 2016), with instrument locations shown in Figure 11c. Location of study region shown in Figure 7a. Seismic traces on both plots show receiver function migrations from Hammond et al. (2011). (c) Comparison of seismic anisotropy in the upper crust from shear wave splitting (green arrows; Keir et al., 2011a, 2011b) and geoelectric strike from MT (blue arrows) for periods related to the low conductive (blue) areas shown in Figures 11a and 11b (1–10 s) (Johnson, 2012). (d) Comparison of seismic anisotropy in the whole crust from receiver functions (red arrows) (Hammond, 2014) and geoelectric strike from MT (blue arrows) for periods related to the highly conductive (red) areas shown in Figures 11a and 11b (100–1,000 s) (Johnson, 2012).

5.2. Magmatic Plumbing System

Constraints on the magma plumbing system come from receiver functions, seismicity, MT, gravity, and magnetic studies. MT data provide unprecedented constraints on the locus and scale of magma plumbing systems that feed dyke intrusion and volcanism in the MHR segment (Desissa et al., 2013; Johnson et al., 2016) (Figure 11). A small-scale, but high melt fraction (≤22%), conductor lies slightly deeper than the inferred source of magma supplying the recent dyking events, determined from geodesy and seismology (e.g., Ebinger et al., 2008; Grandin et al., 2011; Hamling et al., 2009). A much more substantial magma reservoir straddling the Moho (~22 km deep in this area; Hammond et al., 2011) lies ~25 km to the west of the rift axis (Figure 11) where Ferguson et al. (2013) find geochemical evidence for ponding and reequilibration of magma at the top of the mantle, most likely stored in stacked sills. Although the regularized MT inversion model of Figure 11 gives a single conductor, Johnson et al. (2016) show that a series of sills, with a similar total magma volume, fit the data equally well.

A second MT profile in the northwestern MHR was acquired on a trend oblique to the rift and approaching within 10 km of Dabbahu volcano at the northern end of the magmatic segment (Johnson et al., 2016). At its closest point to the volcano, the model has very high (≥12 S/m) conductivity from depths of ~4 km, peaking at 6.5 km depth. Interpretation of these data is a challenge since model conductivities exceed that of basaltic melt at the appropriate temperatures and pressures, even with high water content (Pommier & Le Trong, 2011). However, Field et al. (2012, 2013) found a wide range of erupted products from the Dabbahu volcano, including very evolved, wet rhyolites, which could have crystallized in the top 6 km of the crust. Recent estimates of rhyolite melt conductivity (Guo et al., 2016) are 3–4 times higher than conductivities of basaltic melt at the appropriate temperature, pressure, Na_2O, and water content but still less than the maximum observed in our model. Very high conductivities and hence substantial melt volumes (even using the higher melt conductivities of rhyolitic magmas deduced by Guo et al., 2016) are also detected beneath the Dabbahu volcano, where Field et al. (2012) inferred protracted fractional crystallization of parent basaltic magma in a substantial, long-lived storage region, preferably in sills, between 1.5 km and 5.5 km depth, consistent with the pressured zone imaged with seismicity data (Ebinger et al., 2008); however, MT data cannot be satisfied by a conductor confined to such shallow depths (Johnson et al., 2016). Jointly, the data support the view of sill complexes beneath axial and flank volcanic systems. However, petrological constraints suggest that fractionation starts in the lower crust beneath flank volcanoes and in the upper crust beneath axial volcanoes.

The two most recent eruptions at the northernmost magmatic segment, Erta'Ale, were sourced from dikes and sills in the upper 3 km (Magee et al., 2017; Pagli et al., 2012; Xu et al., 2017) (Figure 7b). The persistent lava lake in the Erta'Ale crater and the frequent eruptions suggest a semipermanent melt-rich sill, as along the magma-rich slow-spreading Reykjanes ridge. Farther south where the MHR segment merges with the Tendaho Graben, high conductivity is again imaged off axis at lower crustal depths (Johnson et al., 2016) (Figure 11) but with smaller inferred volumes than beneath the recently active northern MHR. This coincides with an inferred partially molten gabbroic body that has been intruded into a thinned lower crust deduced from microgravity data (Lewi et al., 2015) (cf. models of MT and gravity data through the Boset volcano in the northern MER; Whaler & Hautot, 2006; Cornwell et al., (2006), section 4.2). Didana et al. (2014, 2015) imaged an upper crustal zone of extensive partial melt fraction (up to 0.13) beneath the Tendaho Graben geothermal prospect to the east of the southern MHR axis, connected to a large intrusive magmatic body underlying the TG and MHR, fed by a mantle source.

Farther south across the currently inactive part of the MHR, lying within the TG, high conductivity is again imaged at lower crustal depths (Profile 3), in this case ~10 km to the east of the rift axis (Johnson et al., 2016) (Figure 11). The maximum conductivity and lateral extent of the conductor, and hence inferred partial melt fraction and total melt volume, are lower than in the off-axis reservoir beneath the recently active northern MHR. In a similar location, Lewi et al. (2015) modeled microgravity data to infer that a partially molten gabbroic body has been intruded into a thinned lower crust. This agreement between MT and gravity results is reminiscent of that found for the location of dense subsurface bodies, interpreted as gabbroic, and conductors across the northern MER through Boset volcano. Didana et al. (2014, 2015) have modeled several MT profiles across the TG geothermal prospect to the southeast of the profile of Johnson et al. (2016) and to the east of the southern MHR axis. Seismic surface wave (Guidarelli et al., 2011), *Pn* (Stork et al., 2013), and body wave tomography (Hammond et al., 2013) studies image slow upper mantle velocities throughout the MHR rift segment, with the most extreme reductions centered on the recently active northern part.

5.3. The Shape and Distribution of Partial Melt

Seismic anisotropy in the upper crust is constrained from shear wave splitting from local earthquakes (Keir et al., 2011a, 2011b) and surface waves (Bastow et al., 2010) (Figure 11d). Large amounts of fault-parallel (NNW) anisotropy are seen only in the area of 2005–2012 diking activity. Outside of this region, anisotropy in the upper crust is lower but remains aligned with major faults. These patterns suggest that the presence of melt enhances a pervasive fracture-parallel anisotropy in this region. Seismic anisotropy in the whole crust can be estimated by looking at azimuthal variations in V_P/V_S from receiver functions. V_P/V_S throughout Afar have values >2, implying that melts are also present (Dugda et al., 2005; Hammond et al., 2011; Stuart et al., 2006). However, Hammond (2014) shows that such high values are an effect of seismic anisotropy, suggesting that if melt is the cause, then it must be preferentially aligned. Inverting the azimuthal variations in

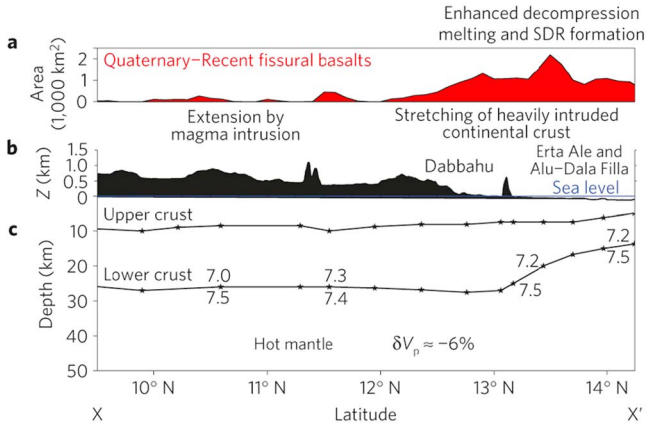

Figure 12. (a) Variation in Quaternary-Recent basaltic volcanism exposed every 0.1° latitude along strike in the Red Sea rift in Afar, with crustal velocity structure largely based on the EAGLE along-axis seismic profile (Maguire et al., 2006) and location shown in Figure 7a. (b) Elevation and (c) crustal thickness. Seismic velocities are in km/s. Note the abrupt thinning of the crust in northern Afar (>13° N), which coincides with subsidence of the rift valley below sea level and a marked pulse in Quaternary-Recent volcanism (after Bastow & Keir, 2011). SDR = seaward dipping reflector; δV_P indicates regional velocity reduction relative to global norm.

V_P/V_S suggests that melt in the lower crust must be stored in interconnected sills, consistent with reflectivity studies in rift zones (e.g., Thybo et al., 2000). Estimates of azimuthal anisotropy for the whole crust have the same orientation as that in the upper crust but with much stronger anisotropy.

Further support for aligned crustal melt pockets comes from measurements of geoelectrical strike orientations determined from the MT profiles outlined in section 5.2 (Johnson, 2012). The presence of electrical anisotropy implies that the aligned melt is interconnected. For periods synonymous with the mostly low-conductivity upper crust (1–10 s), the electrical anisotropy strikes are similar to those from upper crustal earthquake shear wave splitting, and the magnitude of electrical anisotropy (measured as the difference in MT phase for currents flowing along and across geoelectrical strike; see, e.g., Hamilton et al., 2006; Padilha et al., 2006) is relatively low. For periods synonymous with the conductive lower crust (100–1,000 s) the strike of the electrical anisotropy matches well with fast directions from receiver functions and teleseismic shear wave splitting, and the amount of electrical anisotropy is higher (Figure 11). These similarities support the idea that seismic and electrical anisotropy are caused by the preferential alignment of melt, primarily in the lower crust. These patterns suggest that melt can flow within these interconnected networks in the lower crust and feed the relatively localized zones of deformation in the upper crust (Desissa et al., 2013; Hammond, 2014). Note that there are areas with little or no electrical anisotropy, but high conductivities indicating abundant melt, in the upper crust (e.g., close to Dabbahu volcano; Figure 11), suggesting no particular geometry in its arrangement. Here the penetration depth is severely limited, and the 100–1,000 s periods are probably not penetrating the deeper crust.

5.4. Crustal Thinning and Subsidence at Plate Rupture

Wide-angle seismic experiments show that the crust throughout Ethiopia has a consistent layering with lower crustal V_P = 6.7–7.0 km/s, an upper crustal V_P = 6.0–6.3 km/s, and cover rocks of lava flows and sediments with V_P = 2.2–4.5 km/s (Makris & Ginzburg, 1987; Prodehl & Mechie, 1991a, 1991b) (Figures 8, 10, and 12). Excluding the regularly spaced volcanoes marking the centers and tips of magmatic segments, the cover rocks are generally thickest where the crust is thinnest suggesting a strong link between crustal thinning, rift valley subsidence, and resultant accumulation of basin infill (Figure 12). The Danakil basin, which hosts the Erta'Ale magmatic segment, has the thinnest crust in Afar at 15 km thick and is also characterized by the thickest sedimentary basins: ~5 km as opposed to 2–3 km elsewhere (Berckhemer et al., 1975; Makris & Ginzburg, 1987) (Figure 12). The change in crustal thickness along rift from south to north is primarily accounted for by markedly thinned lower crust, although the upper crust is also appreciably thinner (Makris & Ginzburg, 1987). Existing controlled source data do not traverse the rough relief of the currently active magmatic segments where intrusion volumes may be largest.

Spatial variations in crustal thickness in Ethiopia correlate with variations in effective elastic thickness, with the strongest plate ($Te \approx 60$ km) beneath the plateaus and the weakest plate ($Te \approx 6$ km) beneath the Danakil depression (Perez-Gussinyé et al., 2009). Both crustal thickness and effective elastic thickness, a measure of strength over time periods much longer than the earthquake cycle, also correlate to variations in seismogenic layer thickness estimated from local seismicity and teleseisms; seismogenic layer thickness is 25–30 km beneath the Ethiopian Plateau (Keir et al., 2009) but decreases to ~5 km beneath the Danakil depression (Craig et al., 2011; Nobile et al., 2012).

There is debate regarding whether the regions of thinnest crust (~15–20 km) in Afar, such as the Danakil depression, are fully oceanic in nature. In the Danakil depression, the basin floor is at ~120 m below sea level and the Holocene stratigraphy is dominated by intercalated basalts and evaporites (Atnafu et al., 2015). The basin stratigraphy and environment of deposition are similar to that interpreted to form the seaward dipping reflector sequences (at fully rifted margins), and therefore, the Danakil depression could be a modern analog for their formation (Bastow & Keir, 2011; Buck, 2017; Corti et al., 2015). There is at least 50% more melt available

beneath the northern MHR than in the TG segment in the south and likely up to an order of magnitude more. This change is consistent with regional northward increases in the number of Holocene volcanoes as well as the volume of erupted material (Barberi & Varet, 1977), and it is likely a result of a northward increase in thinning of the plate and resultant decompression melting of asthenosphere (Bastow & Keir, 2011).

The most highly extended crust beneath the Danakil depression is 5–10 km thicker than normal oceanic crust. There are two end-member hypotheses to explain the structure and composition of the Danakil crust. In one model, heavily intruded and extended crust deforms by brittle failure at the surface and by magma intrusion and ductile flow in the lower crust (Bastow & Keir, 2011). Unlike thin crust at oceanic rifts, the intrusive material may stall and fractionate to produce peralkaline and rhyolitic lavas, and felsic intrusive material, contributing to the unusual structure. The second model relates to high magma production rates in early-stage seafloor spreading caused by the steep lithosphere-asthenosphere boundary on either side of the rift (e.g., Boutilier & Keen, 1999; Korenaga et al., 2000; Ligi et al., 2011; White & McKenzie, 1989). The high extrusion rates at the weak spreading ridge cause bending above the ridge and may produce seaward dipping reflectors. Our syntheses suggest that both processes are important.

5.5. Summary: Defining Transitional Crust and Plate Rupture Along Magmatic Margins

Passive and controlled source seismic imaging shows that the crust in Afar varies from 15 to 25 km thick, and the crust is heavily modified by solidified mafic intrusion and partial melt currently residing in magma reservoirs through the crust. MT combined with modeling seismic and electrical anisotropy supports the interpretation that the lower crust is an important region of melt ponding. The melt in the lower crust resides in horizontal sills near segment centers, and it is then transported laterally and vertically in dikes that accommodate most of the plate boundary deformation. The central magma chamber that maintains the along-axis segmentation over multiple episodes and the extension via dike intrusion and faulting above the dikes produce columns of new crust with corresponding magnetic stripes. The unusually thick crust (~15 km) matches the thick crust beneath magmatic rifted margins with seaward dipping reflector sequences, pointing to a common mode of emplacement. In contrast, the observed seismic velocity and structure of the crust and the low-silica composition of basalts suggests that seafloor spreading processes are still evolving.

Seismic imaging, gravity, and MT all suggest that the whole crust beneath the rift flanks and the rift axis is heavily modified by magma intrusion. Seismic and electrical anisotropy support the view that magma accumulates in the lower crust as networks of interconnected stacked sills, whereas magma in the upper crust may be both in sill networks and subvertical dikes. Petrological constraints suggest that fractionation starts in the lower crust beneath flank volcanoes during the early stages of rifting, whereas most fractionation occurs in the upper crust beneath axial volcanoes as plate rupture initiates (Rooney et al., 2011, 2014).

6. The Cameroon Volcanic Line

Cameroon's crustal structure has been investigated using both passive and active seismic sources (e.g., Dorbath et al., 1986; Gallacher & Bastow, 2012; Meyers et al., 1998; Plomerova et al., 1993; Stuart et al., 1985; Tokam et al., 2010) and potential field studies (e.g., Fairhead & Okereke, 1987; Tadjou et al., 2009; Toteu et al., 2004) (Figures 3b and 13). Thinned crust (~25 km) resulting from extension is imaged beneath the Garoua rift (Figure 12), while the transition from the CVL to the Congo craton is heralded by a transition in Moho depth from ~36 km to 43–48 km depth (Gallacher & Bastow, 2012; Tokam et al., 2010) (Figure 13). Crustal shear wave velocities also increase into the craton from the CVL, from ~3.7 km/s to ~3.9 km/s (Tokam et al., 2010). Bulk crustal V_P/V_S ratios along the CVL are comparable to those of cratons worldwide (~1.74), an observation that Gallacher and Bastow (2012) cited as evidence for the lack of melt fractionation and intrusion during the ~30 Ma development of the CVL. These seismological results thus corroborate petrological studies that attribute low-volume, high-pressure magmas to melting of subcontinental lithospheric mantle that has experienced only small amounts of crustal fractionation (e.g., Fitton, 1980; Halliday et al., 1990; Marzoli et al., 2000; Suh et al., 2003; Yokoyama et al., 2007). Such low-volume, high-pressure magmas are expected to form within the subcontinental lithospheric mantle and exhibit relatively little fractionation within the crust (e.g., Suh et al., 2003).

Gravity studies in Cameroon (e.g., Fairhead & Okereke, 1987 ; Poudjom Djomani et al., 1992, 1997; Tadjou et al., 2009) highlight various major tectonic features in the region, including the Benue Trough (+ve

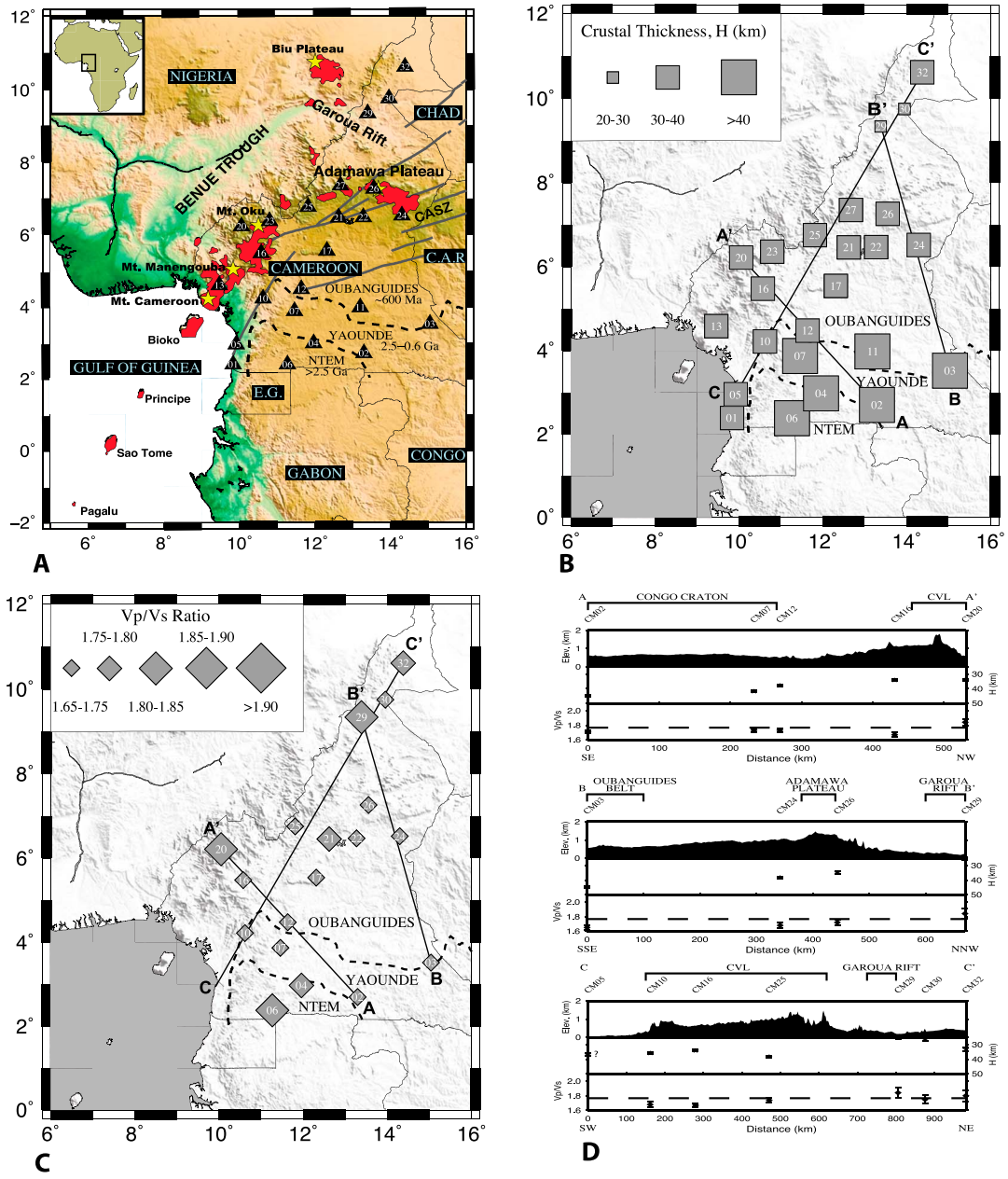

Figure 13. (a) Location map of the CBSE seismograph stations (triangles) superimposed on regional topography. Numbers are station codes. The Ntem Complex boundary and the Yaoundé domain boundary are after Toteu et al. (2004). Stars are selected CVL volcanoes. C.A.R.: Central African Republic; CASZ: Central African Shear Zone; E.G.: Equatorial Guinea. The red areas are regions of Cenozoic volcanism along the CVL taken from Tokam et al. (2010). (b) Variations in crustal thickness. (c) Variations in V_P/V_S ratio across Cameroon from receiver function analysis. (d) The black thick lines A-A′, B-B′, and C-C′ show the orientation of transects. After Gallacher and Bastow (2012).

Bouguer anomaly), uplift of the Adamawa Plateau (−ve anomaly), and the Congo craton (−ve Bouguer anomaly). Evidence for continental collision was found at the northern margin of the Congo craton, as well as a positive anomaly associated with the Central African Shear Zone, which bisects the Adamawa uplift (Figure 13, e.g., Poudjom Djomani et al., 1997; Tadjou et al., 2009).

Recent work by Milelli et al. (2012) and Fourel et al. (2013) has used scaled laboratory models and analytical solutions to investigate the effects of large lateral variations in lithospheric thickness on lithospheric stability. Their work demonstrates that lithospheric instabilities can develop over long timescales with small rates of

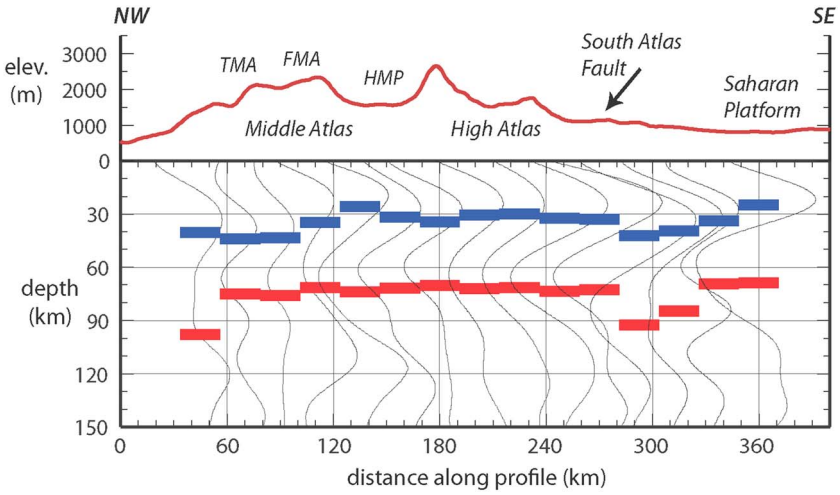

Figure 14. *S* receiver function profile across Atlas Mountains from northwest to southeast as indicated in Figure 3a. Top panel indicates the elevation and primary tectonic features (HMP-High Moulouya platform; FMA-folded Middle Atlas; TMA-Tabular Middle Atlas). *S* receiver function stacks at 40 km spacing are shown for all stations within 20 km of profile and plotted evenly spaced for clarity. Blue and red dashes indicate Moho and lithosphere-asthenosphere boundary, respectively.

upwelling and decompression melting as is observed in Cameroon and consistent with recent hybrid models for magmatism along the CVL (e.g., De Plaen et al., 2014; Gallacher & Bastow, 2012; Reusch et al., 2010).

7. The Atlas Orogen

In contrast to the Mediterranean arcs (Alps, Apennine, Carpathian, Hellenic, and Betic-Rif), the Atlas is subparallel to and south of the convergent margin and on the African plate (Figures 1 and 3a). The mountain belt has high topography (>4,100 m), yet there is no apparent deep crustal root to isostatically support the high elevations of the Atlas (e.g., Ayarza et al., 2005, 2014; Jessell et al., 2016; Miller & Becker, 2014; Missenard et al., 2006; Sandvol et al., 1998; Zeyen et al., 2005) (Figure 3a). Furthermore, only a modest amount of tectonic shortening has been estimated and has been suggested to be achieved through thick-skinned thrusting and folding (e.g., Gomez et al., 2000; Teixell et al., 2003).

Many recent efforts have focused on understanding the crustal- and lithospheric-scale structure of the Atlas to understand the orogenesis. Structural seismological imaging suggests that the lithosphere beneath the Atlas is particularly thin or perhaps the uppermost mantle is abnormally warm with low seismic velocities found at depths of ~65–160 km (e.g., Bezada et al., 2014; Fullea et al., 2007; Miller et al., 2015; Palomeras et al., 2014; Sun et al., 2014). Figure 14 shows *S* receiver function estimates of the Moho and lithosphere-asthenosphere depths along a profile across the Atlas from Miller and Becker (2014). Geophysical modeling indicates that the lithosphere is thin (~65 km) compared with the topographically high, thick lithosphere of the Saharan platform (≥150 km) and the Morocco Atlantic margin along a corridor that is aligned with the highest topography in the Atlas (Fullea et al., 2007; Miller & Becker, 2014; Miller et al., 2015; Missenard et al., 2006; Missenard & Cadoux, 2012; Teixell et al., 2003, 2005) (see Figure 3a). The combination of thinned lithosphere and mantle upwelling has been invoked to explain the unusual high topography, low seismic velocities in the uppermost mantle, and lack of a significant crustal root (Arboleya et al., 2004; Frizon de Lamotte et al., 2009; Fullea et al., 2007; Miller & Becker, 2014; Missenard et al., 2006; Teixell et al., 2005; Zlotnik et al., 2014). The source of the upwelling has been suggested to be part of the Canary plume from geochemical analyses of Quaternary alkali basalts in the Atlas and their spatial location above the low velocity material beneath the mountain range (Anguita & Hernán, 2000; Duggen et al., 2009).

Shear wave splitting analyses (Díaz & Gallart, 2014; Miller et al., 2013) also indicate a strong change in azimuthal anisotropy strength at the northern edge of the Middle Atlas, as well as an alignment of fast polarization orientations parallel to the strike of the Atlas Mountains, suggesting shearing in a mantle channel guided by lithospheric topography (Miller et al., 2013; Miller & Becker, 2014) and deflected by the high-velocity slab

beneath the Alboran Sea (Alpert et al., 2013; Díaz & Gallart, 2014). Miller et al. (2015) interpret the localized volcanism and low velocity anomalies in the sub-lithospheric mantle to be the result of the Canary Island plume flowing sub-horizontally beneath the Atlas. This seismologically based interpretation is supported by numerical experiments of mantle flow that incorporate the effects of the stiff, deep West African cratonic keel and nearly vertical, narrow slab beneath the Alboran (Alpert et al., 2013), numerical experiments of strongly tilted plumes and resulting instabilities (Mériaux et al., 2011), and by scaled analogue models of the Alboran slab and Canary plume interaction (Mériaux et al., 2015). Other hypotheses explaining the Cenozoic uplift of the Atlas and the links to recent volcanism and to upper-mantle structure include: lithospheric delamination (Bezada et al., 2014; Duggen et al., 2009; Levander et al., 2014) and edge-driven convection (Kaislaniemi & van Hunen, 2014; Missenard & Cadoux, 2012). The two edge-driven convection studies (Kaislaniemi & van Hunen, 2014; Missenard & Cadoux, 2012) are based on numerical experiments, which are designed to evaluate the dynamics of the thinned lithosphere and mantle melting processes in the Moroccan Atlas. They also find good agreement with observations of lithospheric thickness and volcanism, but neither incorporate the presence of the subducted slab beneath the Alboran Sea.

Despite the lack of consensus on the origin of the Atlas topography, various recent studies using a range of methods, from the SIMA active source seismic experiment (Ayarza et al., 2014), broadband waveform analysis (Sun et al., 2014), MT (Anahnah et al., 2011; Ledo et al., 2011), body wave (e.g., Bezada et al., 2014), and surface wave (Palomeras et al., 2014) tomography, for example, have suggested the presence of anomalous low-velocity material beneath the lithosphere and in the crust. The temperature of this material is also inferred to be warm, due to the presence of partial melt (Anahnah et al., 2011; Ayarza et al., 2014; Ledo et al., 2011; Sun et al., 2014).

8. Summary

Our synthesis of geophysical studies that aim to image the crust beneath zones of active rifting and orogenesis in Africa shows that magma and volatiles are migrating from the asthenosphere through the plate, leading to changes in rheology and making large contributions to H_2O and CO_2 fluxes globally. The addition of magmatic fluids permanently alters the composition of continental crust accreted during the Proterozoic, and it increases the continental crustal volume. The magma intrusion accommodates plate boundary deformation and masks crustal stretching. In young, weakly extended sectors of the East African rift, volatiles released from upwelling asthenosphere, heated mantle lithosphere, and magma intrusions alter crustal composition and rheology. Even in rifts that formed within the last 7 Myr, ~20% of the crust is new magmatic material intruded as sills in the lower crust (underplate) and as more localized zones of dike intrusion in the middle and upper crust as imaged with seismic, MT, and gravity methods. In the mature Main Ethiopian Rift (MER), the surface area of the rift has doubled in the past ~ 10 Myr, and intrusive volumes are 30%, increasing into the central Afar rift zone where dike intrusion accommodates much of the active extension, and symmetric magnetic anomalies mimic seafloor spreading. Intrusive to extrusive volumes (surface flows plus basin fill) are roughly equivalent but increase with increasing age of rifting and amount of extension and proximity to prerift flood magmatism. In the older, more evolved Horn of Africa, intense episodes of magma intrusion fed from crustal magma chambers beneath segment centers create new columns of mafic crust up to 8 m wide in a process akin to that along slow-spreading ridges. The magma intrusion and faulting above the dikes accommodate centuries of plate boundary opening and suggest that plate rupture is achieved through catastrophic magma intrusion events in 15–20 km thick transitional crust. Regional analyses suggest that progressively smaller screens of continental crust are heated and weakened by repeated episodes of magma intrusion immediately prior to seafloor spreading.

On the western side of the African continent, magmatism with very minor extension over the past 30 Myr has formed the Cameroon Volcanic Line (CVL)—a linear chain of basaltic volcanoes that formed on the broad Adamawa Plateau that lacks the age progression predicted by the traditional hot spot track hypothesis. Intrusive volumes are much smaller than in the Eastern, MER, and Afar rifts, and magmas largely fractionate at subcrustal depths. The comparison with East African crustal structure suggests that extensional forces are much smaller in the CVL, inhibiting the creation and rise of magma into the crust and preventing full-scale rifting. In the Atlas orogen of northwestern Africa, recent magmatism is also primarily along a linear trend from the Canary Islands to the Alboran Sea and linked to the Canary Island hot spot. In contrast to the

magma-rich Horn of Africa, however, magmatism in Cameroon and Morocco has had relatively little impact on crustal structure, but the mantle flow and lithospheric heating cause dynamic uplift supporting the high Atlas mountain range.

Our work highlights consistent patterns and new insights into continental lithospheric deformation processes. Based on our results and complementary crust and mantle xenolith studies, future studies would benefit from constraints on physical properties across a broader range of crustal and magmatic rock compositions, and in particular, relatively low silica, and gas-rich melts. Our work focuses on areas with sometimes dense data coverage, but large sectors of the African continent remain virtually unexplored in terms of crust and upper mantle structure through seismic, MT, heat flow, and detailed structural analyses. Gap-filling studies will tighten the context for studies of active deformation, and they promise new insights into continental lithospheric behavior, given the relative stability of the African continent. Critical areas include the largely amagmatic but remote Western and Southwestern rift zones, the Turkana gap between the Ethiopian and East African Plateaux, the seismically active Indian Ocean margin, and the boundaries of thick Archaean cratons, which have been the locus of plate deformation through multiple Wilson Cycles.

Acknowledgments

We thank two anonymous referees and Editors Jeff Gu and John Geissman for feedback that greatly improved text and figures. C. E. was supported by National Science Foundation grants EAR-1113355 and EAR-1109302. D. K. is supported by Natural Environmental Research Council grant NE/L013932/1. C. E. and D. K. also were supported by a grant from Beach Petroleum and Tanzania Development Corporation. C. T. and S. H. were supported by ANR grant 12-JS06-000. C. E., C. T., and D. K. conducted studies with approval of the Commission for Science and Technology (Tanzania) and the National Council for Science and Technology (Kenya). K. A. W. was supported by NERC grants NER/B/S/2001/00863 and NE/E007147/1 and is currently supported by NERC grant NE/L013932/1. Her MT fieldwork used equipment loaned by the NERC Geophysical Equipment Facility and from the University of Brest and the Geophysical Instrument Pool Potsdam and was supported logistically by Addis Ababa University, the Geological Survey of Ethiopia, and the Petroleum Operations Department of the Ethiopian Ministry of Mines. M. S. M. is supported by NSF Continental Dynamics Program EAR-0809023 and NSF CAREER award EAR-1054638. The facilities of SEIS-UK are supported by the Natural Environment Research Council under agreement R8/H10/64. The facilities of IRIS Data Services, and specifically the IRIS Data Management Center, were used for access to waveforms, related metadata, and/or derived products used in this study. Broadband seismic data collected in Morocco utilized PASSCAL instrumentation and were supported by IRIS. IRIS Data Services are funded through the Seismological Facilities for the Advancement of Geoscience and EarthScope (SAGE) Proposal of the National Science Foundation under Cooperative Agreement EAR-1261681. CRAFTI data (XJ) are available at the IRIS-DMC in 2017 (http://ds.iris.edu/ds/nodes/dmc/).

References

Abdallah, A., Courtillot, V., Kasser, M., Le Dain, A. Y., Lépine, J. C., Robineau, B., … Tarantola, A. (1979). Relevance of afar seismicity and volcanism to the mechanics of accreting plate boundaries. *Nature*, *282*(5734), 17–23. https://doi.org/10.1038/282017a0

Abdelfettah, Y., Tiercelin, J. J., Tarits, P., Hautot, S., Maia, M., & Thuo, P. (2016). Subsurface structure and stratigraphy of the northwest end of the Turkana Basin, northern Kenya rift, as revealed by magnetotellurics and gravity joint inversion. *Journal of African Earth Sciences*, *119*, 120–138. https://doi.org/10.1016/j.jafrearsci.2016.03.008

Abebe, T., Mazzarini, F., Innocenti, F., & Manetti, P. (1998). The Yerer-Tullu Wellel volcanotectonic lineament: A transtensional structure in central Ethiopia and the associated magmatic activity. *Journal of African Earth Sciences*, *26*(1), 135–150. https://doi.org/10.1016/S0899-5362(97)00141-3

Accardo, N., Gaherty, J. B., Shillington, D. J., Ebinger, C. J., Nyblade, A. A., Mbogoni, G. J., … Mruma, A. (2017). Surface-wave imaging of the weakly-extended Malawi Rift from ambient-noise and teleseismic Rayleigh waves. *Geophysical Journal International*, *209*(3), 1892–1905. https://doi.org/10.1093/gji/ggx133

Adams, A., Nyblade, A., & Weeraratne, D. (2012). Upper mantle shear wave velocity structure beneath the East African plateau: Evidence for a deep, plateauwide low velocity anomaly. *Geophysical Journal International*, *189*(1), 123–142. https://doi.org/10.1111/j.1365-246X.2012.05373.x

Ahmed, A., Tiberi, C., Leroy, S., Stuart, G. W., Keir, D., Sholan, J., … Basuyau, C. (2013). Crustal structure of the rifted volcanic margins and uplifted plateau of Western Yemen from receiver function analysis. *Geophysical Journal International*, *193*(3), 1673–1690. https://doi.org/10.1093/gji/ggt072

Ahmed, S., Leroy, D., Keir, F., Korostelev, K., Khanbari, F., Rolandone, G. S., & Obrebski, M. (2014). Crustal structure of the Gulf of Aden southern margin: Evidence from receiver functions on Socotra Island (Yemen). *Tectonophysics*, *637*, 251–267. https://doi.org/10.1016/j.tecto.2014.10.014

Albaric, J., Déverchère, J., Perrot, J., Jakovlev, A., & Deschamps, A. (2014). Deep crustal earthquakes in North Tanzania, East Africa: Interplay between tectonic and magmatic processes in an incipient rift. *Geochemistry, Geophysics, Geosystems*, *15*, 374–394. https://doi.org/10.1002/2013GC005027

Alpert, L. A., Miller, M. S., Becker, T. W., & Allam, A. (2013). Structure beneath the Alboran from geodynamic flow models and seismic anisotropy. *Journal of Geophysical Research*, *118*, 4265–4277. https://doi.org/10.1002/jgrb.50309

Anahnah, F., Galindo-Zald var, J., Chalouan, A., Pedrera, A., Ruano, P., Pous, J., … Asensio, E. (2011). Deep resistivity cross section of the intraplate Atlas Mountains (NW Africa): New evidence of anomalous mantle and related quaternary volcanism. *Tectonics*, *30*, TC5014. https://doi.org/10.1029/2010TC002859

Anguita, F., & Hernán, F. (2000). The Canary Islands origin: A unifying model. *Journal of Volcanology and Geothermal Research*, *103*(1–4), 1–26. https://doi.org/10.1016/S0377-0273(00)00195-5

Arboleya, M. L., Teixell, A., Charroud, M., & Julivert, M. (2004). A structural transect through the High and Middle Atlas of Morocco. *Journal of African Earth Sciences*, *39*(3–5), 319–327. https://doi.org/10.1016/j.jafrearsci.2004.07.036

Ashley, G. M., Tactikos, J. C., & Owen, R. B. (2009). Hominin use of springs and wetlands: Paleoclimate and archaeological records from Olduvai Gorge (~ 1.79–1.74 ma). *Palaeogeography, Palaeoclimatology, Palaeoecology*, *272*(1–2), 1–16. https://doi.org/10.1016/j.palaeo.2008.10.016

Atnafu, B., Kidane, T., Foubert, A., Jaramillo-Vogel, D., Schaegis, J.-C., & Henriet, J.-P. (2015). Reading history in Afar. *Eos*, *96*, 12–15.

Aulbach, S. R. L., Rudnick, R. L., & McDonough, W. F. (2011). Evolution of the lithospheric mantle beneath the East African Rift in Tanzania and its potential signatures in rift magmas. *Geological Society of America Special Papers*, *478*, 105–125. https://doi.org/10.1130/2011.2478

Ayalew, D., Ebinger, C., Bourdon, E., Wolfenden, E., Yirgu, G., & Grassineau, N. (2006). Temporal compositional variation of syn-rift rhyolites along the western margin of the southern Red Sea and northern Main Ethiopian Rift. *Geological Society of London, Special Publication*, *259*(1), 121–130. https://doi.org/10.1144/GSL.SP.2006.259.01.10

Ayarza, P., Alvarez-Lobato, F., Teixell, A., Arboleya, M. L., Tesón, E., Julivert, M., & Charroud, M. (2005). Crustal structure under the central High Atlas Mountains (Morocco) from geological and gravity data. *Tectonophysics*, *400*(1–4), 67–84. https://doi.org/10.1016/j.tecto.2005.02.009

Ayarza, P., Carbonell, R., Teixell, A., Palomeras, I., Martí, D., Kchikach, A., … Amrhar, M. (2014). Crustal thickness and velocity structure across the Moroccan Atlas from long offset wide-angle reflection seismic data: The Sima experiment. *Geochemistry, Geophysics, Geosystems*, *15*, 1698–1717, https://doi.org/10.1002/2013GC005164

Ayele, A., Keir, D., Ebinger, C., Wright, T. J., Stuart, G. W., Buck, W. R., … Sholan, J. (2009). September 2005 mega-dike emplacement in the Manda-Harraro nascent oceanic rift (Afar depression). *Geophysical Research Letters*, *36*, L20306. https://doi.org/10.1029/2009GL039605

Ayele, A. A., Stuart, G., & Kendall, J.-M. (2004). Insights into rifting from shear wave splitting and receiver functions: An example from Ethiopia. *Geophysical Journal International*, *157*(1), 354–362. https://doi.org/10.1111/j.1365-246X.2004.02206.x

Barberi, F., & Varet, J. (1977). Volcanism of Afar: Small-scale plate tectonics implications. *Geological Society of America Bulletin*, *88*(9), 1251–1266. https://doi.org/10.1130/0016-7606(1977)88%3C1251:VOASPT%3E2.0.CO;2

Barnie, T. D., Keir, D., Hamling, I., Hofmann, B., Belachew, M., Carn, S., … Wright, T. (2016). A multidisciplinary study of the final episode of the Manda Hararo dyke sequence, Ethiopia, and implications for trends in volcanism during the rifting cycle. *Geological Society of London, Special Publication*, *420*(1), 149–163. https://doi.org/10.1144/SP420.6

Bastow, I., & Keir, D. (2011). The protracted development of the continent-ocean transition in Afar. *Nature Geoscience*, *4*(4), 248–250. https://doi.org/10.1038/NGEO01095

Bastow, I., Nyblade, A., Stuart, G., Rooney, T., & Benoit, M. (2008). Upper mantle seismic structure beneath the Ethiopian hotspot: Rifting at the edge of the African low-velocity anomaly. *Geochemistry, Geophysics, Geosystems*, *9*, Q12022. https://doi.org/10.1029/2008GC002107

Bastow, I., Pilidou, S., Kendall, J.-M., & Stuart, G. (2010). Melt-induced seismic anisotropy and magma assisted rifting in Ethiopia: Evidence from surface waves. *Geochemistry, Geophysics, Geosystems*, *11*, Q0AB05. https://doi.org/10.1029/2010GC003036

Bastow, I., Stuart, G., Kendall, J.-M., & Ebinger, C. (2005). Upper-mantle seismic structure in a region of incipient continental breakup: Northern Ethiopian rift. *Geophysical Journal International*, *162*(2), 479–493. https://doi.org/10.1111/j.1365-246X.2005.02666.x

Benkhelil, J. (1989). The origin and evolution of the Cretaceous Benue Trough (Nigeria). *Journal of African Earth Sciences*, *8*(2–4), 251–282. https://doi.org/10.1016/S0899-5362(89)80028-4

Berckhemer, H., Baier, B., Bartlesen, H., Behle, A., Burkhardt, H., Gebrande, H., … Vees, R. (1975). Deep seismic soundings in the Afar region and on the highland of Ethiopia. In A. Pilger, & A. Rosler (Eds.), *Afar Depression of Ethiopia* (Vol. I, pp. 89–107). Stuttgart: E. Schweizerbart.

Berhe, S. (1990). Ophiolites in northeast and East Africa: Implications for Proterozoic crustal growth. *Journal of the Geological Society of London*, *147*(1), 41–57. https://doi.org/10.1144/gsjgs.147.1.0041

Beyene, A., & Abdelsalam, M. (2005). Tectonics of the Afar Depression: A review and synthesis. *Journal of African Earth Sciences*, *41*(1–2), 41–59. https://doi.org/10.1016/j.jafrearsci.2005.03.003

Bezada, M. J., Humphreys, E. D., Davila, J. M., Carbonell, R., Harnafi, M., Palomeras, I., & Levander, A. (2014). Piecewise delamination of Moroccan lithosphere from beneath the Atlas Mountains. *Geochemistry, Geophysics, Geosystems*, *15*, 975–985, https://doi.org/10.1002/2013GC005059

Bialas, R., Buck, W., & Qin, R. (2010). How much magma is required to rift a continent? *Earth and Planetary Science Letters*, *292*(1–2), 68–78. https://doi.org/10.1016/j.epsl.2010.01.021

Biggs, J., Bastow, I., Keir, D., & Lewi, E. (2011). Pulses of deformation reveal frequently recurring shallow magmatic activity beneath the Main Ethiopian Rift. *Geochemistry, Geophysics, Geosystems*, *12*, Q0AB10. https://doi.org/10.1029/2011GC003662

Bilham, R., Bendick, R., Larson, K., Mohr, P., Braun, J., Tesfaye, S., & Asfaw, L. (1999). Secular and tidal strain across the Main Ethiopian Rift. *Geophysical Research Letters*, *26*(18), 2789–2792. https://doi.org/10.1029/1998GL005315

Bird, P. (2003). An updated digital model of plate boundaries. *Geochemistry, Geophysics, Geosystems*, *4*(3), 1027. https://doi.org/10.1029/2001GC000252

Birhanu, Y., Bendick, R., Fisseha, S., Lewi, E., Floyd, M., King, R., & Reilinger, R. (2016). GPS constraints on broad scale extension in the Ethiopian Highlands and Main Ethiopian Rift. *Geophysical Research Letters*, *43*, 6844–6851. https://doi.org/10.1002/2016GL069890

Birt, C. S., Maguire, P. K. H., Khan, M. A., Thybo, H., Keller, G. R., & Patel, J. (1997). The influence of pre-existing structures on theS evolution of the southern Kenya Rift Valley—Evidence from seismic and gravity studies. *Tectonophysics*, *278*(1–4), 211–242. https://doi.org/10.1016/S0040-1951(97)00105-4

Bond, G. (1978). Evidence for late Tertiary uplift of Africa relative to North America, South America, Australia and Europe. *Journal of Geology*, *86*(1), 47–65. https://doi.org/10.1086/649655

Bott, M. H. P. (1990). Stress distribution and plate boundary force associated with collision mountain ranges. *Tectonophysics*, *182*(3–4), 193–209. https://doi.org/10.1016/0040-1951(90)90163-3

Boutilier, R. R., & Keen, C. E. (1999). Small-scale convection and divergent plate boundaries. *Journal of Geophysical Research*, *104*(B4), 7389–7403. https://doi.org/10.1029/1998JB900076

Bridges, D., Mickus, K., Gao, S., Abdelsalam, M., & Alemu, A. (2012). Magnetic stripes of a transitional continental rift in Afar. *Geology*, *40*(3), 203–206. https://doi.org/10.1130/G32697.1

Bronner, A., Sauter, D., Manatschal, G., Peron-Pinvidic, G., & Munschy, M. (2011). Magmatic breakup as an explanation for magnetic anomalies at magma-poor rifted margins. *Nature Geoscience*, *4*(8), 549–553, https://doi.org/10.1038.ngeo1201

Brown, C., & Girdler, R. W. (1980). Interpretation of African gravity and its implication for the breakup of the continents. *Journal of Geophysical Research*, *85*(B11), 6443–6455. https://doi.org/10.1029/JB085iB11p06443

Brown, G. (1970). Eastern margin of Red Sea and coastal structures in Saudi Arabia. *Philosophical Transactions of the Royal Society of London A*, *267*(1181), 75–87. https://doi.org/10.1098/rsta.1970.0024

Buck, W. R. (2004). Consequences of asthenospheric variability on continental rifting. *Rheology and Deformation of the Lithosphere at Continental Margins*, *62*, 1–30.

Buck, W. R. (2017). The role of magmatic loads and rift jumps in generating seaward dipping reflectors on volcanic rifted margins. *Earth and Planetary Science Letters*, *466*, 62–69. https://doi.org/10.1016/j.epsl.2017.02.041

Bürgmann, R., & Dresen, G. (2008). Rheology of the lower crust and upper mantle: Evidence from rock mechanics, geodesy, and field observations. *Annual Review of Earth and Planetary Sciences*, *36*(1), 531–567. https://doi.org/10.1146/annurev.earth.36.031207.124326

Burke, K. (1996). The African plate. *South African Journal of Geology*, *99*, 341–409.

Casey, M., Ebinger, C., Keir, D., Gloaguen, R., & Mohamed, F. (2006). Strain accommodation in transitional rifts: Extension by magma intrusion and faulting in Ethiopian rift magmatic segments. *Geological Society of London, Special Publication*, *259*(1), 143–163. https://doi.org/10.1144/GSL.SP.2006.259.01.13

Chakrabarti, R., Basu, A. R., Santo, A. P., Tedesco, D., & Vaselli, O. (2009). Isotopic and geochemical evidence for a heterogeneous mantle plume origin of the Virunga volcanics, Western rift, East African Rift system. *Chemical Geology*, *259*(3–4), 273–289. https://doi.org/10.1016/j.chemgeo.2008.11.010

Chernet, T., Hart, W., Aronson, J., & Walter, R. (1998). New age constraints on the timing of volcanism and tectonism in the northern Main Ethiopian Rift—Southern Afar transition zone (Ethiopia). *Journal of Volcanology and Geothermal Research*, *80*(3–4), 267–280. https://doi.org/10.1016/S0377-0273(97)00035-8

Chesley, J. T., Rudnick, R. L., & Lee, C. T. (1999). Re-Os systematics of mantle xenoliths from the East African Rift: Age, structure, and history of the Tanzanian craton. *Geochimica et Cosmochimica Acta*, *63*(7–8), 1203–1217. https://doi.org/10.1016/S0016-7037(99)00004-6

Christensen, N. (1996). Poisson's ratio and crustal seismology. *Journal of Geophysical Research*, *101*(B2), 3139–3156. https://doi.org/10.1029/95JB03446

Christensen, N. I., & Mooney, W. D. (1995). Seismic velocity structure and composition of the continental crust: A global view. *Journal of Geophysical Research*, *100*(B6), 9761–9788. https://doi.org/10.1029/95JB00259

Cooper, C. M., & Miller, M. S. (2014). Craton formation: Internal structure inherited from closing of the early oceans. *Lithosphere*, *6*(1), 35–42. https://doi.org/10.1130/l321.1

Cornwell, D. G., Mackenzie, G. D., Maguire, P. K. H., England, R. W., Asfaw, L. M., & Oluma, B. (2006). Northern Main Ethiopian Rift crustal structure from new high-precision gravity data. In G. Yirgu, C. J. Ebinger, & P. K. M. Maguire (Eds.), *Structure and evolution of the East African Rift system in the Afar Volcanic Province*, *Geological Society, London Special Publications* (Vol. 259, pp. 269–291). Bath.

Corti, G. (2008). Control of rift obliquity on the evolution and segmentation of the main Ethiopian rift. *Nature Geoscience*, *1*(4), 258–262. https://doi.org/10.1038/ngeo160

Corti, G. (2009). Continental rift evolution: From rift initiation to incipient breakup in the Main Ethiopian Rift, East Africa. *Earth-Science Reviews*, *1*(4), 258–262. https://doi.org/10.1038/ngeo160

Corti, G., Agostini, A., Keir, D., van Wijk, J., Bastow, I. D., & Ranalli, G. (2015). Magma-induced axial subsidence during final-stage rifting: Implications for the development of seaward-dipping reflectors. *Geosphere*, *11*(3), 563–571. https://doi.org/10.1130/GES01076.1

Craig, T., Jackson, J., Priestley, K., & McKenzie, D. (2011). Earthquake distribution patterns in Africa: Their relationship to variations in lithospheric and geological structure, and their rheological implications. *Geophysical Journal International*, *185*(1), 403–434. https://doi.org/10.1111/j.1365-246X.2011.04950.x

Daly, E., Keir, D., Ebinger, C. J., Stuart, G. W., Bastow, I. D., & Ayele, A. (2008). Crustal tomographic imaging of a transitional continental rift: The Ethiopian rift. *Geophysical Journal International*, *172*(3), 1033–1048. https://doi.org/10.1111/j.1365-246X.2007.03682.x

Daniels, K., Bastow, I., Keir, D., Sparks, R., & Menand, T. (2014). Thermal models of dyke intrusion during development of continent-ocean transition. *Earth and Planetary Science Letters*, *385*, 145–153. https://doi.org/10.1016/j.epsl.2013.09.018

De Plaen, R., Bastow, I., Chambers, E., Keir, D., Gallacher, R., & Keane, J. (2014). The development of magmatism along the Cameroon Volcanic Line: Evidence from seismicity and seismic anisotropy. *Journal of Geophysical Research*, *119*, 4233–4252. https://doi.org/10.1002/2013JB010583

Debayle, E., Lévêque, J. J., & Cara, M. (2001). Seismic evidence for a deeply rooted low-velocity anomaly in the upper mantle beneath the northeastern Afro/Arabian continent. *Earth and Planetary Science Letters*, *193*(3–4), 423–436. https://doi.org/10.1016/S0012-821X(01)00509-X

DeMets, C., & Merkouriev, S. (2016). High-resolution estimates of Nubia–Somalia plate motion since 20 Ma from reconstructions of the Southwest Indian Ridge, Red Sea and Gulf of Aden. *Geophysical Journal International*, *207*(1), 317–332. https://doi.org/10.1093/gji/ggw276

Desissa, M., Johnson, N., Whaler, K., Hautot, S., Fisseha, S., & Dawes, G. (2013). A mantle magma reservoir beneath an incipient mid-ocean ridge in Afar, Ethiopia. *Nature Geoscience*, *6*(10), 861–865. https://doi.org/10.1038/ngeo1925

Dewey, J. F., Helman, M. L., Knott, S. D., Turco, E., & Hutton, D. H. W. (1989). Kinematics of the western Mediterranean. *Geological Society of London, Special Publication*, *45*(1), 265–283. https://doi.org/10.1144/GSL.SP.1989.045.01.15

Díaz, J., & Gallart, J. (2014). Seismic anisotropy from the Variscan Core of Iberia to the Western African Craton: New constraints on upper mantle flow at regional scales. *Earth and Planetary Science Letters*, *394*, 48–57. https://doi.org/10.1016/j.epsl.2014.03.005

Didana, Y. L., Thiel, S., & Heinson, G. (2014). Magnetotelluric imaging of upper crustal partial melt at Tendaho graben in Afar, Ethiopia. *Geophysical Research Letters*, *41*, 3089–3095. https://doi.org/10.1002/2014GL060000

Didana, Y. L., Thiel, S., & Heinson, G. (2015). Three dimensional conductivity model of the Tendaho High Enthalpy Geothermal Field, NE Ethiopia. *Journal of Volcanology and Geothermal Research*, *290*, 53–62. https://doi.org/10.1016/j.jvolgeores.2014.11.013

Dixon, J., Clague, D. A., Cousens, B., Monsalve, M. L., & Uhl, J. (2008). Carbonatite and silicate melt metasomatism of the mantle surrounding the Hawaiian plume: Evidence from volatiles, trace elements, and radiogenic isotopes in rejuvenated-stage lavas from Niihau, Hawaii. *Geochemistry, Geophysics, Geosystems*, *9*, Q09005. https://doi.org/10.1029/2008GC002076

Dorbath, C., Dorbath, L., Fairhead, J., & Stuart, G. (1986). A teleseismic delay time study across the Central African Shear Zone in the Adamawa Region of Cameroon, West Africa. *Geophysical Journal International*, *86*(3), 751–766. https://doi.org/10.1111/j.1365-246X.1986.tb00658.x

Doubre, C., Manighetti, I., Dorbath, L., Dorbath, C., Bertil, D., & Delmond, J. C. (2007). Crustal structure and magmato-tectonic processes in an active rift (Asal-Ghoubbet, Afar, East Africa): 2. Insights from the 23-year recording of seismicity since the last rifting event. *Journal of Geophysical Research*, *112*, B05406.

Dugda, M., Nyblade, A., Julià, J., Langston, C., Ammon, C., & Simiyu, S. (2005). Crustal structure in Ethiopia and Kenya from receiver function analysis. *Journal of Geophysical Research*, *110*, B01303. https://doi.org/10.1029/2004JB003065

Dugda, M., & Nyblade, A. A. (2006). New constraints on crustal structure in eastern Afar from the analysis of receiver functions and surface wave dispersion in Djibouti. *Geological Society, London, Special Publications*, *259*(1), 239–251. https://doi.org/10.1144/GSL.SP.2006.259.01.19

Duggen, S., Hoernle, K. A., Hauff, F., Klügl, A., Bouabdellah, M., & Thirlwall, M. (2009). Flow of Canary mantle plume material through a subcontinental lithospheric corridor beneath Africa to the Mediterranean. *Geology*, *37*(3), 283–286. https://doi.org/10.1130/G25426A.1

Duncan, R. A., Hooper, P. R., Rehacek, J., Marsh, J. S., & Duncan, A. R. (1997). The timing and duration of the Karoo igneous event, southern Gondwana. *Journal of Geophysical Research*, *102*(B8), 18,127–18,138. https://doi.org/10.1029/97JB00972

Ebinger, C., & Casey, M. (2001). Continental breakup in magmatic provinces: An Ethiopian example. *Geology*, *29*(6), 527–530. https://doi.org/10.1130/0091-7613(2001)029%3C0527:CBIMPA%3E2.0.CO;2

Ebinger, C., Keir, D., Ayele, A., Calais, E., Wright, T., Belachew, M., … Buck, W. (2008). Capturing magma intrusion and faulting processes during continental rupture: Seismicity of the Dabbahu (Afar) rift. *Geophysical Journal International*, *174*(3), 1138–1152. https://doi.org/10.1111/j.1365-246X.2008.03877.x

Ebinger, C., & Scholz, C. A. (2012). Continental rift basins: The East African perspective. In C. Busby & A. Azor (Eds.), *Tectonics of sedimentary basins: Recent advances* (pp. 183–208). Blackwell, NJ. https://doi.org/10.1002/9781444347166.ch9

Ebinger, C., & Sleep, N. (1998). Cenozoic magmatism throughout East Africa resulting from impact of a single plume. *Nature*, *395*(6704), 788–791. https://doi.org/10.1038/27417

Ebinger, C., Yemane, T., Harding, D., Tesfaye, S., Kelley, S., & Rex, D. (2000). Rift deflection, migration, and propagation: Linkage of the Ethiopian and Eastern rifts, Africa. *Bulletin Geological Society of America*, *112*(2), 163–176. https://doi.org/10.1130/0016-7606(2000)112%3C163:RDMAPL%3E2.0.CO;2

Faccenna, C., Piromallo, C., Crespo-Blanc, A., Jolivet, L., & Rossetti, F. (2004). Lateral slab deformation and the origin of the western Mediterranean Arcs. *Tectonics*, *23*, TC1012. https://doi.org/10.1029/2002TC001488

Fairhead, J. (1988). Mesozoic plate tectonic reconstructions of the central South Atlantic Ocean: The role of the West and Central African rift system. *Tectonophysics*, *155*(1–4), 181–191. https://doi.org/10.1016/0040-1951(88)90265-X

Fairhead, J., & Binks, R. (1991). Differential opening of the Central and South Atlantic Oceans and the opening of the West African rift system. *Tectonophysics*, *187*(1–3), 191–203. https://doi.org/10.1016/0040-1951(91)90419-S

Fairhead, J., & Okereke, C. (1987). A regional gravity study of the West African rift system in Nigeria and Cameroon and its tectonic interpretation. *Tectonophysics*, *143*(1–3), 141–159. https://doi.org/10.1016/0040-1951(87)90084-9

Ferguson, D. J., Maclennan, J., Bastow, I. D., Pyle, D. M., Keir, D., Blundy, J. D., … Yirgu, G. (2013). Melting during late stage rifting in Afar is hot and deep. *Nature*, *499*, 60–73.

Field, L. P., Blundy, J., Brooker, R. A., Wright, T. J., & Yirgu, G. (2012). Magma storage conditions beneath Dabbahu Volcano (Ethiopia) constrained by petrology, seismicity and satellite geodesy. *Bulletin of Volcanology*, *74*(5), 981–1004. https://doi.org/10.1007/s00445-012-0580-6

Field, L. P., Blundy, J., Calvert, A., & Yirgu, G. (2013). Magmatic history of Dabbahu, a composite volcano in the Afar Rift, Ethiopia. *GSA Bulletin*, *125*(1–2), 128–147. https://doi.org/10.1130/B30560.1

Fishwick, S. (2010). Surface wave tomography: Imaging of the lithosphere–asthenosphere boundary beneath central and southern Africa? *Lithos*, *120*(1–2), 63–73. https://doi.org/10.1016/j.lithos.2010.05.011

Fishwick, S., & Bastow, I. D. (2011). Towards a better understanding of African topography: A review of passive-source seismic studies of the African crust and upper mantle. *Geological Society of London, Special Publication*, *357*(1), 343–371. https://doi.org/10.1144/SP357.19

Fitton, J. (1980). The Benue Trough and Cameroon line—A migrating rift system in West Africa. *Earth and Planetary Science Letters*, *51*(1), 132–138. https://doi.org/10.1016/0012-821X(80)90261-7

Flesch, L., & Bendick, R. (2012). The relationship between surface kinematics and deformation of the whole lithosphere. *Geology*, *40*(8), 711–714. https://doi.org/10.1130/G33269.1

Fourel, L., Milelli, L., Jaupart, C., & Limare, A. (2013). Generation of continental rifts, basins, and swells by lithosphere instabilities. *Journal of Geophysical Research*, *118*, 3080–3100. https://doi.org/10.1002/jgrb.50218

Franke, D., Neben, S., Ladage, S., Schreckenberger, B., & Hinz, K. (2007). Margin segmentation and volcano-tectonic architecture along the volcanic margin off Argentina/Uruguay, South Atlantic. *Marine Geology*, *244*(1–4), 46–67. https://doi.org/10.1016/j.margeo.2007.06.009

Freeth, S. (1979). Deformation of the African plate as a consequence of membrane stress domains generated by Post-Jurassic Drift. *Earth and Planetary Science Letters*, *45*(1), 93–104. https://doi.org/10.1016/0012-821X(79)90111-0

Frezzotti, M. L., Ferrando, S., Peccerillo, A., Petrelli, M., Tecce, F., & Perucchi, A. (2010). Chlorine-rich metasomatic H_2O–CO_2 fluids in amphibole-bearing peridotites from Injibara (Lake Tana region, Ethiopian plateau): Nature and evolution of volatiles in the mantle of a region of continental flood basalts. *Geochimica et Cosmochimica Acta*, *74*(10), 3023–3039. https://doi.org/10.1016/j.gca.2010.02.007

Frizon de Lamotte, D. F., Leturmy, P., Missenard, Y., Khomsi, S., Ruiz, G., Saddiqi, O., … Michard, A. (2009). Mesozoic and Cenozoic vertical movements in the Atlas system (Algeria, Morocco, Tunisia): An overview. *Tectonophysics*, *475*(1), 9–28. https://doi.org/10.1016/j.tecto.2008.10.024

Fuis, G. S., & Mooney, W. D. (1990). Lithospheric structure and tectonics from seismic refraction and other data. In R. E. Wallace (Ed.), *The San Andreas Fault System, California*, *U.S. Geological Survey Professional Paper 1515* (pp. 207–236). Washington, DC: US Government Printing Office.

Fullea, J., Fernandez, M., Zeyen, H., & Vergés, J. (2007). A rapid method to map the crustal and lithospheric thickness using elevation, geoid anomaly and thermal analysis. Application to the Gibraltar Arc System, Atlas Mountains and adjacent zones. *Tectonophysics*, *430*(1–4), 97–117. https://doi.org/10.1016/j.tecto.2006.11.003

Furman, T. (2007). Geochemistry of East African Rift basalts: An overview. *Journal of African Earth Sciences*, *48*(2–3), 147–160. https://doi.org/10.1016/j.jafrearsci.2006.06.009

Furman, T., Bryce, J., Rooney, T., Hanan, B., Yirgu, G., & Ayalew, D. (2006). Heads and tails: 30 million years of the Afar plume. *Geological Society, London, Special Publications*, *259*(1), 95–119. https://doi.org/10.1144/GSL.SP.2006.259.01.09

Gallacher, R., & Bastow, I. (2012). The development of magmatism along the Cameroon Volcanic Line: Evidence from teleseismic receiver functions. *Tectonics*, *31*, TC3018. https://doi.org/10.1029/2011TC003028

Gao, S., Davis, P. M., Liu, H., Slack, P. D., Rigor, A. W., Zorin, Y. A., … Logatchev, N. A. (1997). SKS splitting beneath continental rift zones. *Journal of Geophysical Research*, *102*(B10), 22,781–22,797. https://doi.org/10.1029/97JB01858

Gao, S. S., Liu, K. H., Reed, C. A., Yu, Y., Massinque, B., Mdala, H., … Reusch, A. M. (2013). SAFARI-Seismic Arrays for African Rift. *Eos, Transactions American Geophysical Union*, *94*(24), 213–214. https://doi.org/10.1002/2013EO240002

Gomez, F., Beauchamp, W., & Barazangi, M. (2000). Role of the Atlas Mountains (Northwest Africa) within the African-Eurasian Plate-Boundary Zone. *Geology*, *28*(9), 775–778. https://doi.org/10.1130/0091-7613(2000)28%3C775:ROTAMN%3E2.0.CO;2

Grandin, R., Jacques, E., Nercessian, A., Ayele, A., Doubre, C., Socquet, A., … King, G. (2011). Seismicity during lateral dike propagation: Insights from new data in the recent Manda Hararo–Dabbahu rifting episode (Afar, Ethiopia). *Geochemistry, Geophysics, Geosystems*, *12*, Q0AB08. https://doi.org/10.1029/2010GC003434

Green, W. V., Achauer, U., & Meyer, R. P. (1991). A three-dimensional seismic image of the crust and upper mantle beneath the Kenya rift. *Nature*, *354*(6350), 199–203. https://doi.org/10.1038/354199a0

Guerri, M., Cammarano, F., & Connolly, J. A. (2015). Effects of chemical composition, water and temperature on physical properties of continental crust. *Geochemistry, Geophysics, Geosystems*, *16*(7), 2431–2449. https://doi.org/10.1002/2015GC005819

Guidarelli, M., Stuart, G., Hammond, J. O. S., Kendall, J. M., Ayele, A., & Belachew, M. (2011). Surface wave tomography across afar, Ethiopia: Crustal structure at a rift triple-junction zone. *Geophysical Research Letters*, *38*, L24313. https://doi.org/10.1029/2011GL046840

Guo, X., Zhang, L., Behrens, H., & Ni, H. (2016). Probing the status of felsic magma reservoirs: Constraints from the P–T–H_2O dependences of electrical conductivity of rhyolitic melt. *Earth and Planetary Science Letters*, *433*, 54–62. https://doi.org/10.1016/j.epsl.2015.10.036

Guth, A. L. (2016). Volcanic volumes associated with the Kenya Rift: Recognition and correction of preservation biases. *Geological Society of London, Special Publication*, *420*(1), 31–42. https://doi.org/10.1144/SP420.3

Hacker, B. R., Kelemen, P. B., & Behn, M. D. (2015). Continental lower crust. *Annual Review of Earth and Planetary Sciences*, *43*(1), 167–205. https://doi.org/10.1146/annurev-earth-050212-124117

Halldórsson, S. A., Hilton, D. R., Scarsi, P., Abebe, T., & Hopp, J. (2014). A common mantle plume source beneath the entire East African Rift System revealed by coupled helium-neon systematics. *Geophysical Research Letters*, *41*, 2304–2311. https://doi.org/10.1002/2014GL059424

Halliday, A., Davidson, J., Holden, P., DeWolf, C., Lee, D., & Fitton, J. (1990). Trace-element fractionation in plumes and the origin of HIMU mantle beneath the Cameroon line. *Nature*, *347*(6293), 523–528. https://doi.org/10.1038/347523a0

Hamilton, M. P., Jones, A. G., Evans, R. L., Evans, S., Fourie, C. J. S., Garcia, X., … Team, S. M. (2006). Electrical anisotropy of South African lithosphere compared with seismic anisotropy from shear-wave splitting analyses. *Physics of the Earth and Planetary Interiors*, *158*(2–4), 226–239. https://doi.org/10.1016/j.pepi.2006.03.027

Hamling, I., Ayele, A., Bennati, L., Calais, E., Ebinger, C., Keir, D., … Yirgu, G. (2009). Geodetic observations of the ongoing Dabbahu rifting episode: New dyke intrusions in 2006 and 2007. *Geophysical Journal International*, *178*(2), 989–1003. https://doi.org/10.1111/j.1365-%20246X.2009.04163.x

Hammond, J., Kendall, J.-M., Stuart, G., Ebinger, C., Bastow, I., Keir, D., … Wright, T. J. (2013). Mantle upwelling and initiation of rift segmentation beneath the Afar Depression. *Geology*, *41*(6), 635–638. https://doi.org/10.1130/G33925.1

Hammond, J., Kendall, J.-M., Stuart, G., Keir, D., Ebinger, C., Ayele, A., & Belachew, M. (2011). The nature of the crust beneath the Afar triple junction: Evidence from receiver functions. *Geochemistry, Geophysics, Geosystems*, *12*, Q12004. https://doi.org/10.1029/2011GC003738

Hammond, J. O. S. (2014). Constraining melt geometries beneath the Afar depression, Ethiopia from teleseismic receiver functions: The anisotropic H-K stacking technique. *Geochemistry, Geophysics, Geosystems*, *15*, 1316–1332. https://doi.org/10.1002/2013GC005186

Hautot, S., & Tarits, P. (2015). Rift structure and basin control revealed by 3-D magneto telluric data: Examples of Turkana and Northern Tanzania. In *First EAGE Eastern Africa Petroleum Geoscience Forum*. Dar es Salaam, Tanzania. https://doi.org/10.3997/2214-4609.201414466

Hautot, S., Tarits, P., Whaler, K., Le Gall, B., Tiercelin, J. J., & Le Turdu, C. (2000). Deep structure of the Baringo Rift Basin (central Kenya) from three-dimensional magnetotelluric imaging: Implications for rift evolution. *Journal of Geophysical Research*, *105*(B10), 23493–23518. https://doi.org/10.1029/2000JB900213

Hayward, N., & Ebinger, C. (1996). Variations in the along-axis segmentation of the Afar rift system. *Tectonics*, *15*(2), 244–257. https://doi.org/10.1029/95TC02292

Hendrie, D. B., Kusznir, N. J., Morley, C. K., & Ebinger, C. J. (1994). Cenozoic extension in northern Kenya: A quantitative model of rift basin development in the Turkana region. *Tectonophysics*, *236*(1–4), 409–438. https://doi.org/10.1016/0040-1951(94)90187-2

Hodgson, I., Illsley-Kemp, F., Keir, D., Ebinger, C. J., & Mtelela, K. (2017). Crustal structure at a young continental rift: A receiver function study from the Tanganyika Rift. *Tectonics*, *36*. https://doi.org/10.1002/2017TC004477

Hübert, J., Whaler, K., & Fisseha, S. (2016). From 'shoulder to shoulder'—A cross-rift magnetotelluric transect through Aluto volcano, Ethiopia, Abstract for the 23rd Electromagnetic Induction in the Earth Workshop, Chiang Mai, Thailand.

Hutchison, W., Biggs, J., Mather, T. A., Pyle, D. M., Lewi, E., Yirgu, G., … Fischer, T. P. (2016). Causes of unrest at silicic calderas in the East African Rift: New constraints from InSAR and soil-gas chemistry at Aluto volcano, Ethiopia. *Geochemistry, Geophysics, Geosystems*, *17*, 3008–3030. https://doi.org/10.1002/2016GC006395

Ibs-von Seht, M., Blumenstein, S., Wagner, R., Hollnack, D., & Wohlenberg, J. (2001). Seismicity, seismotectonics and crustal structure of the southern Kenya rift-new data from the Lake Magadi area. *Geophysical Journal International*, *146*(2), 439–453. https://doi.org/10.1046/j.0956-540x.2001.01464.x

Jessell, M. W., Begg, G. C., & Miller, M. S. (2016). The geophysical signatures of the West African Craton. *Precambrian Research*, *274*, 3–24. https://doi.org/10.1016/j.precamres.2015.08.010

Johnson, N.E. (2012). Magnetotelluric studies of the crust and upper mantle in a zone of active continental breakup, Afar, Ethiopia, unpublished PhD thesis, University of Edinburgh.

Johnson, N. E., Whaler, K. A., Hautot, S., Fisseha, S., Desissa, M., & Dawes, G. J. K. (2016). Magma imaged magnetotellurically beneath an active and an inactive magmatic segment in Afar, Ethiopia. *Geological Society of London, Special Publication*, *420*(1), 105–125. https://doi.org/10.1144/SP420.11

Jones, A. P., Smith, J. V., Dawson, J. B., & Hansen, E. C. (1983). Metamorphism, partial melting, and K-metasomatism of garnet-scapolite-kyanite granulite xenoliths from Lashaine, Tanzania. *Journal of Geology*, *91*(2), 143–165. https://doi.org/10.1086/628753

Kaislaniemi, L., & van Hunen, J. (2014). Dynamics of lithospheric thinning and mantle melting by edge-driven convection: Application to Moroccan Atlas mountains. *Geochemistry, Geophysics, Geosystems*, *15*, 3175–3189. https://doi.org/10.1002/2014GC005414

Keir, D., Bastow, I., Corti, G., Mazzarini, F., & Rooney, T. (2015). The origin of along-rift variations in faulting and magmatism in the Ethiopian Rift. *Tectonics*, *34*, 464–477. https://doi.org/10.1002/2014TC003698

Keir, D., Bastow, I., Whaler, K., Daly, E., Cornwell, D., & Hautot, S. (2009). Lower crustal earthquakes near the Ethiopian rift induced by magmatic processes. *Geochemistry, Geophysics, Geosystems*, *10*, Q0AB02. https://doi.org/10.1029/2009GC002382

Keir, D., Belachew, M., Ebinger, C. J., Kendall, J.-M., Hammond, J. O. S., Stuart, G. W., … Rowland, J. V. (2011a). Mapping the evolving strain field during continental breakup from crustal anisotropy in the Afar Depression. *Nature Communications*, *2*, 285. https://doi.org/10.1038/ncomms1287

Keir, D., Belachew, M., Ebinger, C., Kendall, J.-M., Hammond, J., Stuart, G., … Rowland, J. (2011b). Mapping the evolving strain field during continental breakup from crustal anisotropy in the Afar Depression. *Nature Communications*, *2*, 285. https://doi.org/10.1038/ncomms1287

Keller, G. R., Mechie, J., Braile, L. W., Mooney, W. D., & Prodehl, C. (1994). Seismic structure of the uppermost mantle beneath the Kenya rift. *Tectonophysics*, *236*(1–4), 201–216. https://doi.org/10.1016/0040-1951(94)90177-5

Kendall, J. M., & Lithgow-Bertelloni, C. (2016). Why is Africa rifting? *Geological Society, London, Special Publications*, *420*(1), 11–30. https://doi.org/10.1144/SP420.17

Keranen, K., Klemperer, S., Gloaguen, R., & EAGLE Working Group (2004). Three-dimensional seismic imaging of a protoridge axis in the main Ethiopian rift. *Geology*, *32*(11), 949–952. https://doi.org/10.1130/G20737.1

Keranen, K., & Klemperer, S. L. (2008). Discontinuous and diachronous evolution of the Main Ethiopian Rift: Implications for development of continental rifts. *Earth and Planetary Science Letters*, *265*(1–2), 96–111. https://doi.org/10.1016/j.epsl.2007.09.038

Keranen, K. M., Klemperer, S. L., Julia, J., Lawrence, J. F., & Nyblade, A. A. (2009). Low lower crustal velocity across Ethiopia: Is the Main Ethiopian Rift a narrow rift in a hot craton? *Geochemistry, Geophysics, Geosystems*, *10*, Q0AB01. https://doi.org/10.1029/2008GC002293

Khan, M. A., Mechie, J., Birt, C., Byrne, G., Gaciri, S., Jacob, B., … Patel, J. P. (1999). The lithospheric structure of the Kenya Rift as revealed by wide-angle seismic measurements. *Geological Society, London, Special Publications*, *164*(1), 257–269. https://doi.org/10.1144/GSL.SP.1999.164.01.13

Kim, S., Nyblade, A. A., Rhie, J., Baag, C.-E., & Kang, T.-S. (2012). Crustal S-wave velocity structure of the Main Ethiopian Rift from ambient noise tomography. *Geophysical Journal International*, *191*(2), 865–878. https://doi.org/10.1111/j.1365-246x.2012.05664.x

King, S., & Anderson, D. (1998). Edge-driven convection. *Earth and Planetary Science Letters*, *160*(3–4), 289–296. https://doi.org/10.1016/S0012-821X(98)00089-2

King, S., & Ritsema, J. (2000). African hot spot volcanism: Small-scale convection in the upper mantle beneath cratons. *Science*, *290*(5494), 1137–1140. https://doi.org/10.1126/science.290.5494.1137

Korenaga, J., Holbrook, W. S., Kent, G. M., Kelemen, P. B., Detrick, R. S., Larsen, H.-C., … Dahl-Jensen, T. (2000). Crustal structure of the southeast Greenland margin from joint refraction and reflection seismic tomography. *Journal of Geophysical Research*, *105*(B9), 21,591–21,614. https://doi.org/10.1029/2000JB900188

Korostelev, F., Weemstra, C., Leroy, S., Boschi, L., Keir, D., Ren, Y., … Ayele, A. (2015). Magmatism on rift flanks: Insights from ambient-noise phase velocity in Afar region. *Geophysical Research Letters*, *42*, 2179–2188. https://doi.org/10.1002/2015GL063259

Kgaswane, E. M., Nyblade, A. A., Julià, J., Dirks, P. H. G. M., Durrheim, R. J., & Pasyanos, M. E. (2009). Shear wave velocity structure of the lower crust in southern Africa: Evidence for compositional heterogeneity within Archaean and Proterozoic terrains. *Journal of Geophysical Research*, *114*, B12304. https://doi.org/10.1029/2008JB006217

Last, R. J., Nyblade, A. A., Langston, C. A., & Owens, T. J. (1997). Crustal structure of the East African Plateau from receiver functions and Rayleigh wave phase velocities. *Journal of Geophysical Research*, *102*(B11), 24,469–24,483. https://doi.org/10.1029/97JB02156

Ledo, J., Jones, A. G., Siniscalchi, A., Campanyà, J., Kiyan, D., Romano, G., … TopoMed MT Team (2011). Electrical signature of modern and ancient tectonic processes in the crust of the Atlas mountains of Morocco. *Physics of the Earth and Planetary Interiors*, *185*(3–4), 82–88. https://doi.org/10.1016/j.pepi.2011.01.008

Lee, H., Muirhead, J. D., Fischer, T., Ebinger, C. J., Kattenhorn, S., & Kianji, G. (2016). Tectonic degassing of mantle-derived CO2 along faults in the East African Rift. *Nature Geoscience*, *9*(2), 145–149. https://doi.org/10.1038/ngeo2622

Leroy, S., d'Acremont, E., Tiberi, C., Basuyau, C., Autin, J., Lucazeau, F., & Sloan, H. (2010). Recent off-axis volcanism in the eastern Gulf of Aden: Implications for plume–ridge interaction. *Earth and Planetary Science Letters*, *293*(1–2), 140–153. https://doi.org/10.1016/j.epsl.2010.02.036

Levander, A., Bezada, M. J., Niu, F., Humphreys, E. D., Palomeras, I., Thurner, S. M., … Miller, M. S. (2014). Subduction-driven recycling of continental margin lithosphere. *Nature*, *515*(7526), 253–256. https://doi.org/10.1038/nature13878

Lewi, E., Keir, D., Birhanu, Y., Blundy, J., Stuart, G., Wright, T., & Calais, E. (2015). Use of a high-precision gravity survey to understand the formation of oceanic crust and the role of melt at the southern Red Sea rift in Afar, Ethiopia. In T. J. Wright, et al. (Eds), *Magmatic rifting and active volcanism*. *Geological Society, London, Special Publications*, *420*, 165–180. https://doi.org/10.1144/SP420.13

Ligi, M., Bonatti, E., Tonotini, F. C., Cipriani, A., Cocchi, L., Schettino, A., … Rasul, N. (2011). Initial burst of oceanic crust accretion in the Red Sea due to edge-driven mantle convection. *Geology*, *39*(11), 1019–1022. https://doi.org/10.1130/G32243.1

Lowry, A. R., & Pérez-Gussinyé, M. (2011). The role of crustal quartz in controlling cordilleran deformation. *Nature*, *471*(7338), 353–357. https://doi.org/10.1038/nature09912

Maccaferri, F., Bonafede, M., & Rivalta, E. (2011). A quantitative study of the mechanisms governing dike propagation, dike arrest and sill formation. *Journal of Volcanology and Geothermal Research*, *208*(1–2), 39–50. https://doi.org/10.1016/j.jvolgeores.2011.09.001

Macdonald, R. (1994). Petrological evidence regarding the evolution of the Kenya Rift Valley. *Tectonophysics*, *236*(1–4), 373–390. https://doi.org/10.1016/0040-1951(94)90185-6

Mackenzie, G., Thybo, H., & Maguire, P. (2005). Crustal velocity structure across the Main Ethiopian Rift: Results from 2-dimensional wide-angle seismic modelling. *Geophysical Journal International*, *162*(3), 994–1006. https://doi.org/10.1111/j.1365-246X.2005.02710.x

Magee, C., Bastow, I. D., de Vries, B. V. W., Jackson, C. A. L., Hetherington, R., Hagos, M., & Hoggett, M. (2017). Structure and dynamics of surface uplift induced by incremental sill emplacement. *Geology*, *45*(5), 431–434. https://doi.org/10.1130/G38839.1

Maguire, P., Keller, G., Klemperer, S., Mackenzie, G., Harder, S., O'Reilly, B., … Amha, M. (2006). Crustal structure of the northern Main Ethiopian Rift from the EAGLE controlled-source survey: A snapshot of incipient lithospheric break-up. In G. Yirgu, C. J. Ebinger, & P. K. H. Maguire (Eds.), *The Afar Volcanic Province within the East African Rift System*, *Geological Society, London Special Publications* (Vol. 259, pp. 271–293).

Maguire, P. K. H., Swain, C. J., Masotti, R., & Khan, M. A. (1994). A crustal and uppermost mantle cross-sectional model of the Kenya Rift derived from seismic and gravity data. *Tectonophysics*, *236*(1–4), 217–249. https://doi.org/10.1016/0040-1951(94)90178-3

Mahatsente, R., Jentzsch, G., & Jahr, T. (1999). Crustal structure of the Main Ethiopian Rift from gravity data: 3-dimensional modeling. *Tectonophysics*, *313*(4), 363–382. https://doi.org/10.1016/S0040-1951(99)00213-9

Makris, J., & Ginzburg, A. (1987). The Afar Depression: Transition between continental rifting and sea floor spreading. *Tectonophysics*, *141*(1–3), 199–214. https://doi.org/10.1016/0040-1951(87)90186-7

Mana, S., Furman, T., Carr, M. J., Mollel, G. F., Mortlock, R. A., Feigenson, M. D., … Swisher, C. C. (2012). Geochronology and geochemistry of the Essimingor volcano: Melting of metasomatized lithospheric mantle beneath the North Tanzanian Divergence zone (East African Rift). *Lithos*, *155*, 310–325. https://doi.org/10.1016/j.lithos.2012.09.009

Mana, S., Furman, T., Turrin, B. D., Feigenson, M. D., & Swisher, C. C. (2015). Magmatic activity across the East African North Tanzanian Divergence Zone. *Journal of the Geological Society*, *2014-072*.

Mancilla, F., & Diaz, J. (2015). High resolution Moho topography map beneath Iberia and Northern Morocco from receiver function analysis. *Tectonophysics*, *663*, 203–211. https://doi.org/10.1016/j.tecto.2015.06.017

Manighetti, I., Tapponnier, P., Gillot, P. Y., Jacques, E., Courtillot, V., Armijo, R., … King, G. (1998). Propagation of rifting along the Arabia-Somalia plate boundary: Into Afar. *Journal of Geophysical Research*, *103*(B3), 4947–4974. https://doi.org/10.1029/97JB02758

Mansur, A. T., Manya, S., Timpa, S., & Rudnick, R. L. (2014). Granulite-facies xenoliths in rift basalts of northern Tanzania: Age, composition and origin of lower crust. *Journal of Petrology*, *55*(7), 1243–1286. https://doi.org/10.1093/petrology/egu024

Marty, B., & Yirgu, G. (1996). Helium isotopic variations in Ethiopian plume lavas: Nature of magmatic sources and limit on lower mantle contribution. *Earth and Planetary Science Letters*, *144*(1–2), 223–237. https://doi.org/10.1016/0012-821X(96)00158-6

Marzoli, A., Piccirillo, E., Renne, P., Bellieni, G., Iacumin, M., Nyobe, J., & Tongwa, A. (2000). The Cameroon volcanic line revisited: Petrogenesis of continental basaltic magmas from lithospheric and asthenospheric mantle sources. *Journal of Petrology*, *41*(1), 87–109. https://doi.org/10.1093/petrology/41.1.87

Mattsson, H. B., Nandedkar, R. H., & Ulmer, P. (2013). Petrogenesis of the melilititic and nephelinitic rock suites in the Lake Natron–Engaruka monogenetic volcanic field, northern Tanzania. *Lithos*, *179*, 175–192. https://doi.org/10.1016/j.lithos.2013.07.012

Mazzarini, F., Rooney, T., & Isola, I. (2013). The intimate relationship between strain and magmatism: A numerical treatment of clustered monogenetic fields in the Main Ethiopian Rift. *Tectonics*, *32*, 49–64. https://doi.org/10.1029/2012TC003146

McKenzie, D., & Davies, D. (1970). Plate tectonics of the Red Sea and East Africa. *Nature*, *226*(5242), 243–248. https://doi.org/10.1038/226243a0

Mechie, J., Fuchs, K., & Altherr, R. (1994). The relationship between seismic velocity, mineral composition and temperature and pressure in the upper mantle—With an application to the Kenya Rift and its eastern flank. *Tectonophysics*, *236*(1–4), 453–464. https://doi.org/10.1016/0040-1951(94)90189-9

Mechie, J., Keller, G. R., Prodehl, C., Gaciri, S., Braile, L. W., Mooney, W. D., … Sandmeier, K. J. (1994). Crustal structure beneath the Kenya Rift from axial profile data. *Tectonophysics*, *236*(1–4), 179–200. https://doi.org/10.1016/0040-1951(94)90176-7

Medynski, S., Pik, R., Burnard, P., Vye-Brown, C., France, L., Schimmelpfennig, I., … Yirgu, G. (2015). Stability of rift axis magma reservoirs: Spatial and temporal evolution of magma supply in the Dabbahu rift segment (Afar, Ethiopia) over the past 30 kyr. *Earth and Planetary Science Letters*, *409*, 278–289. https://doi.org/10.1016/j.epsl.2014.11.002

Meju, M. A., & Sakkas, V. (2007). Heterogeneous crust and upper mantle across southern Kenya and the relationship to surface deformation as inferred from magnetotelluric imaging. *Journal of Geophysical Research*, *112*, B04103. https://doi.org/10.1029/2005JB004028

Mériaux, C. A., Duarte, J. C., Duarte, S. S., Schellart, W. P., Chen, Z., Rosas, F., … Terrinha, P. (2015). Capture of the Canary mantle plume material by the Gibraltar arc mantle wedge during slab rollback. *Geophysical Journal International*, *201*(3), 1717–1721. https://doi.org/10.1093/gji/ggv120

Mériaux, C. A., Mansour, J. A., Moresi, L. N., Kerr, R. C., & May, D. A. (2011). On the rise of strongly tilted mantle plume tails. *Physics of the Earth and Planetary Interiors*, *184*(1–2), 63–79. https://doi.org/10.1016/j.pepi.2010.10.013

Meyers, J., Rosendahl, B., Harrison, G., & Ding, Z.-D. (1998). Deep–imaging seismic and gravity results from the offshore Cameroon Volcanic Line, and speculation of African hotlines. *Tectonophysics*, *284*(1–2), 31–63. https://doi.org/10.1016/S0040-1951(97)00173-X

Milelli, L., Fourel, L., & Jaupart, C. (2012). A lithospheric instability origin for the Cameroon Volcanic Line. *Earth and Planetary Science Letters*, *335–336*, 80–87. https://doi.org/10.1016/j.epsl.2012.04.028

Miller, M. S., Allam, A., Becker, T. W., Di Leo, J. F., & Wookey, J. (2013). Constraints on the tectonic evolution of the westernmost Mediterranean and Northwestern Africa from shear wave splitting analysis. *Earth and Planetary Science Letters*, *375*, 234–243. https://doi.org/10.1016/j.epsl.2013.05.036

Miller, M. S., & Becker, T. W. (2014). Reactivated lithospheric-scale discontinuities localize dynamic uplift of the Moroccan Atlas Mountains. *Geology*, *42*(1), 35–38. https://doi.org/10.1130/g34959.1

Miller, M. S., O'Driscoll, L. J., Butcher, A. J., & Thomas, C. (2015). Imaging Canary Island hotspot material beneath the lithosphere of Morocco and Spain. *Earth and Planetary Science Letters*, *431*, 186–194. https://doi.org/10.1016/j.epsl.2015.09.026

Missenard, Y., & Cadoux, A. (2012). Can Moroccan Atlas lithospheric thinning and volcanism be induced by edge-driven convection? *Terra Nova*, *24*(1), 27–33. https://doi.org/10.1111/j.1365-3121.2011.01033.x

Missenard, Y., Zeyen, H., Frizon de Lamotte, D., Leturmy, P., Petit, C., Sébrier, M., & Saddiqi, O. (2006). Crustal versus asthenospheric origin of relief of the Atlas Mountains of Morocco. *Journal of Geophysical Research*, *111*, B03401. https://doi.org/10.1029/2005JB003708

Mohr, P. (1972). Surface structure and plate tectonics of Afar. *Tectonophysics*, *15*(1–2), 3–18. https://doi.org/10.1016/0040-1951(72)90045-5

Mohr, P. (1989). Nature of the crust under Afar—New igneous, not thinned continental. *Tectonophysics*, *167*(1), 1–11. https://doi.org/10.1016/0040-1951(89)90290-4

Mohriak, W. U., Szatmari, P., & Anjos, S. (2012). Salt: Geology and tectonics of selected Brazilian basins in their global context. *Geological Society of London, Special Publication*, *363*(1), 131–158. https://doi.org/10.1144/SP363.7

Moreau, C., Regnoult, J., Déruelle, B., & Robineau, B. (1987). A new tectonic model for the Cameroon Line, Central Africa. *Tectonophysics*, *141*(4), 317–334. https://doi.org/10.1016/0040-1951(87)90206-X

Morley, C. K., Karanja, F. M., Wescott, W. A., Stone, D. M., Harper, R. M., Wigger, S. T., & Day, R. A. (1999). *AAPG Studies in Geology# 44, chapter 2: Geology and geophysics of the Western Turkana Basins* (pp. 19–54). Tulsa, OK: AAPG Publishing.

Morley, C. K., Wescott, W. A., Stone, D. M., Harper, R. M., Wigger, S. T., & Karanja, F. M. (1992). Tectonic evolution of the northern Kenyan Rift. *Journal of the Geological Society of London*, *149*(3), 333–348. https://doi.org/10.1144/gsjgs.149.3.0333

Morrissey, A., & Scholz, C. A. (2014). Paleohydrology of Lake Turkana and its influence on the Nile River system. *Palaeogeography, Palaeoclimatology, Palaeoecology*, *403*, 88–100. https://doi.org/10.1016/j.palaeo.2014.03.029

Muhongo, S., & Lenoir, J. L. (1994). Pan-African granulite-facies metamorphism in the Mozambique Belt of Tanzania: U-Pb zircon geochronology. *Journal of the Geological Society*, *151*(2), 343–347. https://doi.org/10.1144/gsjgs.151.2.0343

Muirhead, J. D., Kattenhorn, S. A., Lee, H., Fischer, T. P., Mana, S., Turrin, B., … Stamps, D. S. (2016). Evolution of upper crustal faulting assisted by magmatic volatile release during continental rift initiation in the East Africa Rift. *Geosphere*, *12*(6), 1670–1700. https://doi.org/10.1130/GES01375.1

Mulibo, G. D., & Nyblade, A. A. (2009). The 1994–1995 Manyara and Kwamtoro earthquake swarms: Variation in the depth extent of seismicity in Northern Tanzania. *South African Journal of Geology*, *112*(3–4), 387–404. https://doi.org/10.2113/gssajg.112.3-4.387

Mulibo, G. D., & Nyblade, A. A. (2013). The P and S wave velocity structure of the mantle beneath eastern Africa and the African superplume anomaly. *Geochemistry, Geophysics, Geosystems*, *14*, 2696–2715. https://doi.org/10.1002/ggge.20150

Nguuri, T. K., Gore, J., James, D. E., Webb, S. J., Wright, C., Zengeni, T. G., … Snoke, J. A. (2001). Crustal structure beneath southern Africa and its implications for the formation and evolution of the Kaapvaal and Zimbabwe cratons. *Geophysical Research Letters*, *28*(13), 2501–2504. https://doi.org/10.1029/2000GL012587

Niemeijer, A. R., & Spiers, C. J. (2006). Velocity dependence of strength and healing behaviour in simulated phyllosilicate-bearing fault gouge. *Tectonophysics*, *427*(1–4), 231–253. https://doi.org/10.1016/j.tecto.2006.03.048

Nkouathio, D., Kagou Dongmo, A., Bardintzeff, J., Wandji, P., Bellon, H., & Pouclet, A. (2008). Evolution of volcanism in graben and horst structures along the Cenozoic Cameroon Line (Africa): Implications for tectonic evolution and nantle source composition. *Mineralogy and Petrology*, *94*(3–4), 287–303. https://doi.org/10.1007/s00710-008-0018-1

Nobile, A., Pagli, C., Keir, D., Wright, T., Ayele, A., Ruch, J., & Acocella, V. (2012). Dike-fault interaction during the 2004 Dallol intrusion at the northern edge of the Erta Ale Ridge (Afar, Ethiopia). *Geophysical Research Letters*, *39*, L19305. https://doi.org/10.1029/2012GL053152

Nyblade, A. A., Pollack, H. N., Jones, D. L., Podmore, F., & Mushayandebvu, M. (1990). Terrestrial heat flow in east and southern Africa. *Journal of Geophysical Research*, *95*(B11), 17,371–17,384. https://doi.org/10.1029/JB095iB11p17371

Nyblade, A. A., & Robinson, S. W. (1994). The African superswell. *Geophysical Research Letters*, *21*(9), 765–768. https://doi.org/10.1029/94GL00631

O'Donnell, J. P., Adams, A., Nyblade, A. A., Mulibo, G. D., & Tugume, F. (2013). The uppermost mantle shear wave velocity structure of eastern Africa from Rayleigh wave tomography: Constraints on rift evolution. *Geophysical Journal International*, *194*(2), 961–978. https://doi.org/10.1093/gji/ggt135

Padilha, A., Vitorello, I., Pádua, M., & Bologna, M. (2006). Lithospheric and sublithospheric anisotropy beneath central-southeastern Brazil constrained by long period magnetotelluric data. *Physics of the Earth and Planetary Interiors*, *158*(2–4), 190–209. https://doi.org/10.1016/j.pepi.2006.05.006

Pagli, C., Wright, T. J., Ebinger, C. J., Yun, S. H., Cann, J. R., Barnie, T., & Ayele, A. (2012). Shallow axial magma chamber at the slow-spreading Erta Ale Ridge. *Nature Geoscience*, *5*(4), 284–288. https://doi.org/10.1038/ngeo1414

Palomeras, I., Thurner, S., Levander, A., Liu, K., Villasenor, A., Carbonell, R., & Harnafi, M. (2014). Finite-frequency Rayleigh wave tomography of the Western Mediterranean: Mapping its lithospheric structure. *Geochemistry, Geophysics, Geosystems*, *15*, 140–160. https://doi.org/10.1002/2013GC004861.

Perez-Gussinyé, M., Metois, M., Fernandez, M., Verges, J., Fullea, J., & Lowry, A. (2009). Effective elastic thickness of Africa and its relationship to other proxies for lithospheric structure and surface tectonics. *Earth and Planetary Science Letters*, *287*(1–2), 152–167. https://doi.org/10.1016/j.epsl.2009.08.004

Persaud, P., Ma, Y., Stock, J. M., Hole, J. A., Fuis, G. S., & Han, L. (2016). Fault zone characteristics and basin complexity in the southern Salton trough, California. *Geology*, *44*(9), 747–750. https://doi.org/10.1130/G38033.1

Pik, R., Marty, B., & Hilton, D. R. (2006). How many mantle plumes in Africa? The geochemical point of view. *Chemical Geology*, *226*(3–4), 100–114. https://doi.org/10.1016/j.chemgeo.2005.09.016

Pique, A., Tricart, P., Guiraud, R., Laville, E., Bouaziz, S., Amrhar, M., & Ait Ouali, R. (2002). The Mesozoic–Cenozoic Atlas Belt (North Africa): An overview. *Geodinamica Acta*, *15*(3), 185–208.

Plasman, M., Tiberi, C., Ebinger, C., Roecker, S., Gautier, S., Albaric, J., … Gama, R. (2017). Lithospheric structure of the North Tanzanian Divergence, East African rift, estimated from receiver functions. *Geophysical Journal International*, *210*(1), 465–481. https://doi.org/10.1093/gji/ggx177

Plomerova, J., Babuska, V., Dorbath, C., Dorbath, L., & Lillie, R. (1993). Deep lithospheric structure across the central African shear zone in Cameroon. *Geophysical Journal International*, *115*(2), 381–390. https://doi.org/10.1111/j.1365-246X.1993.tb01193.x

Pommier, A., & Le Trong, E. (2011). SIGMELTS: A web portal for electrical conductivity calculations in geosciences. *Computers and Geosciences*, *37*(9), 1450–1459. https://doi.org/10.1016/j.cageo.2011.01.002

Poudjom Djomani, Y., Diament, M., & Albouy, Y. (1992). Mechanical behaviour of the lithosphere beneath the Adamawa Uplift (Cameroon, West Africa) based on gravity data. *Journal of African Earth Sciences*, *15*(1), 81–90. https://doi.org/10.1016/0899-5362(92)90009-2

Poudjom Djomani, Y., Diament, M., & Wilson, M. (1997). Lithospheric structure across the Adamawa Plateau (Cameroon) from gravity studies. *Tectonophysics*, *273*(3–4), 317–327. https://doi.org/10.1016/S0040-1951(96)00280-6

Prodehl, C., Jacob, A. W. B., Thybo, H., Dindi, E., & Stangl, R. (1994). Crustal structure on the northeastern flank of the Kenya rift. *Tectonophysics*, *236*(1–4), 271–290. https://doi.org/10.1016/0040-1951(94)90180-5

Prodehl, C., & Mechie, J. (1991a). Large-scale variation in lithospheric structure along and across the Kenya rift. *Nature*, *354*(6350), 223.

Prodehl, C., & Mechie, J. (1991b). Crustal thinning in relationship to the evolution of the Afro-Arabian rift system: A review of seismic refraction data. *Tectonophysics*, *198*(2–4), 311–327. https://doi.org/10.1016/0040-1951(91)90158-O

Purcell, P. (1976). The Marda fault zone, Ethiopia. *Nature*, *261*(5561), 569–571. https://doi.org/10.1038/261569a0

Redfield, T., Wheeler, W., & Often, M. (2003). A kinematic model for the development of the Afar Depression and its paleogeographic implications. *Earth and Planetary Science Letters*, *216*(3), 383–398. https://doi.org/10.1016/S0012-821X(03)00488-6

Reed, C. A., Almadani, S., Gao, S. S., Elsheikh, A. A., Cherie, S., Abdelsalam, M. G., … Liu, K. H. (2014). Receiver function constraints on crustal seismic velocities and partial melting beneath the Red Sea rift and adjacent regions, Afar Depression. *Journal of Geophysical Research*, *119*, 2138–2152. https://doi.org/10.1002/2013JB010719

Reisberg, L., Lorand, J. P., & Bedini, R. M. (2004). Reliability of Os model ages in pervasively metasomatized continental mantle lithosphere: A case study of Sidamo spinel peridotite xenoliths (East African Rift, Ethiopia). *Chemical Geology*, *208*(1–4), 119–140. https://doi.org/10.1016/j.chemgeo.2004.04.008

Reusch, A., Nyblade, A., Wiens, D., Shore, P., Ateba, B., Tabod, C., & Nnange, J. (2010). Upper mantle structure beneath Cameroon from body wave tomography and the origin of the Cameroon Volcanic Line. *Geochemistry, Geophysics, Geosystems*, *11*, Q10W07. https://doi.org/10.1029/2010GC003200

Ritsema, J., van Heijst, H. J., & Woodhouse, J. H. (1999). Complex shear wave velocity structure imaged beneath Africa and Iceland. *Science*, *286*(5446), 1925–1928. https://doi.org/10.1126/science.286.5446.1925

Roecker, S., Ebinger, C., Tiberi, C., Mulibo, G., Ferdinand-Wambura, R., Mtelela, K., … Peyrat, S. (2017). Subsurface images of the Eastern Rift, Africa, from the joint inversion of body waves, surface waves, and gravity: Investigating the role of fluids in early-stage continental rifting. *Geophysical Journal International*, *210*(2), 931–950. https://doi.org/10.1093/gji/ggx220

Rooney, T., Bastow, I., & Keir, D. (2011). Insights into extensional processes during magma assisted rifting: Evidence from aligned scoria cones. *Journal of Volcanology and Geothermal Research*, *201*(1–4), 83–96. https://doi.org/10.1016/j.jvolgeores.2010.07.019

Rooney, T., Bastow, I., Keir, D., Mazzarini, F., Movsesian, E., Grosfils, E., … Yirgu, G. (2014). The protracted development of focused magmatic intrusion during continental rifting. *Tectonics*, *33*, 875–897. https://doi.org/10.1002/2013TC003514

Rooney, T., Furman, T., Bastow, I., Ayalew, D., & Yirgu, G. (2007). Lithospheric modification during crustal extension in the Main Ethiopian Rift. *Journal of Geophysical Research*, *112*, B10201. https://doi.org/10.1029/2006JB004916

Rooney, T. O., Mohr, P., Dosso, L., & Hall, C. (2013). Geochemical evidence of mantle reservoir evolution during progressive rifting along the western Afar margin. *Geochimica et Cosmochimica Acta*, *102*, 65–88. https://doi.org/10.1016/j.gca.2012.08.019

Rooney, T. O., Nelson, W. R., Ayalew, D., Hanan, B., Yirgu, G., & Kappelman, J. (2017). Melting the lithosphere: Metasomes as a source for mantle-derived magmas. *Earth and Planetary Science Letters*, *461*, 105–118. https://doi.org/10.1016/j.epsl.2016.12.010

Rosenbaum, G., & Lister, G. S. (2004). Formation of arcuate orogenic belts in the western Mediterranean region. *Geological Society of America Special Papers*, *383*, 41–56.

Rudnick, R. L., McDonough, W. F., & Chappell, B. W. (1993). Carbonatite metasomatism in the northern Tanzanian mantle: Petrographic and geochemical characteristics. *Earth and Planetary Science Letters*, *114*(4), 463–475. https://doi.org/10.1016/0012-821X(93)90076-L

Ruegg, J. C. (1975). Main results about the crustal and upper mantle structure of the Djibouti region (TFAI). *Afar Depression of Ethiopia*, *1*, 120–134.

Sakkas, V., Meju, M. A., Khan, M. A., Haak, V., & Simpson, F. (2002). Magnetotelluric images of the crustal structure of Chyulu Hills volcanic field, Kenya. *Tectonophysics*, *346*(3–4), 169–185. https://doi.org/10.1016/S0040-1951(01)00276-1

Samrock, F., Kuvshinov, A., Bakker, J., Jackson, A., & Fisseha, S. (2015). 3-D analysis and interpretation of magnetotelluric data from the Aluto-Langano geothermal field, Ethiopia. *Geophysical Journal International*, *202*(3), 1923–1948. https://doi.org/10.1093/gji/ggv270

Sandvol, E., Seber, D., Calvert, A., & Barazangi, M. (1998). Grid search modelling of receiver functions: Implications for crustal structure in the Middle East and North Africa. *Journal of Geophysical Research*, *103*(B11), 26,899–26,917. https://doi.org/10.1029/98JB02238

Saria, E., Calais, E., Stamps, D. S., Delvaux, D., & Hartnady, C. J. H. (2014). Present-day kinematics of the East African Rift. *Journal of Geophysical Research*, *119*, 3584–3600.

Schmandt, B., & Humphreys, E. (2010). Complex subduction and small-scale convection revealed by body-wave tomography of the western United States upper mantle. *Earth and Planetary Science Letters*, *297*(3–4), 435–445. https://doi.org/10.1016/j.epsl.2010.06.047

Selway, K., Yi, J., & Karato, S. I. (2014). Water content of the Tanzanian lithosphere from magnetotelluric data: Implications for cratonic growth and stability. *Earth and Planetary Science Letters*, *388*, 175–186. https://doi.org/10.1016/j.epsl.2013.11.024

Sembroni, A., Faccenna, C., Becker, T. W., Molin, P., & Bekele, A. (2016). Long-term, deep-mantle support of the Ethiopia-Yemen Plateau. *Tectonics*, *35*, 469–488. https://doi.org/10.1002/2015TC004000

Sengör, A. M., & Burke, K. (1978). Relative timing of rifting and volcanism on Earth and its tectonic implications. *Geophysical Research Letters*, *5*(6), 419–421. https://doi.org/10.1029/GL005i006p00419

Serpelloni, E., Vannucci, G., Pondrelli, S., Argnani, A., Casula, G., Anzidei, M., … Gasperini, P. (2007). Kinematics of the Western Africa-Eurasia plate boundary from focal mechanisms and GPS data. *Geophysical Journal International*, *169*(3), 1180–1200. https://doi.org/10.1111/j.1365-246X.2007.03367.x

Shackleton, R. M. (1986). Precambrian collision tectonics in Africa. *Geological Society, London, Special Publications*, *19*(1), 329–349. https://doi.org/10.1144/GSL.SP.1986.019.01.19

Shillington, D. J., Gaherty, J. B., Ebinger, C. J., Scholz, C. A., Selway, K., Nyblade, A. A., … Elliott, J. (2016). Acquisition of a unique onshore/offshore geophysical and geochemical dataset in the Northern Malawi (Nyasa) Rift. *Seismological Research Letters*, *87*(6), 1406–1416. https://doi.org/10.1785/0220160112

Shudofsky, G. N., Cloetingh, S., Stein, S., & Wortel, R. (1987). Unusually deep earthquakes in East Africa: Constraints on the thermo-mechanical structure of a continental rift system. *Geophysical Research Letters*, *14*(7), 741–744. https://doi.org/10.1029/GL014i007p00741

Simiyu, S. M. (2010). Status of geothermal exploration in Kenya and future plans for its development. In *Proceedings World Geothermal Congress* (pp. 25–29). Bali, Indonesia.

Simmons, N. A., Forte, A. M., & Grand, S. P. (2007). Thermochemical structure and dynamics of the African superplume. *Geophysical Research Letters*, *34*, L02301. https://doi.org/10.1029/2006GL028009

Simpson, F. (2000). A three-dimensional electromagnetic model of the southern Kenya Rift: Departure from two dimensionality as a possible consequence of a rotating stress field. *Journal of Geophysical Research*, *105*(B8), 19,321–19,334. https://doi.org/10.1029/2000JB900106

Sippel, J., Meeßen, C., Cacace, M., Mechie, J., Fishwick, S., Heine, C., … Strecker, M. R. (2017). The Kenya rift revisited: Insights into lithospheric strength through data-driven 3-D gravity and thermal modelling. *Solid Earth*, *8*(1), 45–81. https://doi.org/10.5194/se-8-45-2017

Skogseid, J., Planke, S., Faleide, J. I., Pedersen, T., Eldholm, O., & Neverdal, F. (2000). NE Atlantic continental rifting and volcanic margin formation. *Geological Society of London, Special Publication*, *167*(1), 295–326. https://doi.org/10.1144/GSL.SP.2000.167.01.12

Spieker, K., Wölbern, I., Thomas, C., Harnafi, M., & El Moudnib, L. (2014). Crustal and upper-mantle structure beneath the Western Atlas Mountains in SW Morocco derived from receiver functions. *Geophysical Journal International*, *198*(3), 1474–1485. https://doi.org/10.1093/gji/ggu216

Stab, M., Bellahsen, N., Pik, R., Quidelleur, X., Ayalew, D., & Leroy, S. (2016). Modes of rifting in magma-rich settings: Tectono-magmatic evolution of Central Afar. *Tectonics*, *35*, 2–38. https://doi.org/10.1002/2015TC003893

Stamps, D. S., Flesch, L. M., Calais, E., & Ghosh, A. (2014). Current kinematics and dynamics of Africa and the East African Rift System. *Journal of Geophysical Research: Solid Earth*, *119*, 5161–5186.

Stork, A. L., Stuart, G. W., Henderson, C. M., Keir, D., & Hammond, J. O. S. (2013). Uppermost mantle (Pn) velocity model for the Afar region, Ethiopia: An insight into rifting processes. *Geophysical Journal International*, *193*(1), 321–328. https://doi.org/10.1093/gji/ggs106

Stuart, G. W., Bastow, I. D., & Ebinger, C. J. (2006). Crustal structure of the northern Main Ethiopian Rift from receiver function studies. *Geological Society, London, Special Publications*, *259*(1), 253–267. https://doi.org/10.1144/GSL.SP.2006.259.01.20

Stuart, G. W., Fairhead, J. D., Dorbath, L., & Dorbath, C. (1985). A seismic refraction study of the crustal structure associated with the Adamawa Plateau and Garoua Rift, Cameroon, West Africa. *Geophysical Journal International*, *81*(1), 1–12. https://doi.org/10.1111/j.1365-246X.1985.tb01346.x

Suh, C., Ayonghe, S., Sparks, R., Annen, C., Fitton, J., Nana, R., & Luckman, A. (2003). The 1999 and 2000 eruptions of Mount Cameroon: Eruption behaviour and Petrochemistry of Lava. *Bulletin of Volcanology*, *65*(4), 267–281. https://doi.org/10.1007/s00445-002-0257-7

Sun, D., Miller, M. S., Holt, A., & Becker, T. W. (2014). Hot upwelling conduit beneath the Atlas Mountains, Morocco. *Geophysical Research Letters*, *41*, 8037–8044. https://doi.org/10.1002/2014GL061884

Tadjou, J., Nouayou, R., Kamguia, J., Kande, H., & Manguelle-Dicoum, E. (2009). Gravity analysis of the boundary between the Congo Craton and the Pan-African Belt of Cameroon. *Austrian Journal of Earth Sciences: An International Journal of the Austrian Geological Society*, *102*(1), 71–79.

Teixell, A., Arboleya, M.-L., Julivert, M., & Charroud, M. (2003). Tectonic shortening and topography in the Central High Atlas (Morocco), *Tectonics*, *22*(5), 1051. https://doi.org/10.1029/2002TC001460

Teixell, A., Ayarza, P., Zeyen, H., Fernandez, M., & Arboleya, M.-L. (2005). Effects of mantle upwelling in a compressional setting: The Atlas Mountains of Morocco. *Terra Nova*, *17*(5), 456–461. https://doi.org/10.1111/j.1365-3121.2005.00633.x

Tessema, A., & Antoine, L. A. G. (2004). Processing and interpretation of the gravity field of the East African Rift: Implication for crustal extension. *Tectonophysics*, *394*(1–2), 87–110. https://doi.org/10.1016/j.tecto.2004.07.057

Thybo, H., & Artemieva, I. M. (2013). Moho and magmatic underplating in continental lithosphere. *Tectonophysics*, *609*, 605–619. https://doi.org/10.1016/j.tecto.2013.05.032

Thybo, H., Maguire, P. K. H., Birt, C., & Perchuć, E. (2000). Seismic reflectivity and magmatic underplating beneath the Kenya Rift. *Geophysical Research Letters*, *27*(17), 2745–2748. https://doi.org/10.1029/1999GL011294

Tiberi, C., Ebinger, C., Ballu, V., Stuart, G., & Oluma, B. (2005). Inverse models of gravity data from the Red Sea-Aden-East African rifts triple junction zone. *Geophysical Journal International*, *163*(2), 775–787. https://doi.org/10.1111/j.1365-246X.2005.02736.x

Tokam, A., Tabod, C., Nyblade, A., Julià, J., Wiens, D., & Pasyanos, M. (2010). Structure of the crust beneath Cameroon, West Africa, from the joint inversion of Rayleigh wave group velocities and receiver functions. *Geophysical Journal International*, *183*(2), 1061–1076. https://doi.org/10.1111/j.1365-246X.2010.04776.x

Toteu, S., Penaye, J., & Djomani, Y. (2004). Geodynamic evolution of the Pan-African Belt in central Africa with special reference to Cameroon. *Canadian Journal of Earth Sciences*, *41*(1), 73–85. https://doi.org/10.1139/e03-079

Trestrail, K. R., Rooney, T. O., Girard, G., Svoboda, C., Yirgu, G., Ayalew, D., & Kappelman, J. (2017). Sub-continental lithospheric mantle deformation in the Yerer-Tullu Wellel Volcanotectonic lineament: A study of peridotite xenoliths. *Chemical Geology*, *455*, 249–263. https://doi.org/10.1016/j.chemgeo.2016.10.013

Tugume, F., Nyblade, A., & Julià, J. (2012). Moho depths and Poisson's ratios of Precambrian crust in East Africa: Evidence for similarities in Archean and Proterozoic crustal structure. *Earth and Planetary Science Letters*, *355*, 73–81.

Turner, S., Regelous, M., Kelley, S., Hawkesworth, C., & Mantovani, M. (1994). Magmatism and continental break-up in the South Atlantic: High precision 40Ar-39Ar geochronology. *Earth and Planetary Science Letters*, *121*(3–4), 333–348. https://doi.org/10.1016/0012-821X(94)90076-0

Vail, J. (1983). Pan-African crustal accretion in northeast Africa. *Journal of African Earth Sciences*, *1*(3–4), 285–294. https://doi.org/10.1016/S0731-7247(83)80013-5

Van Avendonk, H. J., Lavier, L. L., Shillington, D. J., & Manatschal, G. (2009). Extension of continental crust at the margin of the eastern Grand Banks, Newfoundland. *Tectonophysics*, *468*(1–4), 131–148. https://doi.org/10.1016/j.tecto.2008.05.030

Van Hinsbergen, D. J. J., Buiter, S. J. H., Torsvik, T. H., Gaina, C., & Webb, S. J. (2011). The formation and evolution of Africa from the Archaean to Present: Introduction. *Geological Society of London, Special Publication*, *357*(1), 1–8. https://doi.org/10.1144/SP357.1

Van Ngoc, P., Boyer, D., Le Mouél, J.-L., & Courtillot, V. (1981). Identification of a magma chamber in the Ghoubbet-Asal rift (Djibouti) from a magnetotelluric experiment. *Earth and Planetary Science Letters*, *372*, 372–380.

Vauchez, A., Dineur, F., & Rudnick, R. (2005). Microstructure, texture and seismic anisotropy of the lithospheric mantle above a mantle plume: Insights from the Labait volcano xenoliths (Tanzania). *Earth and Planetary Science Letters*, *232*(3–4), 295–314. https://doi.org/10.1016/j.epsl.2005.01.024

Veevers, J. J., Cole, D. I., & Cowan, E. J. (1994). Southern Africa: Karoo basin and Cape fold belt. *Geological Society of America Memoirs*, *184*, 223–280. https://doi.org/10.1130/MEM184-p223

Velasco, A., Kaip, G., Wamalwa, A., & Patlan, E. (2011). Seismic characterization of Menengai Crater, Kenya (Menengai), FDSN Database. https://doi.org/10.7914/SN/1C

Wada, I., Wang, K., He, J., & Hyndman, R. D. (2008). Weakening of the subduction interface and its effects on surface heat flow, slab dehydration, and mantle wedge serpentinization. *Journal of Geophysical Research*, *113*, B04402. https://doi.org/10.1029/2007JB005190

Wang, Y. F., Zhang, J. F., Jin, J. M., & Green, H. W. (2012). Mafic granulite rheology: Implications for a weak continental lower crust. *Earth and Planetary Science Letters*, *353*, 99–107.

Weeraratne, D. S., Forsyth, D. W., Fischer, K. M., & Nyblade, A. A. (2003). Evidence for an upper mantle plume beneath the Tanzanian craton from Rayleigh wave tomography. *Journal of Geophysical Research*, *108*(B9), 2427. https://doi.org/10.1029/2002JB002273

Weinstein, A., Oliva, S. J., Ebinger, C. J., Roecker, S., Tiberi, C., Witkin, E., … Rodzianko, A. (2017). Active deformation and magmatism during early stage rifting of Archaean lithosphere in the Eastern rift, Africa. *Geochemistry, Geophysics, Geosystems*, *18*, 3662–3686. https://doi.org/10.1002/2017GC007027

Whaler, K., & Hautot, S. (2006). The electrical resistivity structure of the crust beneath the northern Ethiopian rift. In G. Yirgu, C. J. Ebinger, & P. K. H Maguire (Eds.), *The Afar Volcanic Province within the East African Rift System*, *Geological Society, London, Special Publications* (Vol. 256, pp. 293–305).

Wheildon, J., Morgan, P., Williamson, K. H., Evans, T. R., & Swanberg, C. A. (1994). Heat flow in the Kenya rift zone. *Tectonophysics*, *236*(1–4), 131–149. https://doi.org/10.1016/0040-1951(94)90173-2

White, R., & McKenzie, D. (1989). Magmatism at rift zones: The generation of volcanic continental margins and flood basalts. *Journal of Geophysical Research*, *94*(B6), 7685–7729. https://doi.org/10.1029/JB094iB06p07685

Wölbern, I., Rümpker, G., Schumann, A., & Muwanga, A. (2010). Crustal thinning beneath the Rwenzori region, Albertine rift, Uganda, from receiver-function analysis. *International Journal of Earth Sciences*, *99*(7), 1545–1557. https://doi.org/10.1007/s00531-009-0509-2

Woldegabriel, G., Aronson, J. L., & Walter, R. C. (1990). Geology, geochronology, and rift basin development in the central sector of the Main Ethiopia Rift. *Geological Society of America Bulletin*, *102*(4), 439–458.

Wolfenden, E., Ebinger, C., Yirgu, G., Deino, A., & Ayalew, D. (2004). Evolution of the northern main Ethiopian rift: Birth of a triple junction. *Earth and Planetary Science Letters*, *224*(1–2), 213–228. https://doi.org/10.1016/j.epsl.2004.04.022

Wolfenden, E., Ebinger, C., Yirgu, G., Renne, P., & Kelley, S. (2005). Evolution of a volcanic rifted margin: Southern Red Sea, Ethiopia. *Bulletin Geological Society of America*, *117*(7), 846–864. https://doi.org/10.1130/B25516.1

Wortel, M. J. R., & Spakman, W. (2000). Subduction and slab detachment in the Mediterranean-Carpathian region. *Science*, *290*(5498), 1910–1917. https://doi.org/10.1126/science.290.5498.1910

Xu, W., Rivalta, E., & Li, X. (2017). Magmatic architecture within a rift segment: Articulate axial magma storage at Erta Ale volcano, Ethiopia. *Earth and Planetary Science Letters*, *476*, 79–86. https://doi.org/10.1016/j.epsl.2017.07.051

Yang, Z., & Chen, W. P. (2010). Earthquakes along the East African Rift System: A multiscale, system-wide perspective. *Journal of Geophysical Research*, *115*, B12309. https://doi.org/10.1029/2009JB006779

Yokoyama, T., Kusakabe, M., & Nakamura, E. (2007). Plume-lithosphere interaction beneath Mt. Cameroon volcano, West Africa: Constraints from 238U- 230Th-226Ra and Sr-Nd-Pb isotope systematics. *Geochimica et Cosmochimica Acta*, *71*(7), 1835–1854. https://doi.org/10.1016/j.gca.2007.01.010

Zeyen, H., Ayarza, P., Fernandez, M., & Rimi, A. (2005). Lithospheric structure under the western African-European plate boundary: A transect across the Atlas Mountains and the Gulf of Cadiz. *Tectonics*, *24*, TC2001. https://doi.org/10.1029/2004TC001639

Zlotnik, S., Jiménez-Munt, I., & Fernàndez, M. (2014). Coupled mantle dripping and lateral dragging controlling the lithosphere structure of the NW-Moroccan margin and the Atlas Mountains: A numerical experiment. *Lithos*, *189*, 16–27. https://doi.org/10.1016/j.lithos.2013.10.016